5-2024

Test and Evaluation Model for Midwater Docking of Autonomous Underwater Vehicles

Parker Baillon
Florida Institute of Technology, pbaillon2019@my.fit.edu

Test and Evaluation Model for Midwater Docking of Autonomous Underwater Vehicles

by

Parker Baillon

A thesis submitted to the Department of Ocean Engineering and Marine Sciences
at Florida Institute of Technology
in partial fulfillment of the requirements
for the degree of

Master of Science
in
Ocean Engineering

Melbourne, Florida
May, 2024

We, the undersigned committee, hereby approve the attached thesis,
"Test and Evaluation Model for Midwater Docking of Autonomous Underwater Vehicles"
by
Parker Baillon

_____

Stephen Wood, Ph.D., P.E.
Professor
Ocean Engineering and Marine Sciences
Major Advisor

_____

Ronnal Reichard, Ph.D.
Professor
Ocean Engineering and Marine Sciences

_____

Ilya Mingareev, Ph.D.
Assistant Professor
Mechanical and Civil Engineering

_____

Richard B. Aronson, Ph.D.
Professor and Department Head
Ocean Engineering and Marine Sciences

Abstract

Title: Test and Evaluation Model for Midwater Docking of Autonomous Underwater Vehicles

Author: Parker Baillon

Major Advisor: Stephen Wood, Ph.D., P.E.

This research created a Test and Evaluation (T&E) model for midwater Autonomous Underwater Vehicle (AUV) capture. The creation of this model will allow for a better assessment of the feasibility of midwater AUV capture. To achieve this, the T&E model was exposed to various flow conditions to assess stability. Capturing an AUV in midwater, the area below the wave-affected zone to the sea floor, has many benefits for an AUV and its mission. AUVs basing missions from a midwater dock will not be affected by wave motions. A midwater dock can be transported to any mission site and deployed with similar operating procedures to surface docking stations.

For this project, requirements and specifications were given by the Naval Surface Warfare Center, Carderock Division (NSWCCD). The main requirements of this project were to create a docking station that measured 12 ft in length, 1ft tall and 1ft wide, 200 lbs in water, and eight onboard thrusters. Each thruster was required to be independently controlled and set up to maintain the pitch and yaw angles of the docking station. The main objective given by NSWCCD was to examine the motions, limitations, and power requirements of the dock when subjected to ocean currents. The unit was tested at NSWCCD's Circulating Water Channel (CWC) to do this. At this testing facility, the unit was exposed to different flow velocities, allowing the unit to try and maintain different yaw angles while stabilizing the pitch. Information about the time it takes to move to a position and the accuracy of the position will be measured with an underwater motion capture system.

Testing revealed the unit could maintain its yaw position at all current speeds. The unit was stable in pitch and yaw, with ample thrust available from the onboard thrusters. This research indicated that capturing an AUV in the midwater would be feasible with additional control system development and advanced tunning profiles.

Table of Contents

List of Figures

List of Tables

Terminology

AUV – Autonomous Under Water Vehicle

T&E - Test and Evaluation

NSWCCD – Naval Surface Warfare Center Carderock Division

PID – Proportional Integral Control

ROV – Remotely Operated Vehicle

HCWS – Heave Compensated Winch System

IMU – Inertial Measurement Unit

MoCap – Motion Capture

CAD – Computer Aided Design

COTS – Commercial off the Shelf Component

DoF – Degree of Freedom

FEA – Finite Element Analysis

NEMA 6P – Nation Electrical Manufactures Association Water Resistance Rating

SPI – Serial Peripheral Interface

I2C – Inter-Integrated Circuit

Acknowledgement

Thank you to Code 881 and NSWC Carderock Division for supporting this project. Without the support and expertise of the incredible staff, this research would not have been possible.

Thank you to my thesis committee for their expertise and support through this research. Being able to ask questions and receive guidance and recommendations from this group of talented professors was extremely valuable.

Thank you, Dr. Wood, for all your support of me through my undergraduate and now graduate degree. Without the experience I gained working on your projects and hearing your stories I would not be the student and engineer I am today. Thank you for inviting me to your lab back in my freshman year.

Dedication

I dedicate this thesis research to my wife, Maria, who has always supported me through my toughest times and toughest projects. You are everything to me, and I am so thankful for your love and support.

Chapter 1
Introduction and Background

Introduction

The primary purpose of this research was to create a physical test and evaluation (T&E) model of an Autonomous Underwater Vehicle (AUV) midwater docking station that will allow for a better assessment of technology feasibility. Current AUV docking devices are traditionally located on the seafloor or the ocean surface. Each of these locations presents its advantages and disadvantages. Mounting a docking station on the seafloor provides a stable, established reference point for the AUV to return to. Seafloor-mounted systems can interface with subsea cable networks to connect to the mainland (1), making them ideal for areas where continuous AUV mission coverage is desirable. However, the installation of these devices is complicated and expensive. Target location bathymetry may make installation of a seafloor dock not feasible due to depth or lack of subsea infrastructure.

On the other hand, capturing the AUV on the ocean surface allows for maximum mission mobility but exposes the AUV to surface effects like wind and waves. The AUV can be transported to almost any target location and deployed from the surface vessel. High sea states can make recovery of an AUV dangerous and possibly harm the vehicle or the recovery crew. To maximize the deployment conditions, the technique of midwater docking can be used for the launch and recovery of an AUV. The unit would be suspended on a heave-compensated winch system (HCWS) to enhance docking further. An HCWS is a device located on a ship that analyzes its motion and adjusts the length of the line going to the unit to keep it at a level depth (2). Docking an AUV in midwater, while attached to a stable surface mount, allows the vehicle to be submerged below the effects of wind and waves, reducing the forces perturbing the AUV.

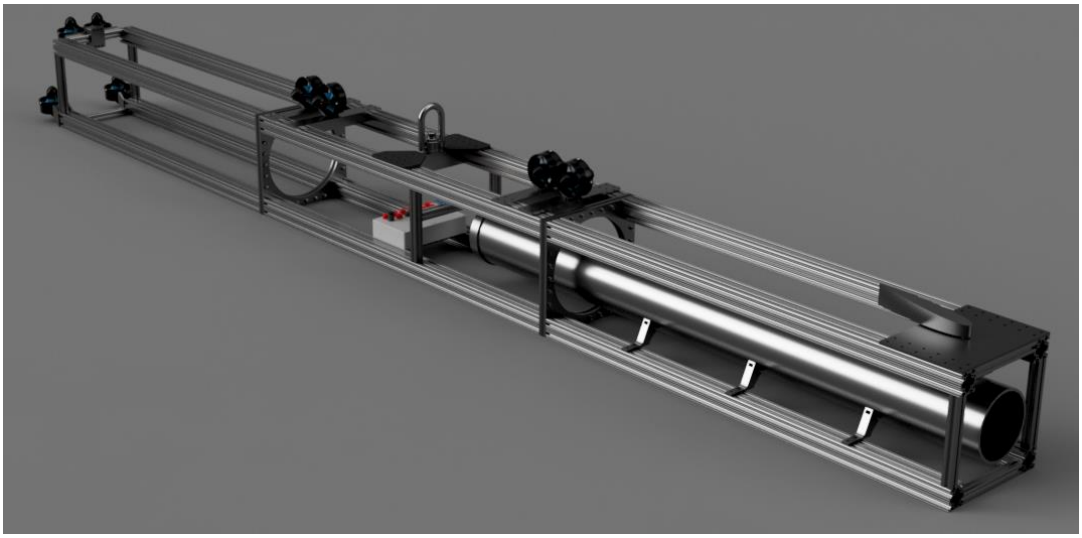

Figure 1: Docking Station CAD Model

The above testing model was used to examine the feasibility of midwater AUV Capture. The customer, NSWCCD, gave the physical dimensions of the docking station and thruster placements. The following section outlines the requirements for which the system was designed.

The docking station T&E model was used to understand how the unit will move during actual in-water operations. To capture an AUV with low maneuverability, the docking station will need to be stable and capable of holding a variety of attitudes. The more stable and adjustable the platform is, the easier it will be for the AUV to align and complete its docking sequence. Testing the T&E model allowed important control and stability information to be gathered.

The T&E model proposed for this research was rigorously tested in an ideal flow environment at NSWCCD, ensuring the reliability and accuracy of the results. The model was experimentally tested through a variety of orientations and flow speeds to better understand and quantify the docking station's feasibility. An underwater motion capture system captured all 6DoF motions, providing comprehensive data for analysis. The testing at NSWCCD identified the system's power requirements, range of motion, and yaw/pitch response rates.

Motivations

As AUV systems continue to advance, creating effective capturing solutions for performing missions in various environments will be necessary. Midwater docking has the potential to capture AUVs in a wide range of sea states without the need for complex infrastructure, which would limit mission mobility. Examining the controllability of the T&E model will advance the field's understanding of unstable tow bodies that utilize active compensation. Traditional tow bodies are naturally stable at a given orientation, such as a required pitch angle for a sensor like a side scan sonar. However, with an AUV, the recovery frame must adapt to different AUV trajectories independently of flow. The thrusters fully control the frame to achieve this, and there is no unpowered stable state. Potential end users for this technology and research are groups that deploy AUV systems in high wave height environments, which pose a hazard to the vehicle or recovery team using traditional surface methods.

Project Requirements

With collaboration from NSWCCD, a set of model requirements and testing requirements were produced. These requirements will drive the detailed design of the model and its control system.

Model requirements:

- The system will be no larger than 12ft x 1ft x 1ft.
- Provide internal storage capacity for a 6-inch diameter x 62-inch-long payload.
- Wet weight of 150lbs – 250lbs.
- Dry weight not to exceed 300 lbs.
- Include lifting mount(s) to support lifting by crane.
- Waterproof for complete submersion up to 10m depth.
- Maintain position at various yaw angles from 0-90 degrees port and starboard.
- Incorporate sensors to measure yaw orientation. This may be accomplished using a measurement of true heading, magnetic heading, or sideslip angle relative to flow.

But will need to be accurate to within +-0.5 degrees and serve as feedback in the yaw controller.

- Operating current 0.25kts – 1.5kts.
- Adjustable Center of Buoyancy and Center of Gravity.
- Active yaw and pitch compensation.
- Adjustable Thruster Mounting locations to accommodate different thruster layouts for up to 8 independently controlled thrusters.
- Each individual thruster shall be able to produce 0-8lbs of thrust in either direction and be controllable such that thrust output capacity can be limited if desired.
- Configurable command and control software.
- Surface powered for extended testing runs.
- LED light array for visibility with underwater motion capture.
- Removable panels to direct water flow around the unit.
- Shippable on a single standard wood pallet.
- The system will be able to be mounted in the Circulating Water Facility using existing facility infrastructure and equipment as provided by NSWC Carderock.

Test requirements:

- Evaluate system stability in different positions and current speeds.
- Evaluate the performance of the closed-loop controller algorithm.
- Collect data on the system:
    - Attitude (roll, pitch, and yaw)
    - Position (surge, sway, and heave)
    - Depth
    - Current Speed
    - Controller Performance (gain, input, and response)
    - Thruster Power
- Simulate the heave motion of the support vessel (if existing equipment to enable this is available and feasible to use).

Research Objectives

The goal of this master thesis research was to create a T&E model of an AUV capturing system. This model was adaptable for different garage sizes, thruster layouts, and control architectures. The model was tested in the Circulating Water Channel (CWC) at NSWCCD. The CWC will provide a controlled-current environment where different docking station attitudes can be examined for stability. The development and testing of this model contributed to a better understanding of the feasibility of midwater capture of AUV systems while also creating a platform ready for further development and testing.

Objective 1: Create a physical working model for understanding the stability motions of an AUV docking system.

Objective 2: Create configurable control software programmable through MATLAB Simulink.

Objective 3: Collect data on a model's motion and controller performance.

Objective 4: Develop a better understanding of the feasibility of midwater AUV capture.

Hypothesis: The creation of a T&E model of an AUV docking station will allow for a better assessment of the feasibility of midwater AUV capture.

Background Information

Docking Stations:

Launching underwater vehicles from depth is the preferred option for many subsea operations. Commercial Remotely Operated Vehicles (ROVs) have long been deployed from garage systems. The garage system can be deployed from a shipboard crane, A-frame, or moon pool. The benefit of this system is that the ROV will not be subjected to surface effects while docking. The cage also allows the ROV to be connected via a dual tether system. The main lifting tether connects to the garage and provides the lifting capacity needed, while a smaller, spooled tether in the garage is used to deploy the ROV onto the location. This smaller tether is lighter and less obtrusive. This dual combination dramatically increases the depth range and sea conditions in which the vehicle can operate (3).

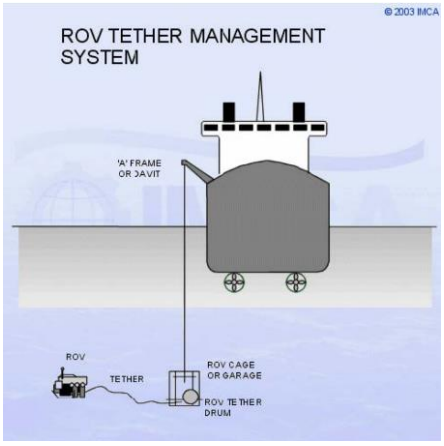

Figure 3: ROV Garage System (4)

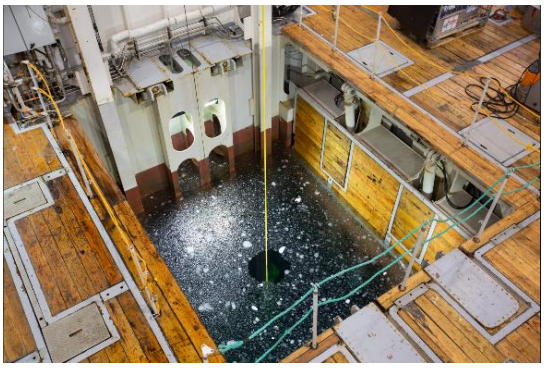

Figure 2: Research Ship Moon Pool (5)

AUVs, however, present challenges for a garage-type recovery system as there is no operator. AUVs do not have an operator, so the onboard computer fully commands the motions. Due to this, the motion behavior of the garage system needs to be minimal and predictable so that the onboard computer system can be trained to dock with the garage. Additionally, AUVs generally have a different geometry than ROVs. An ROV is commonly used for work or exploration where precise motions are required, often fully controlled in 6 degrees of freedom (DoF), while an AUV will be controlled in 5 DoF. An

AUV is often designed for extended, continuous survey areas of the ocean floor, making their shape long, slender, and hydrodynamic (6).

Figure 5: Commercial Class ROV (7)

Figure 4: Remus 100 AUV (8)

The difference in geometry and control authority for the AUV system necessitates a different type of garage system than one used for an ROV. The garage will need to be longer and conform to the torpedo shape of the AUV. The development of a garage system for an AUV will allow for a more effective launch and recovery of the AUV.

Another unique possible use for a midwater garage capturing system is capturing underwater gliders. These ocean observation instruments glide up and down the water column with a buoyancy engine (6). The buoyancy engine adjusts the vehicle's buoyancy from negative to positive, causing the glider to rise or fall in the ocean. This form of propulsion limits the control of the vehicle, so for vehicle recovery, it floats passively on the surface, waiting to be captured by a crew aboard a vessel. The gliders can be captured with a net or attachment of a lifting line. This makes the glider susceptible to waves and marine traffic (9). The midwater capture garage would allow the glider to be recovered during a dive or ascent where the control authority is the greatest. Capturing the glider during its mission would prevent it from getting damaged by waves or surface traffic. This capture will require a predictable and highly stable platform for the vehicle to fly into for docking.

The system must pitch up or down for the unit to capture an underwater glider. Since a glider is most controllable during its dive and ascent, the dock would need to capture the system in the middle of this action. Since the T&E docking unit can control its pitch, it can be compatible with the dive paths of an underwater glider, as shown in the figure below.

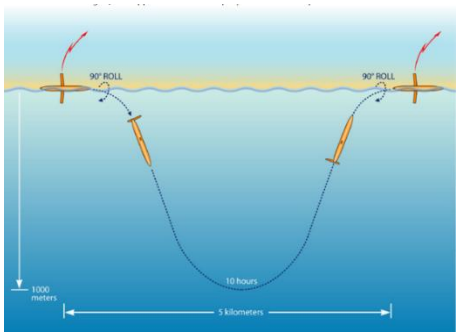

Figure 6: Slocum Glider Example Mission (10)

Another ocean system that could utilize the midwater docking system would be hybrid ocean gliders. These systems fly similarly to a standard ocean glider but also include an active thruster on the back that can be operated for increased control authority. An example of this type of system is shown in the figure below.

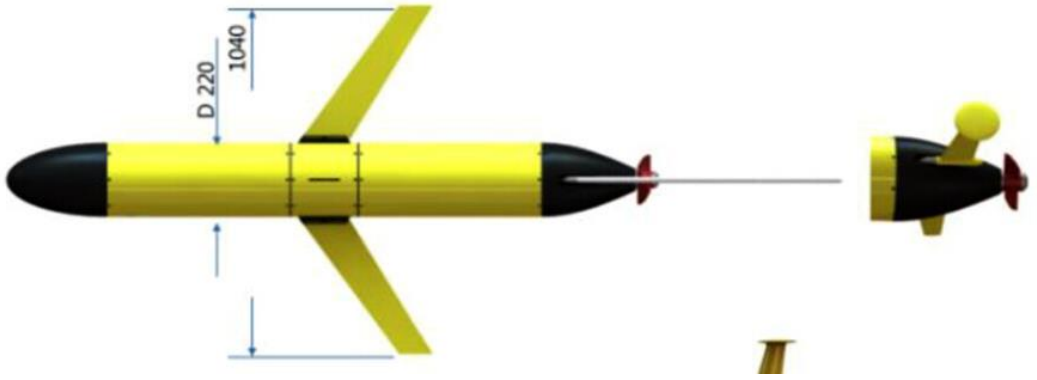

Figure 7: Hybrid Ocean Glider with Rear Thruster (36)

This type of ocean glider could follow the slopping path of a traditional glider or re-position its self-level to the capturing frame. More complex hybrid systems are being developed for survey and inspection use. These next-generation vehicles incorporate the rear thruster onto the glider and add horizontal bow and stern thrusters to the glider system. This combination of active thrusters gives the vehicle control like a ROV. This type of vehicle would be able to integrate well with the underwater docking station due to its strong control authority. The vehicle shown below would require minimum compensation from the proposed AUV dock.

Figure 8: Hybrid Ocean Glider Prototype (35)

Control Theory:

A vital component of the AUV docking system is the control of the yaw and pitch axes. These two motions will have the most significant impact on the system's success. As an AUV goes to dock with the unit, the vehicle may collide with the unit if the yaw or pitch cannot remain stable. For the context of this thesis research, the goal for the unit was to develop a set of closed-loop controllers for yaw and pitch in a simplistic but effective manner.

When creating controllers for motion control, the two main types are open-loop and closed-loop control. Open-loop control does not consider the system's response. In an open-loop setup, the actuator is commanded to move, and the system does not consider its resulting action.

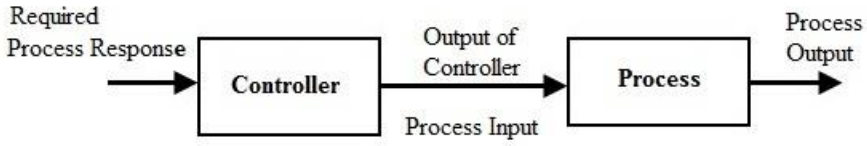

Figure 9: Open Loop Control Example (11)

A closed-loop controller considers the system's response. There are several types of closed-loop control, but the most common in underwater robotics and many industries is the Proportional, Integral, and Derivative controller (PID). This controller and the other portion of a closed-loop system are outlined and defined below.

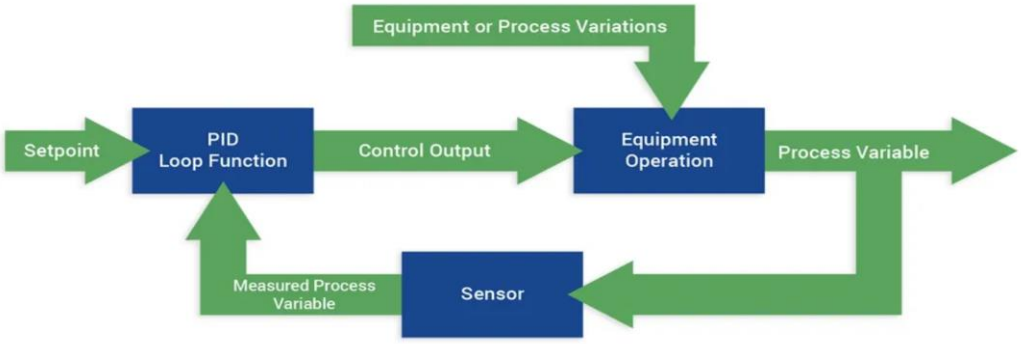

Figure 10: Basic PID loop diagram (12)

Based on the above diagram, the major sections of a closed-loop control setup are defined below:

Setpoint: Targeted value for the system; this is normally set by the user, and for this T&E model, it will be the value for pitch/yaw that the vehicle will try to maintain.

PID Loop Function: This loop is a summation of three different functions.

$$u(t) = K_c \left(e(t) + \frac{1}{T_i} \int_0^t e(t')dt' + T_d \frac{de(t)}{dt} \right) + b \qquad \text{Equation 1}$$

The proportional response part of Equation 1 calculates the direct error between the current setpoint and the measured process variable. This component of the PID controller often causes the majority of the response, but if the gain for this variable is too high, the system may oscillate rather than settle at the setpoint. The integral response of the PID loop sums the error of the setpoint and measured process variable over time. If error persists in the system, this term will help bring the system into equilibrium. The derivative response will cause a decrease in output if the measured process variable is changing too quickly. This portion of the PID loop helps make the control loop less reactive. However, the term is susceptible to noise in the measured process variable signal. If too much noise exists, the derivative response will fluctuate rapidly and cause the system to be unstable. A good solution to this issue is applying a filter to the measured process variable.

Process Variation: External forces that will act on the system. For the T&E model, these forces were hydrodynamic loads.

Equipment Operation: This section is the actual operation of the equipment. This portion accepts the output of the PID controller and commands the equipment accordingly. For the testing model, the input is the error in the angle setpoint. The equipment interprets this and commands the thrusters on the unit to make the required adjustments.

Process Variable: This is the quantity the setpoint tries to control. For the AUV dock, this will be the yaw and pitch value of the vehicle.

Sensor: This is the equipment that will measure the process variable. For the AUV dock, this will be the 9 DOF Inertial Measurement Unit (IMU) and current vane.

Measured Process Variable: The measured value of the process variable captured by the sensor.

This closed-loop control was implemented with MATLAB Simulink. This program allows for control loops to be easily set up and tuned. Additionally, the hardware for the model is controlled directly through Simulink. This Simulink controller setup allowed simple integration with final hardware and real-time system tuning. Future control systems can be added with little modifications if they already exist in the Simulink environment.

When implementing a PID controller, a transfer function will often be used to estimate the system's response. A transfer function is a mathematical model that converts a specified input to a specified output in the same way a real-life process would. Transfer functions can be used to model simple linear systems or complex nonlinear systems. The operation of the AUV docking station is likely to be complex and nonlinear, as stated in the Handbook of Marine Craft Hydrodynamics and Motion Control (13). Two main areas will need to be investigated when examining the creation of the model's transfer function for this docking system. Hydrodynamics and thruster mechanics will have the most significant effect on the system's response. Various hydrodynamic coefficients will be needed to predict the motion of the system to create the transfer function. Past studies have used a

combination of Computational Fluid Dynamics (CFD) and in-water tests. To model the thruster performance hardware, performance testing from Blue Robotics (14) and the thesis "6-DoF Modelling and Control of a Remotely Operated Vehicle" (15) could be used to build a thruster model. Due to the scope of the project, the creation of a complex dynamic model for the system was omitted from the PID tuning process.

As seen in Equation 1, the PID function has several gains that affect each response's output. Tunning of a closed-loop control system is finding the best set of gains for each portion of the PID loop. Several different techniques can be used. If a mathematical model is known, the built-in tunning software found in Simulink can be utilized. This tunning tool will run through different sets of PID gains until the system achieves the desired performance. When a mathematical model of the system is not known, the PID gains can be tuned from the response of the real hardware. This is often not done in industry, as the response can be erratic and uncontrolled when tuning the system. However, tuning the gain on real hardware is possible in a controlled testing setting, where the equipment can be isolated. Most methods of tuning hardware are focused on trial and error; this research used the Ziegler-Nichols closed-loop tuning method. This method utilizes the ultimate gain value and ultimate period of oscillation to calculate the initial PID controller gains.

In the Ziegler-Nichols closed-loop tuning method, the first goal is to find the value of K_u which is the ultimate gain. This proportional gain value results in the system oscillating indefinitely (16). From the system's oscillation, the value for the ultimate period of oscillation, P_u, can be measured. From P_u and K_u, the loop-tunning constants K_c, T_i, and T_d can be calculated using the following procedure (16).

1. Remove the response of the integral and derivative portion of the PID loop.
2. Change the setpoint of the system to initiate a small disturbance.
3. Adjust the gain of the proportional term until the oscillation becomes constant.
4. Record the value of K_u and P_u
5. Use the table below to calculate the remaining constants.

	K_c	T_I	T_D
P	$K_u/2$		
PI	$K_u/2.2$	$P_u/1.2$	
PID	$K_u/1.7$	$P_u/2$	$P_u/8$

Figure 11: Ziegler-Nichols closed-loop tuning method Calculation Table (16)

The performance of the PID system will be verified by tracking the process parameter compared to the setpoint. A graph plotting the commanded position and measured position will be produced. This will help determine if the controller is stable and able to fulfill its requirements. An example of this is shown in the figures below.

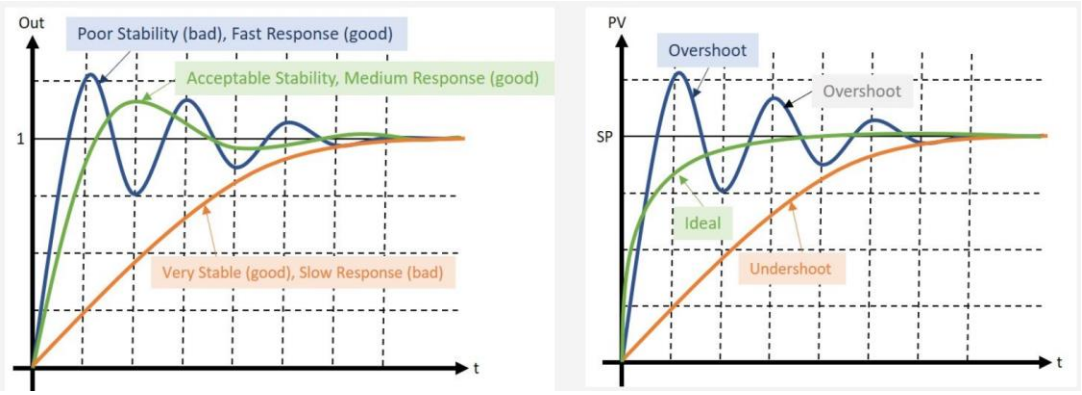

Figure 12: Example PID Process Outputs (17)

The figures above depict the stability and response of different PID process loops. The system's performance can be determined simplistically with three parameters: Stability, Response, and Overshoot/Undershoot. The stability of the system measures how much oscillation is occurring. The system is considered unstable if a system continues oscillating and can never achieve the desired setpoint. The response of the system is the time it takes for the process variable to reach the setpoint. Overshoot/Undershoot is the measure of how far the measured process variable is from the setpoint. If the loop is overshooting, then the measured value will be greater than the setpoint. The inverse is true for undershoot scenarios. The end goal of system tunning is to create a set of constants that will create the desired system response.

Underwater Motion Capture:

During testing of the docking station at the Naval Surface Warfare Center Carderock Division (NSWCCD), motion capture technology was used to capture the absolute position of the unit. Motion capture technology utilizes a series of cameras tracking reflective markers. Each camera finds the position of the markers in its 2D view. Meshing the 2D position data across a series of cameras positioned in 3D allows for the position of each marker to be resolved in 3D space. The system used was the OptiTrack Prime 13 camera; this camera has many desirable attributes for motion capture work and has the following specifications, shown below in Figure 13.

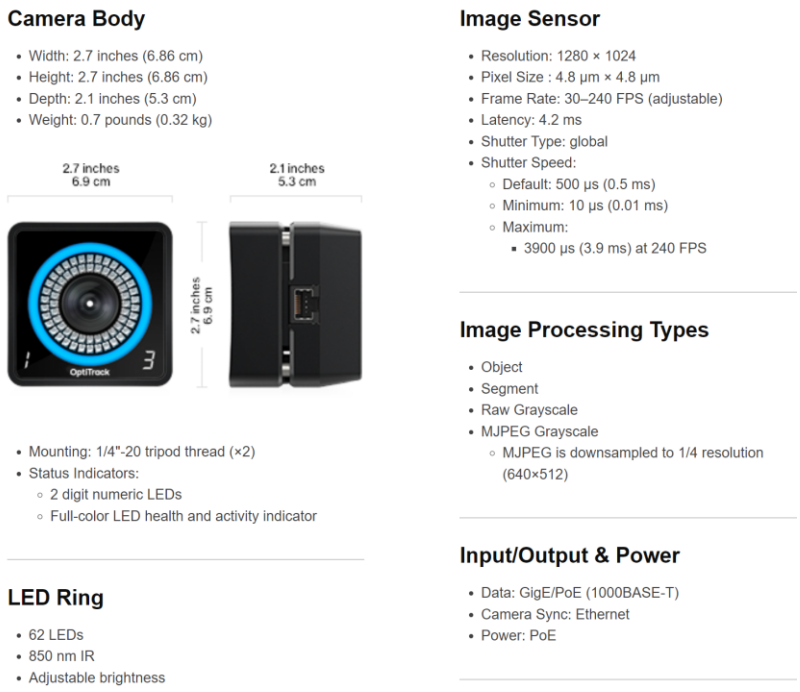

Figure 13: Prime 13 Camera Specifications (18)

The OptiTrack Prime 13 camera is a good choice for motion capture as it captures in a high resolution at a high frame rate. High resolution allows for the camera to capture more detail of each marker. Frame rate controls the frequency of data collection. Higher frame rates are good for capturing fast-moving, high-detail systems. Another strong benefit of the Prime

13 camera is its exposure settings. Exposure controls the timing at which the sensor is open. The longer the exposure, the more light will be captured, resulting in brighter images for the camera to process. The form factor of the Prime 13 is compact, which allows it to be mounted in tight spaces. Lastly, the camera is powered and communicates through Power over Ethernet (PoE). This makes interfacing the camera into a test setup simple; a single cord can be run on each camera and back to the host computer.

Each camera in the system has a set of IR LEDs that emit light toward the target area. This light is then reflected off a marker to the camera. IR is used in air systems as it travels far and can be distinguished from the visual light. The Prime 13 camera has a filter that will only allow IR wavelengths, greatly decreasing possible noise. The process of the IR light reflection is shown in the diagram below.

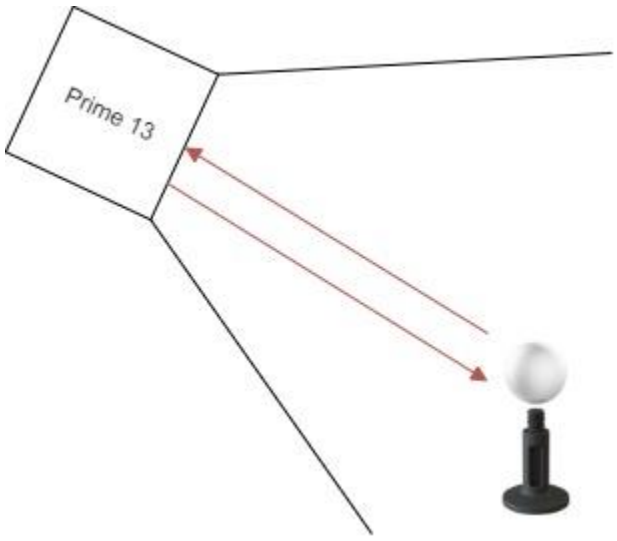

Figure 14: Reflective Marker Example – OptiTrack Marker (18)

To resolve the position of the markers, a minimum of two cameras are required. However, the more cameras added to the system with greater overlap between them, the better the calculated marker position will be. In most cases, being able to place cameras in full 360-degree coverage is ideal as shown in Figure 15. The cameras are connected through an ethernet switch and a PC running the OptiTrack Motive software. This software controls

the timing, performance, and calibration of the cameras. In traditional fixed-position in-air systems, the typical resolution for this setup is < 0.5mm (19).

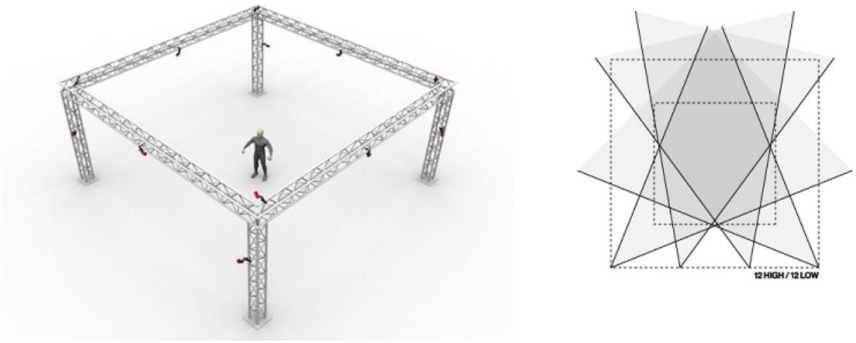

Figure 15: In-air Opti Track Setup (18)

When using an in-air camera system underwater, many challenges must be managed. The first issue is waterproofing the system. To do this, NSWCCD has created small underwater enclosures with Blue Robotics components to house the cameras. The camera enclosures are rugged and protect the camera during testing. On the rear of the enclosures are connectors that pass the ethernet signals. The camera enclosures to be used for testing are shown below.

Figure 16: Prime 13 Underwater Enclosure

The next major issue is how the cameras will see the markers on the testing unit. The built-in IR LEDs on the camera will have extremely poor performance underwater. IR wavelengths 700 nm-1000 nm (20) travel less than 2m in water (21). The built-in LEDs will also reflect against the housing and fully blind the camera. Utilizing a visual light

marker system with wavelengths 400 nm- 700 nm (20) is a great choice for underwater use. A visual light system often uses a blue (475 nm) or green (550 nm) light source. The light source will be in either a reflecting or projecting layout. In a reflecting layout, the light source points into the capture volume. Reflective markers on the unit bounce the light back so the camera can see. If the visual light is placed on the target body, the light will shine towards the camera. In this setup, the distance traveled is half that of the reflective setup. Since the distance is less, along with eliminating losses due to the reflector projection setups will appear brighter to the camera.

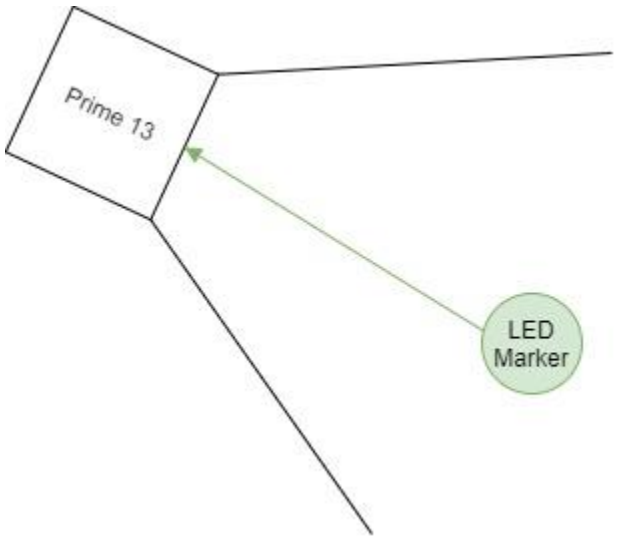

Figure 17: Active Marker Example

The brighter the marker is, the better the camera system's performance will be. A major factor for underwater motion capture performance is the exposure of the system for maximizing the light in the camera. As the capture rate is increased, the maximum exposure will decrease. By utilizing the active markers, the capture rate can be increased while still maintaining a good view of the marker positions.

For underwater motion capture, the placement of cameras and markers is important for system success. Utilizing projecting markers will help the camera system isolate the markers. However, errors caused by the water's surface still need to be minimized. The

most effective way to reduce the reflection seen from the surface is to angle the camera system downwards so it cannot “see” the water’s surface. A 2D cross-section of an underwater motion capture setup with ideal camera positioning is shown below.

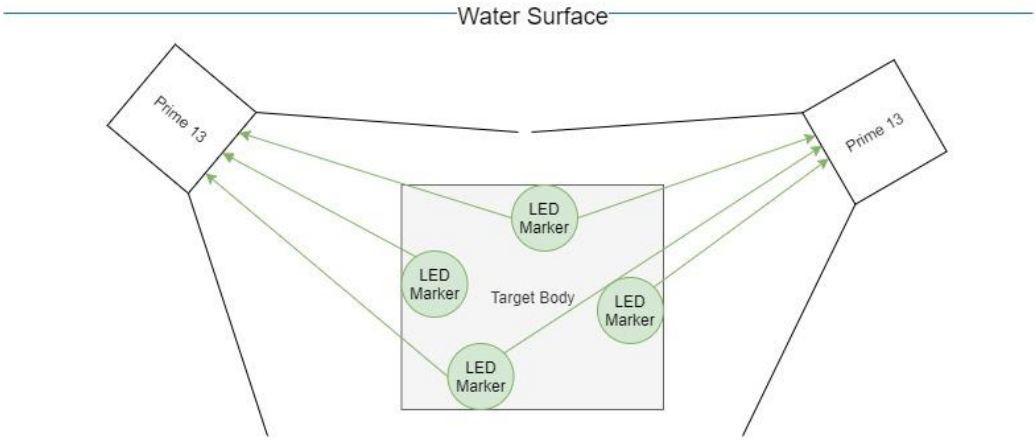

Figure 18: 2D Cross Section of Underwater Motion Capture

Inside the motion capture software, Motive, many different settings can be used to isolate the marker position and filter out the noise. The two primary filters used are the size and circularity filters. The size filter removes points that are either too big or too small. As the testing unit moves through the water some markers will appear larger/smaller to the cameras. Setting the correct size filter is important for system success. The circularity filter helps to remove reflections caused by refraction through the water surface or off the docking station’s structure. An example of these filtering options is shown below. Since the markers used for this model have a high brightness, an aggressive set of filters can be used. This set of filters will decrease errors in the motion capture data.

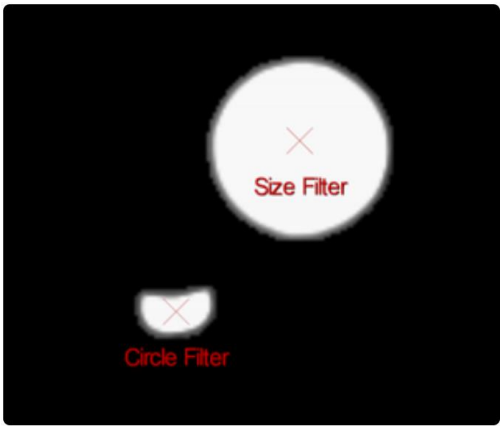

Figure 19: Filter Example from Motive (18)

A major component of the motion capture setup is calibration. The camera system needs a calibration procedure to establish the relative position of all the cameras. To do this in the air, a reflective wand is waved through the capture volume. The calibration wand is a set of reflective markers placed at exact distances apart from one another.

Figure 20: OptiTrack Calibration Wand (18)

The Motive software captures the data as to where the calibration wand is in each camera view. Then, by knowing the exact distance between each marker and using the built-in software algorithms, the position of each camera can be resolved once enough data has been collected. Figure 21 below shows the collected data for an example calibration. The

colored section represents a time series of collected data points. The more filled in each camera view, the more data collected. The goal is for each camera to have a large amount of data points. When calibration is completed, Motive will give statistics on the calibration quality.

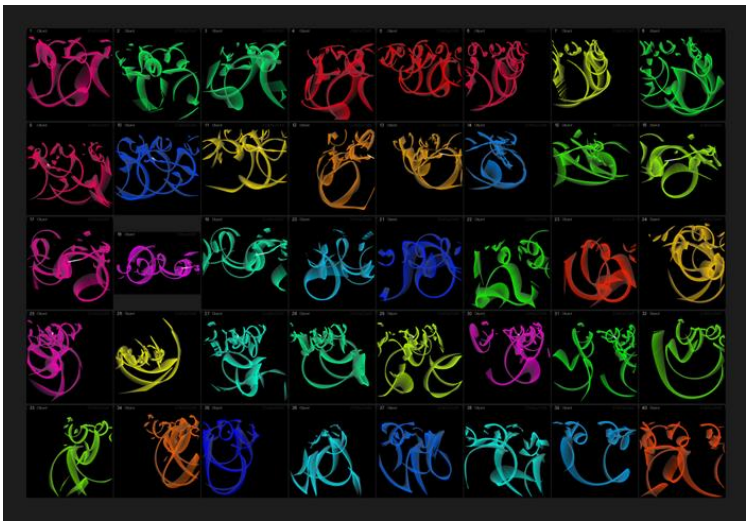

Figure 21: Captured Calibration data for an OptiTrack System (18)

Once calibrated, the position of the cameras cannot be modified, making stable placement and positioning especially important. For an underwater motion capture system that will be utilizing active markers, a different calibration tool must be used. Instead of a reflective wand, an LED wand connected to a long dock pole is used to sweep through the underwater capture volume. Like the in-air calibration, the software collects the needed data and resolves the position of each camera. After calibration is completed, a reference ground plane is placed to orientate the camera positions and establish the coordinate frame.

After the system is set up, a post-calibration test is performed to verify the system's performance. This test consists of taking the calibration wand back through the capture volume and collecting the positions of each marker. Since the exact position of the wand markers is known, a difference can be calculated from the reported marker position. This difference is the error at a given point in the capture volume. This error can be found for

each axis at every point in the capture volume. Knowing what the error is throughout the volume is critical to ensure that the system will perform as expected and that the data gathered can be used.

The final step before testing is setting up the rigid bodies the cameras will track. For this test, the rigid body will be the docking station. A rigid body in Motive is a set of marker points the software will bundle together and track the position of. To do this, markers must be asymmetrical and distributed throughout the body. The goal is to have multiple points for the camera to track so that if some become blocked, the software can still resolve the body's exact location. For the underwater docking station, these markers will be LED lights positioned at various locations along the outside of the frame. An example of marker placement is shown below on in-air quadcopters.

Figure 22: Drones with Reflective Markers (22)

With the system set, calibrated, and verified, it is now ready to begin recording live testing data. The recording is triggered manually or by a 5V high signal. Once recorded, the position of every marker and ridged body is saved. This data can be played back via Motive or exported for further processing.

Processing of the motion capture data begins by reconstructing the 3D data gathered by the system. This step goes back and solves all the rigid body information from the cameras. Sometimes, when a rigid body is very complex, or the system slows during capturing, certain frames of 3D data can be missed. Resolving the 3D data will fill these gaps and ensure the system outputs its most correct estimation of position (23). After completing this step, the data can be exported as a .csv for processing in another program. The motion capture data for this research was processed using a combination of Excel and MATLAB. Below is an example of captured data for a rigid body's x, y, and z positions.

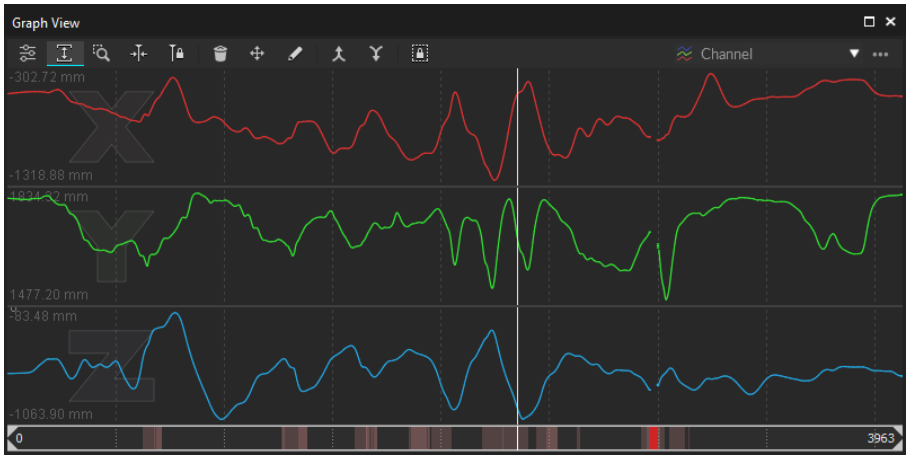

Figure 23: Example data recoded from Motive (18)

Coordinate Systems:

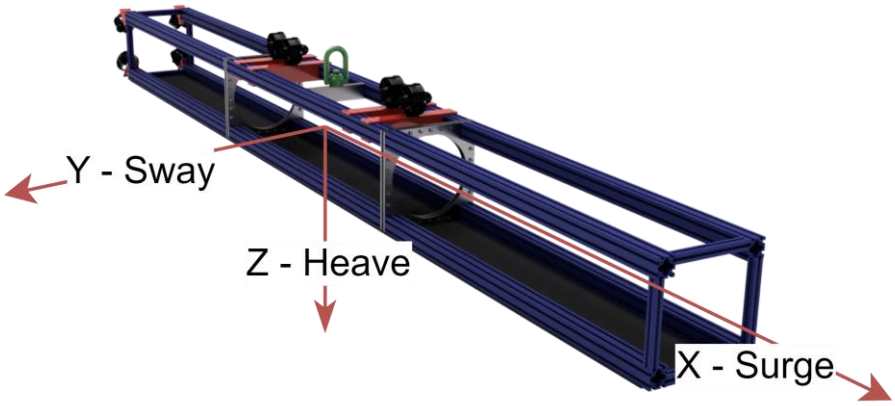

Figure 24: Underwater Vehicle Coordinate System

Measurements taken from the docking stations Inertial Measurement Unit (IMU) will follow the Inertial Frame coordinate system with the Z-axis downward. Motions in this coordinate system will follow the naming convention found in Figure 24. Measurements that are not taken in this coordinate frame will be transformed through standard coordinate transformations laid out by Kris Hauser from the University of Illinois (24). A known system that will need transformation will be the data from the OptiTrack motion capture system. With a standard setup, this system utilizes a Y-up coordinate system shown in the figure below.

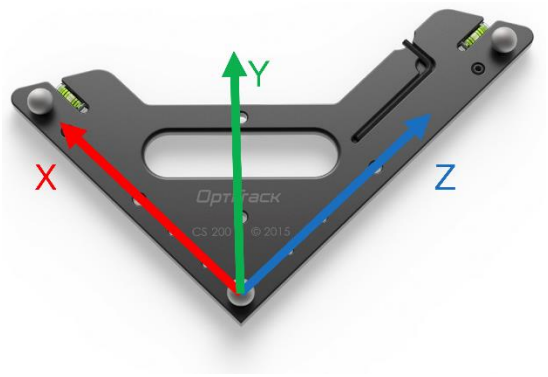

Figure 25: OptiTrack Ground Plate Coordinate System (25)

The figure above shows the ground plane calibration tool. This device allows the software to orientate the cameras and establish the coordinate system used for measurement. If this system cannot be adjusted in the software, the following rotation matrixes will be used to transform the data.

3D Rotation Matrix Base Form: $R = \begin{matrix} r_{11} & r_{12} & r_{13} \\ r_{21} & r_{22} & r_{23} \\ r_{31} & r_{32} & r_{33} \end{matrix}$ Equation 2

To rotate the Y-up coordinate frame to Z-down, one axis rotation will be needed. The first rotation will be 90 degrees around the X-axis.

$$R_x(90^\circ) = \begin{matrix} 1 & 0 & 0 \\ 0 & \cos(90^\circ) & -\sin(90^\circ) \\ 0 & \sin(90^\circ) & \cos(90^\circ) \end{matrix}$$ Equation 3

The resulting coordinate frame will follow the Z-down convention shown in Figure 24.

Additive Manufacturing Techniques:

This project utilizes various additive manufacturing techniques to develop the prototype model. Fused Deposition Modeling (FDM) was used to construct many mounting structures that interface with thrusters, sensors, and other equipment. These custom structures can be developed quickly and cheaply by implementing this form of additive manufacturing. The printing system utilized was the Prusa MK3, as this printer is highly reliable and capable of printing a wide range of materials. This system is set up to run a single filament type through one extruder. Parts were sliced with the Prusa Slicer software.

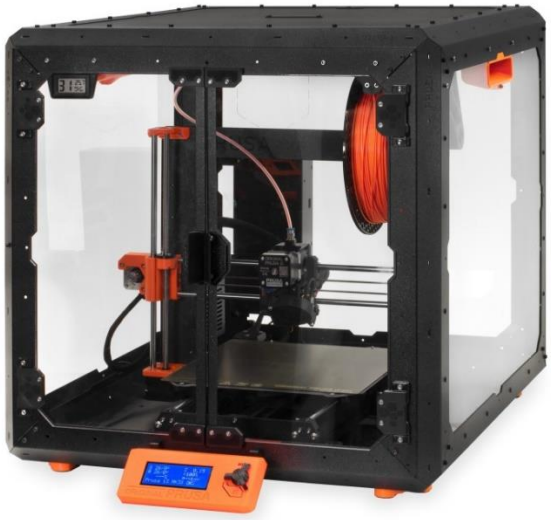

Figure 26: Prusa I3 (26)

Since the docking station will be used underwater, the final parts will be made of PETG filament with a large wall thickness to limit water absorption. All FDM parts that will hold structural loads will be printed at 100% infill.

MSLA will be utilized to create waterproof prints for many of the electronics that will support the function and testing of the docking station. Following the procedure and data in the paper “Stereolithography 3D Printed Resin Pressure Enclosures Applied in the Marine Environment,” pressure enclosures for different electronic sensors and hardware will be produced (27). The printer to be utilized for the pressure enclosures is the Anycubic Photon Mono X. This Masked Stereolithography (MSLA) printer is high resolution, and it has a 192 x 120 x 245 (mm) build volume (28). The Sryatec Sculpt Clear resin will be used to produce the pressure enclosures. This resin has been shown to be strong and capable of being used in an underwater environment (27).

Figure 27: Any Cubic Photon Mono X (28)

Waterproof pressure enclosures will be manufactured and sealed with O-rings following the procedures given by the Parker O-ring manual (29). In-water trials will be used before placing electronics in the enclosures for testing to validate the performance of the enclosures. This will ensure that the enclosures will not leak at the required operational testing depths. An example of these enclosures is shown in the figure below.

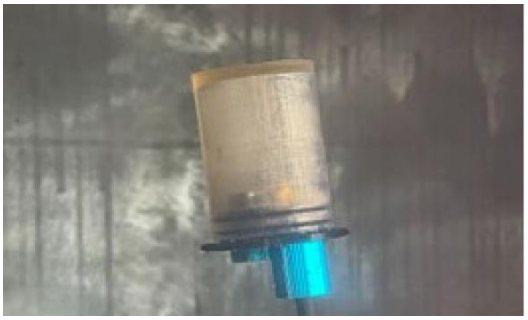

Figure 28: Example SLA Pressure Enclosure (27)

Chapter 2
Test & Evaluation Model Design

Unit Concept Overview

Based on the feedback and requirements from Carderock, the proposed design is a simple, rectangular frame with large open sections for attaching thrusters, electronics canisters, and sensors. To facilitate modularity, brackets for all the components will be 3D printed and clamped onto the frame to allow easy reconfiguration.

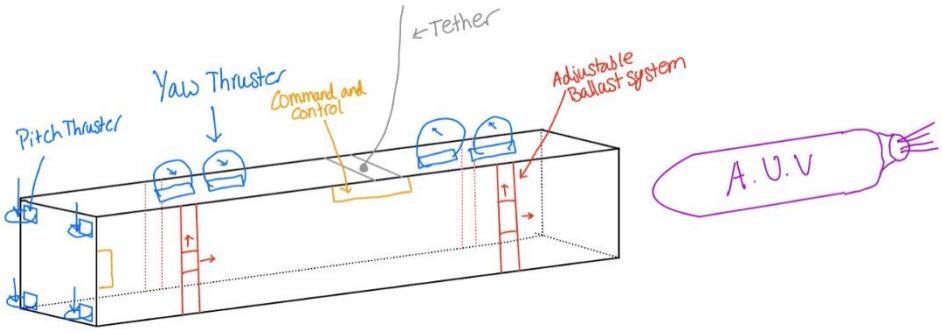

Figure 29: Hand Drawn Initial Concept

The main factors that will impact the system performance will be available thrust, thruster positioning, power, and unit weight. During testing, isolating how much thrust is needed to control the unit at a specific current speed will be valuable information for building a fully functional system. To do this, up to 8 thrusters will be supported by the unit. Each thruster will be able to run above the customer requirement of 8 lbf of thrust. The weight and balance of the unit will be adjusted by moving steel weights along the frame of the unit.

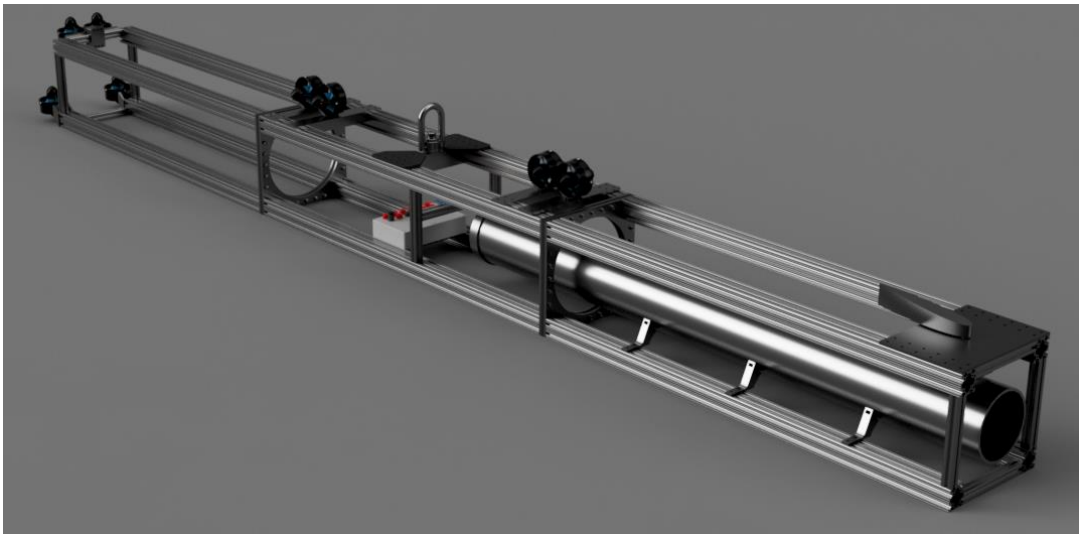

Figure 30: Test and Evaluation Model CAD Design

The figure above shows the design for the T&E unit. The frame is constructed from 2”x2” ¼” thick aluminum tube extrusion. Centered on the frame is a load-rated, universal joint lifting eye. This lifting point will allow the unit to freely move in pitch, yaw, and roll. The tube located forward simulates the size of a payload for the system. Located at the center of the vehicle is an IMU that measures pitch. At the front of the vehicle is the heading sensor, which uses current flow to measure the yaw angle. Located near the IMU is an underwater enclosure that houses the connections for sensors and motion capture lights. Surface power supplies power all of the thrusters to reduce the risk of electrical shock through the water.

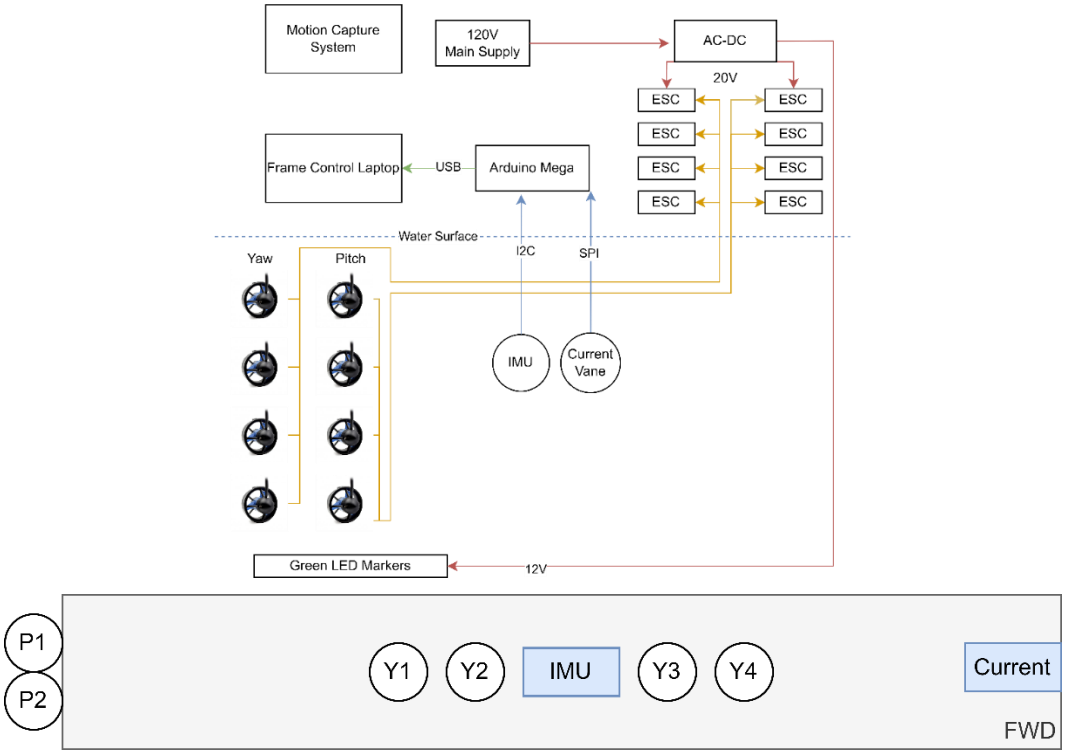

Figure 31: System Connection Diagram

The block diagram above depicts the system layout of the AUV docking device. The goal of the device is to be effective at testing what is being investigated, while remaining simple and economical to build. Many system components used were COTS, and those requiring customization were made using additive manufacturing techniques. The control system was hosted onboard an Arduino Mega R3. This board is a standard microcontroller with robust software and community support. The Arduino board will connect to the sensors and motor controllers. The test unit is controlled by a topside laptop connected through a USB to ethernet converter. On board the unit, the primary sensors are a 9DoF IMU and a current vane. The combination of these sensors will feed into the control loops for pitch and yaw. The system records data and uses it in the overall stability analysis. Also located on the unit are green, underwater LEDs; these provide visibility to the underwater motion capture system.

Mechanical Analysis

To meet the requirements set forth by NSWCCD, a module and strong test frame was needed. Due to the length requirement of 12ft, it was important that the model could be broken down into smaller sections for transport. Breaking the model into three sections introduced a possible point of failure in the frame. The areas shown in the figure below are the bulkheads where the sections meet. If this joint were not strong enough to support the weight of the test frame and additional ballast, the unit would be at risk of failure.

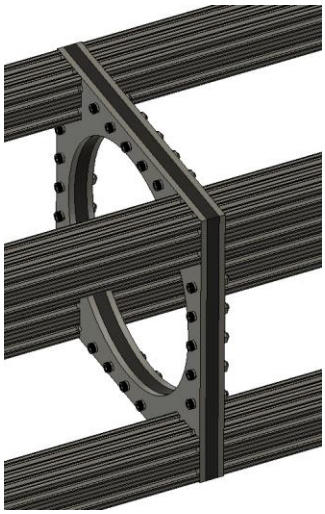

Figure 32: Section Bulkhead

Finite Element Analysis (FEA) was completed to ensure that the bulkhead would be suitable for use and not fail. For the analysis, the bulkhead was simplified to be just the ¼" aluminum plate. On the aluminum plate, the center bolts were fixed, and loads were applied to the corners where the frame would be pulled. A load of 200 lbs was applied in tension for the top corners of the aluminum plate. This load would represent the maximum possible load applied to the section.

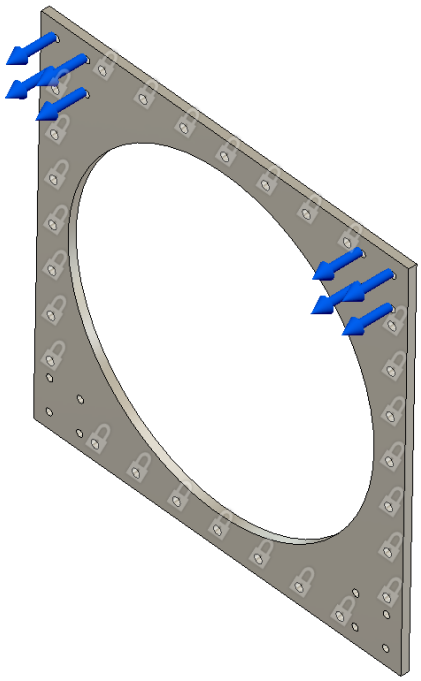

Figure 33: Bulkhead FEA Setup

The FEA setup above was created inside of Fusion 360. Fusion 360 is a free-to-students Computer Aided Design (CAD) software created by Autodesk. The FEA tools inside Fusion 360, utilize the Nastran FEA solver. The diagram from the figure above is converted into constraints, loads, and materials inside of Fusion 360. This model was then solved, and the following output was produced.

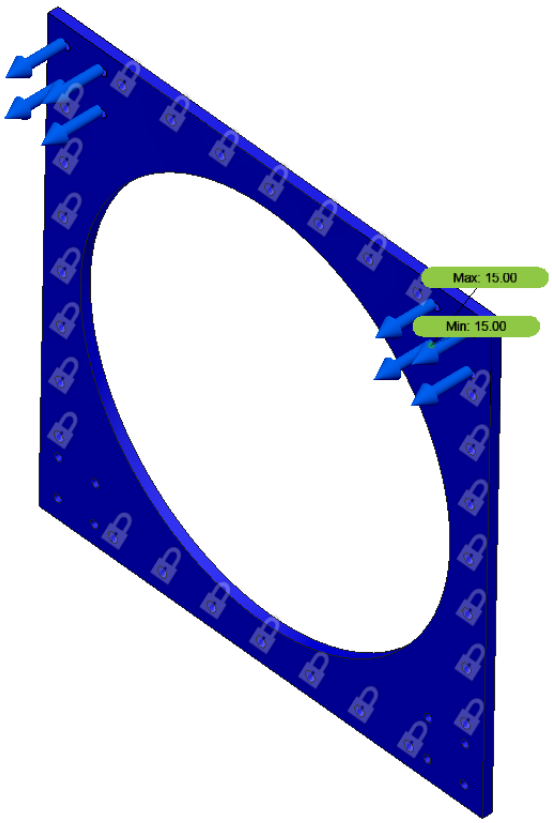

Figure 34: FEA Bulkhead Safety Factor Result

The figure above shows the result of solving the FEA. Shown is a visual representation of the safety factor. The safety factor for the entire plate is above eight, indicating it will not yield and cause failure. The safety factor was not the only metric examined, however. The total deflection of the plate was also significant; if it deflected too much, the frame would no longer be straight and could cause adverse effects.

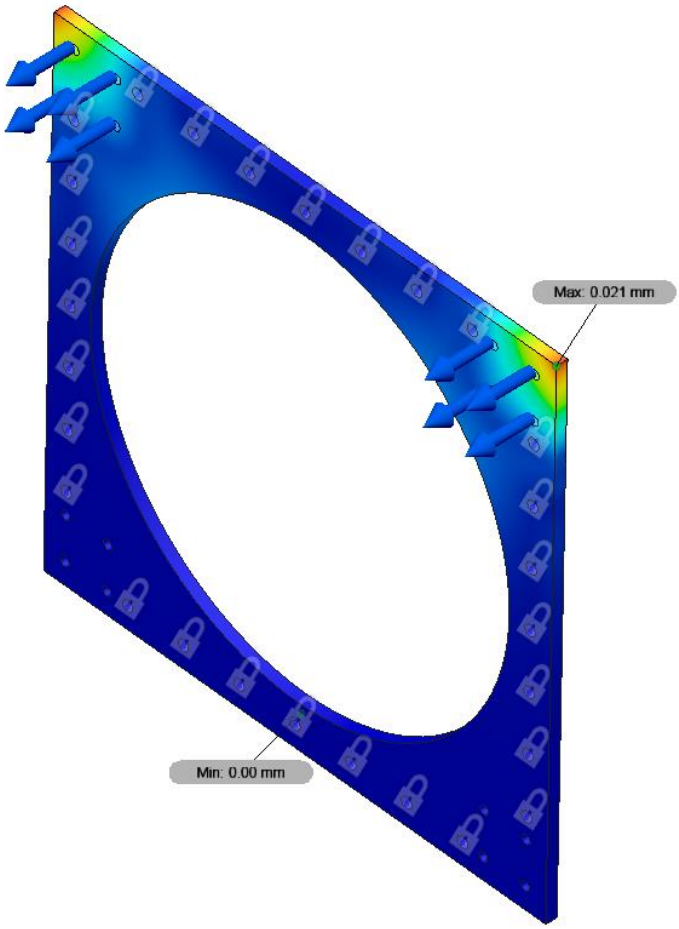

Figure 35: Bulkhead FEA Total Defections

The figure above shows the deflection of the aluminum plate when placed under the given load. The maximum deflection observed was 0.021 mm. This is a low amount of deflection and should not interfere with the unit's operation.

The next critical mechanical section is the lift point connection for the test frame. A swivel hoist ring was used to support the load of the frame and allow for pitch and rotation. The swivel hoist ring allowed the test frame to move freely, but a strong single mount point location was required. The connection of the hoist ring to the test frame is shown below.

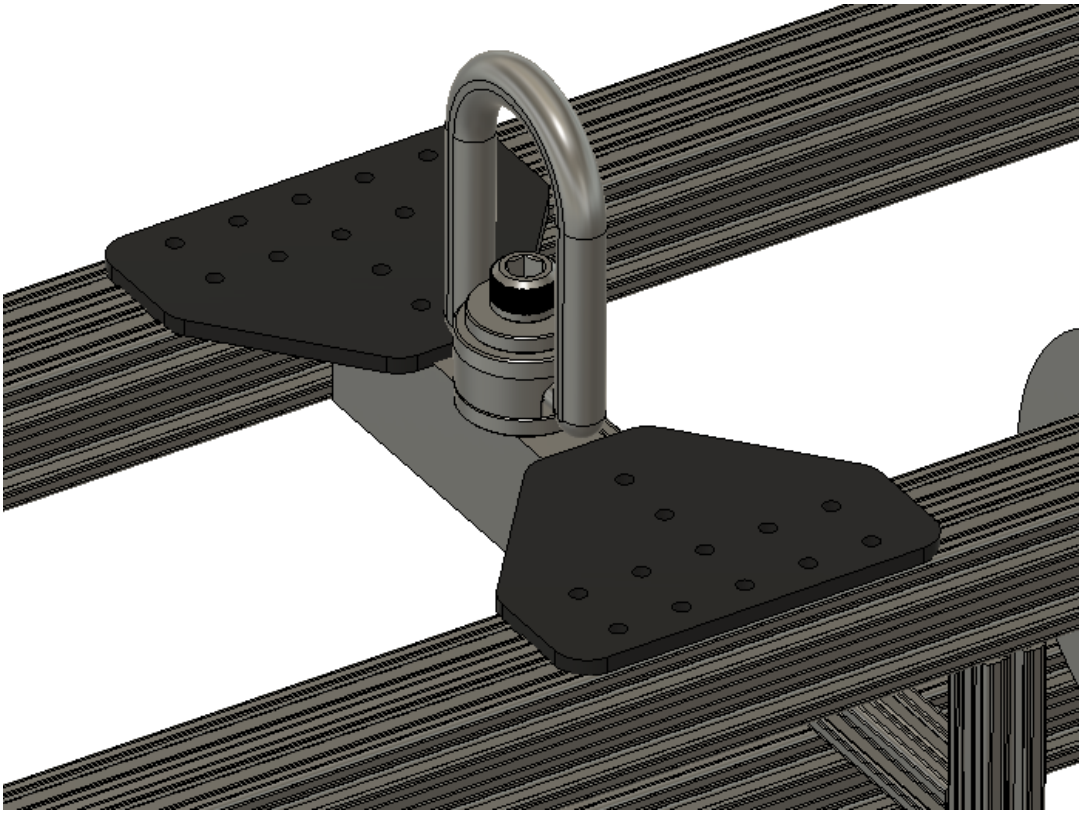

Figure 36: Swivel Hoist Ring

In the figure above, the main support holding the steel bar and hoist ring into place is held into place with large aluminum plates. These large aluminum plates are the weak link in the lifting system. Like the bulkhead section, FEA was completed to check if the plates would yield or deflect. To do this, a section at the top of the test frame model was isolated. The aluminum extrusion bars were simplified to square tubes and fixed into place on the ends. A load of 300 lbs was applied to the hoist ring to represent a maximum load case. The results of the FEA solve are shown in the figures below.

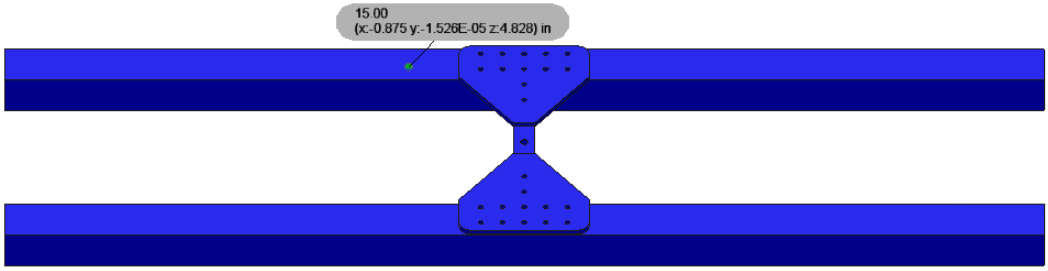

Figure 37: Lift Point Safety Factor

The results for the safety factor show a minimum safety factor of 15. This indicates the aluminum plates and steel bar would not yield.

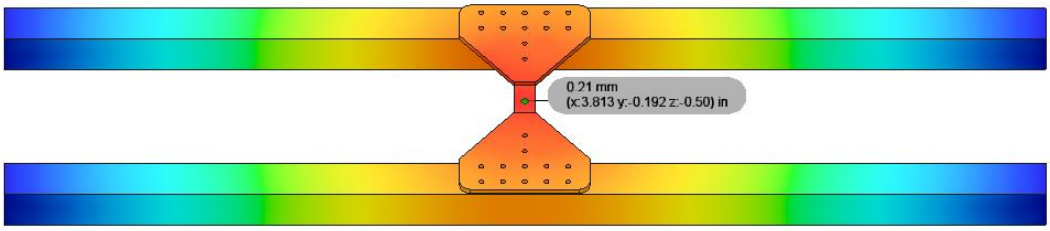

Figure 38: Lift Point Total Deflection

The total deflection at the lifting point was 0.21mm. This was a small deflection compared to the total length of the frame rails. This small deflection would not cause adverse effects during the unit testing.

Overall, the mechanical analysis for the test system revealed that the section design would not weaken the strength of the frame and that the lift point would be strong enough for lifting and testing. This step of the design process was critical to ensure the test unit would perform as expected and not suffer any debilitating mechanical failures.

Yaw Sensor

When operating from a ship in open water, a full suite of sensors will be available to track the position of the unit. A Doppler Velocity Logger (DVL) and Inertial Navigation System (INS) can be used to have an accurate measurement for the heading and location of underwater systems (34). Implementing a DVL and INS is impractical for this system due to cost and development effort. To supply the model with accurate heading information, a different method needs to be implemented. The solution utilized is a current vane that will measure the offset between the device and the current. Since the CWC creates a uniform current flow, the difference in angle will be the yaw angle of the device.

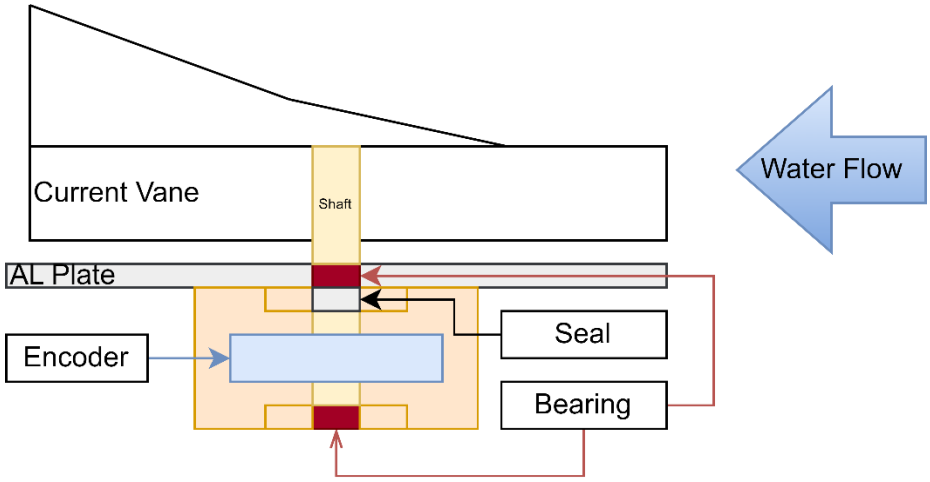

Figure 39: Yaw Sensor Sketch

A detailed model for the current sensor was developed from the above concept. To decrease the manufacturing time, a pre-made aluminum enclosure from Bud Industries (37) was used to protect the encoder. A hole was drilled into the top of the case, and a 3D-printed flange was used to seal the shaft entering the case. This assembly was then bolted to the bottom of the current plate via a 3D-printed mount.

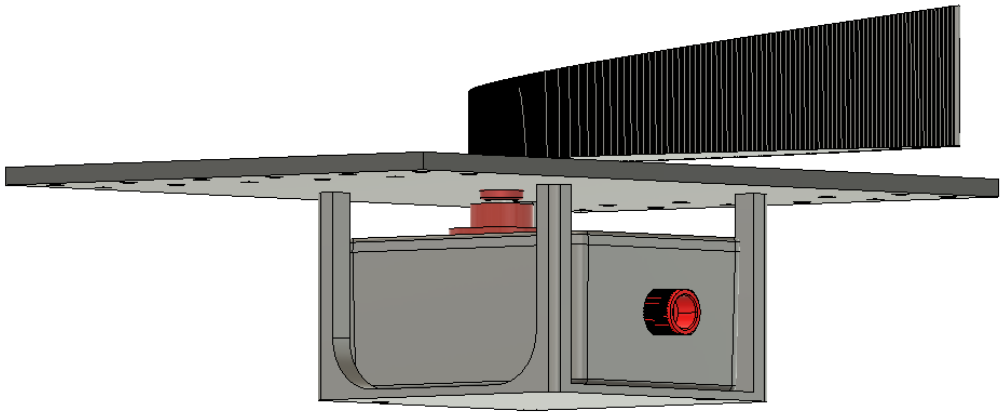

Figure 40: Yaw Sensor CAD Design

Dual bearings were used to support the shaft in connecting the current vane to the encoder. Bearings located inside the top plate and at the bottom of the sensor housing provide support for the shaft. Supporting the shaft minimizes deflection while under load, which ensures the integrity of the O-ring shaft seal. The O-ring seal was designed in accordance with the Parker O-Ring handbook (29). The O-ring groove profile and support bearings can be seen in the section analysis located below.

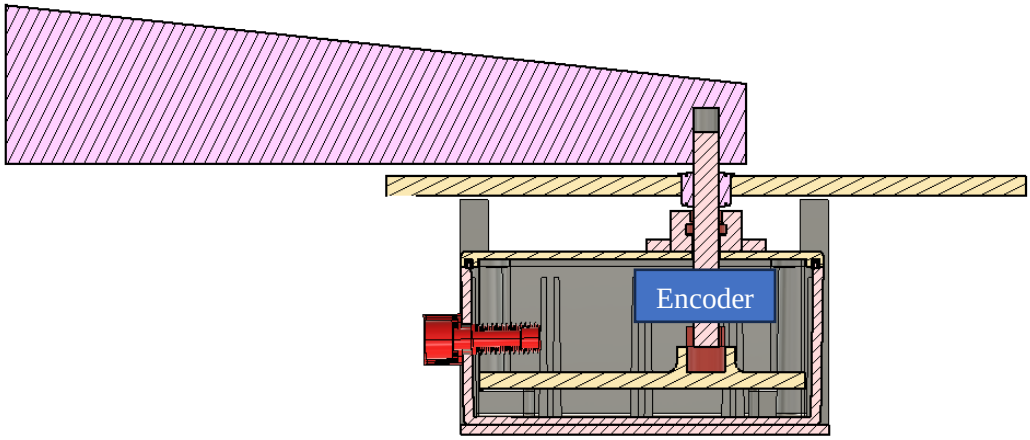

Figure 41: Current Vane Section View

The encoder used in this sensor was the AMT22 from CUI Devices. This encoder has a 16-bit resolution, which allows it to measure angular change of 0.2 degrees (38). The encoder was connected to the control setup through an SPI connection.

An SPI connection is a synchronous data bus, which uses separate lines for data and a clock signal. This aims to keep both the host and peripheral in sync. The clock signal lets the host controller know when to sample the data line. An SPI connection is great for connections that require time synchronization and a robust connection between the host and peripheral. The SPI connection utilizes the following pins to communicate with the Arduino (39).

MISO – Master In Slave Out – Pin where the Arduino sends output when acting as the controller

MOSI – Master Out Slave In – Pin where the sensor sends output when acting as the peripheral

CS – Chip Select – This pin tells the peripheral when to wake and begin transmitting on the data lines. Since this research only uses a single SPI connection, the CS line will be set statically.

Pitch Sensor

An IMU was placed at the model's center to measure the testing model's pitch angle. When located here, the IMU can measure the pitch angle of the vehicle and report this to the controller as Euler angles. Euler angles are used to describe the rotation of a body with respect to a fixed coordinate frame (40). The IMU connects to the Arduino through an Inter-Integrated Circuit (I2C), a communication method known for its simplicity and ease of integration. The I2C connection, consisting of two signals, Serial Data (SDA) and Serial Clock (SCL), is controlled by the bus controller (41). These two lines allow peripherals to communicate with the host with just two wire connections, simplifying the integration process. Data is transmitted by pulling the clock line high and then pulling SDA to low. The address of the sensor is sent then, followed by data. The host device reads the address and data, making the system's integration straightforward.

The pitch sensor was housed in an underwater housing made by Bud Industries. Inside the housing was a 3D-printed bracket to hold the IMU in place. An additional mount was created to adjust the enclosure's position on the testing model. This mount was easily removable and allowed for sensor calibration before final system testing. Below, a cross-section view shows the components of the pitch sensor.

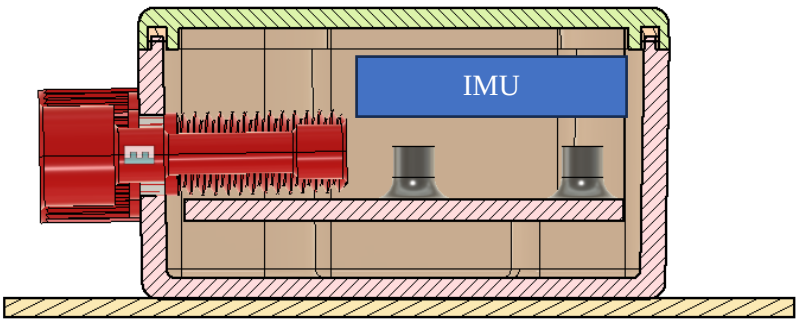

Figure 42: Pitch Sensor Section Analysis

Model Power Setup

To support extended testing efforts required for this test, where the unit may be in the water for 4-6 hours, powering the unit through batteries would not be a realistic or cost-effective solution. Additionally, batteries in the CWC workspace need special permissions to ensure environmental safety. To work around these issues, a surface power-supplied unit was required. Due to safety concerns from Carderock, the power supplies used to run the test frame must be located above the waterline so no 120V AC power goes into the CWC testing basin. Following this requirement will ensure that those supporting the test are not at risk for fatal electric shock.

To calculate the surface power needed to run the system at the required capacity, thruster performance tables from blue robotics were used to identify maximum current draws.

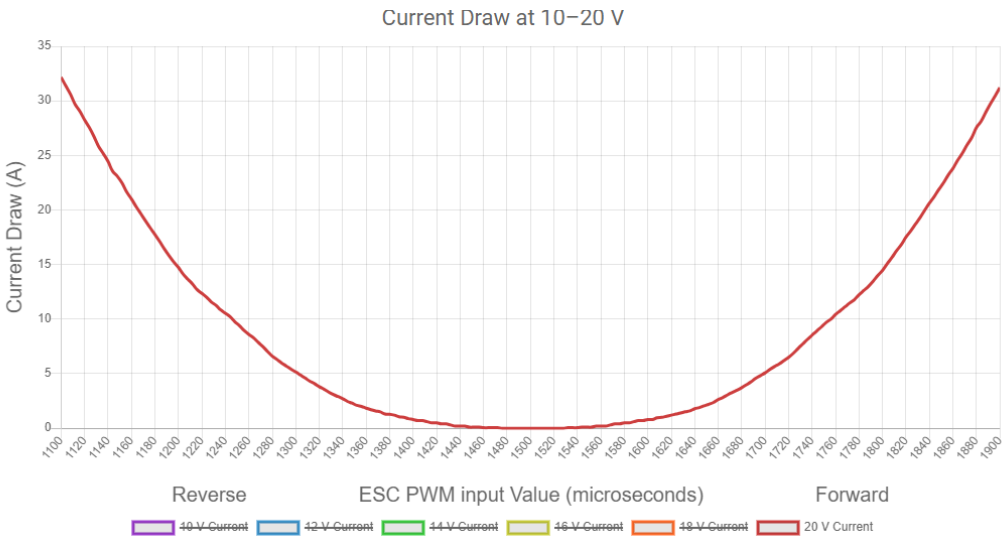

Figure 43: Blue Robotics Thruster Power Curve (42)

Based on the system's thrust requirements, the unit must have 2000w of 20v DC power available, which will be split between the thrusters and the control system. This powering specification will allow the unit to exceed the thrust requirement of each motor, giving ample room to ramp the thrusters up and down to test different power configuration setups.

Power supply selection required balancing power demands, cost, and simplicity. While a single or dual power supply setup would result in a small topside and less wiring, implementing this equipment would have been more costly than using multiple lower-capacity power supplies. The following table compares the difference between a 2 and 8 power supply setup.

Table 1: Power Supply Comparison

	2 Power Supplies	**8 Power Supplies**
Individual Power	1000w	400w
Total Power	2000w	3200w
Price	$500	$312

Due to the difference in cost, the eight individual power supply option was selected. The power supply used for this research was the Dork 24V 480W (43). This unit features user-settable voltage from 0V-24V with a maximum current 20 amps. Blue Robotics' basic Electronic Speed Controller (ESC) are connected to each power supply. The basic ESC can drive brushless motors up to a maximum power of 780W (44).

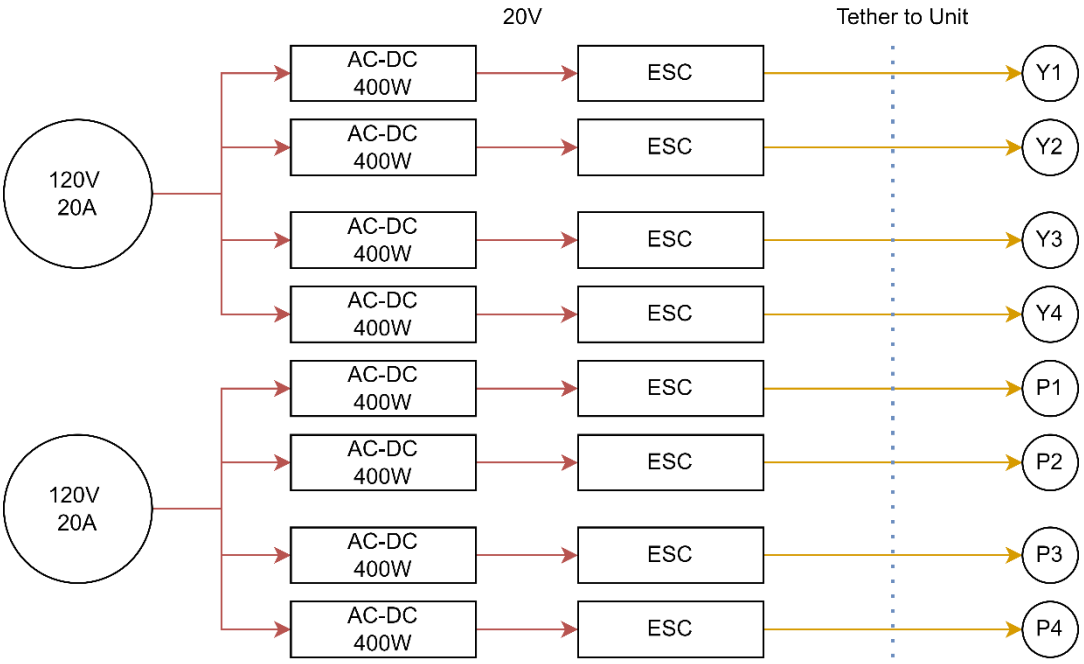

Figure 44: Power Distribution Setup

The power setup locates AC-DC power supplies above the waterline along with corresponding motor controllers. The output from the motor controllers will be passed down to the test frame. The positioning of the power supplies above the water is needed to ensure safety during testing. Heavy gauge tri-plex wire connects the power supplies and motor controllers to the test frame. Each tri-plex wire is rated for 60amps of current throughput. While this current rating is far higher than what was required for an individual thruster, the larger AWG wire was needed to reduce voltage loss over the wire run. The diagram below shows how the wires run from the test frame to the support board.

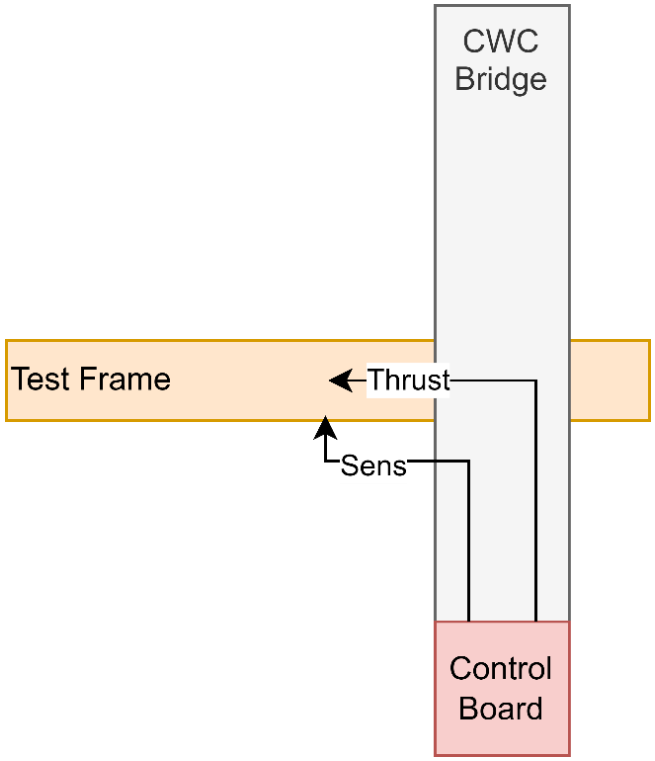

Figure 45: Tether Connection Cable Runs

Wires connecting to each thruster were 25ft long. The following calculations were used to find voltage loss for 12AWG wires carrying the output from the Blue Robotics' basic ESC.

$$V_{drop} = \sqrt{3} * \ I_{wire}(A) * R_{wire}(\Omega) = 1.732 * 20A * 0.0397(\Omega) = \mathbf{1.3V}$$

Based on the calculations above, it is shown that the power setup for this test did not limit the system's performance. At the maximum power loss of 6%, the unit can still output a thrust of 8lbs from each thruster.

Model Tether Setup

Several different options exist to connect the unit to the surface laptop. The conventional technique for ROVs is to use a network interface that can link the ROV and topside via a differential signal like ethernet (31). While this technique allows for communication up to 100m, a more cost-effective method can be used for this testing. This method utilizes COTS Universal Serial Bus (USB to ethernet adapters); these devices are driverless and are not seen by the host computer or Arduino. This allows Simulink to connect directly to the Arduino located on the unit. This method of connection is suitable for applications less than 50m (32).

Figure 46: USB - Ethernet Adapters (32)

A structural tether is required to secure the docking unit to the surface and suspend its weight in the water. This tether must be able to support the maximum wet weight of the unit, 200 lbs. The tether selected was a wire cable with a ¼” diameter. This cable had a working load of 300 lbs, which was greater than the vehicle's maximum weight. The wire cable held the weight of the unit during testing.

To connect the sensors and onboard motion capture LEDs to the topside power board, dual CAT 6 ethernet cables were repurposed. The conductors of the cables were wired according to the following wiring table. For the motion capture system, dual wire pairs were used to increase the maximum current the lighting system could carry. To limit noise that may be induced by the high-powered thrusters, shielded cables were used to connect the testing unit. The cable chosen was flexible for ease of rigging but also tough to limit the risk of a hole being punctured into the jacket. The wiring and cable setup for this research provided a strong, yet cost effective strategy for connecting an underwater vehicle to the surface.

Table 2: Primary Wire Configuration

Pin	**Wire Color**	**Function**
1	Green – White	Sensor Power (+)
2	Green	Sensor Power (-)
3	Blue - White	SDA
4	Blue	SCL
5	White - Orange	Chip Select
6	Orange	MISO
7	Brown – White	MOSI
8	Brown	SCLK

Motion Capture Integration

When designing the motion capture system for this testing model, a key feature was the type of green light that would be attached to the system. To support the motion capture system, the green light needed to be bright and rated for underwater use. After searching through COTS databases, the green light from FXC was chosen for its luminosity, cost, and simple mounting method. This green light was tested in a pool prior to installation on the testing frame. The purpose of this pool test was to evaluate the brightness of the light in a gray-scale image. The images below are from the pool test.

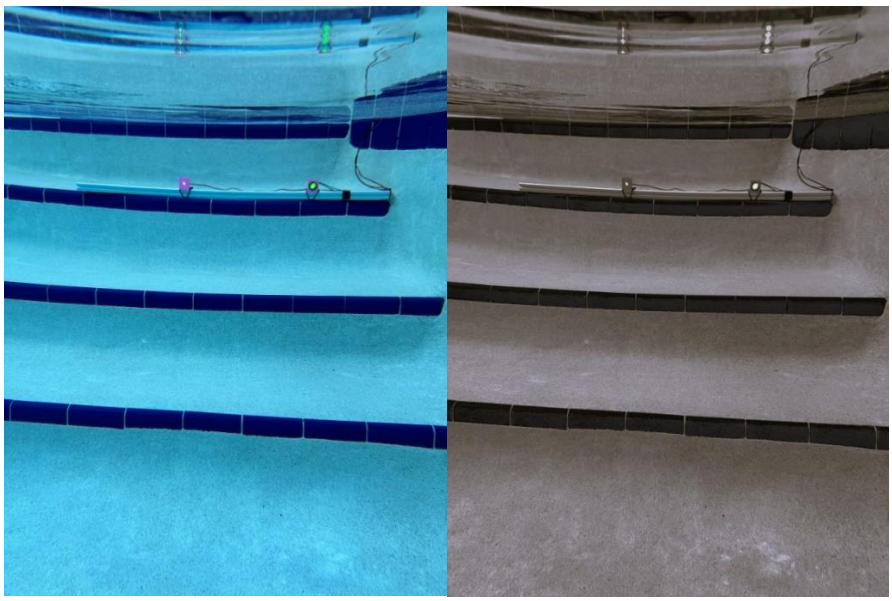

Figure 47: Motion Capture Light Test

The gray-scale images above show the LED on the right side of the bar as being the brightest. This hot spot shown on the gray-scale image indicates the motion capture system will be able to identify each marker well.

Mounting the markers was accomplished with 3D-printed L brackets. The light had a rubber sleeve that fit inside the L bracket, securing it into place, as shown in the section view below.

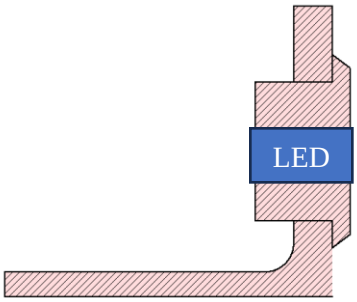

Figure 48: Marker Bracket Section View

The placement of the markers onboard the testing unit was aimed at being asymmetric. To allow the cameras to resolve the position of the rigid body better, markers should be placed with little symmetry, which could allow for an incorrect position to be resolved. Markers were more concentrated toward the rear of the unit as the rear section would be closer to the cameras. The distributions of markers along the body followed the count shown in the diagram below.

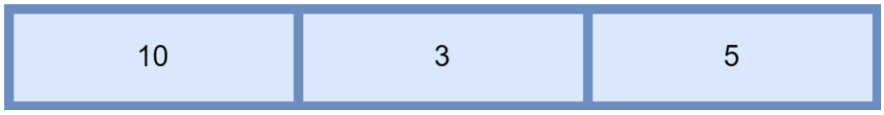

Figure 49: Motion Capture Marker Count

Based on the vehicle's geometry, there will be differences in levels of accuracy between different measurements of the marker's position. The motion capture is more accurate when the separation between markers increases. Due to the unit's 12ft length, the measurements of yaw and pitch will be very accurate. Roll measurements will be the least accurate as the distance between markers in this position is the smallest.

The motion capture lights were strategically wired into light strings, allowing for their distribution along the frame in various directions. This thoughtful design ensured that the motion capture lights were connected inside the electrical distribution box, conveniently located near the center of the testing unit.

Chapter 3
Test & Evaluation Model Building

Frame Construction

The assembly of the test frame was completed using a variety of hand- and computer-controlled tools. Building and assembly of the unit followed the order described below.

Materials for this project were procured and cut using a combination of tools. The aluminum extrusions were cut using a horizontal band saw. The horizontal band saw is a very effective tool for cutting bar stock.

Figure 50: Horizontal Band Saw Cutting Frame Components

The next major component that needed to be cut was the plates for the bulkhead section connections. These plates were cut and drilled using a combination of the water jet and a hand drill. Due to the plates' size, the water jet could not cut the holes along the outside edges of the connection plates. These outside holes were drilled using a template and match drilling. The center hole that allowed the payload tube to pass through was cut using the water jet. The following diagram shows the areas cut by the water jet and those drilled by hand.

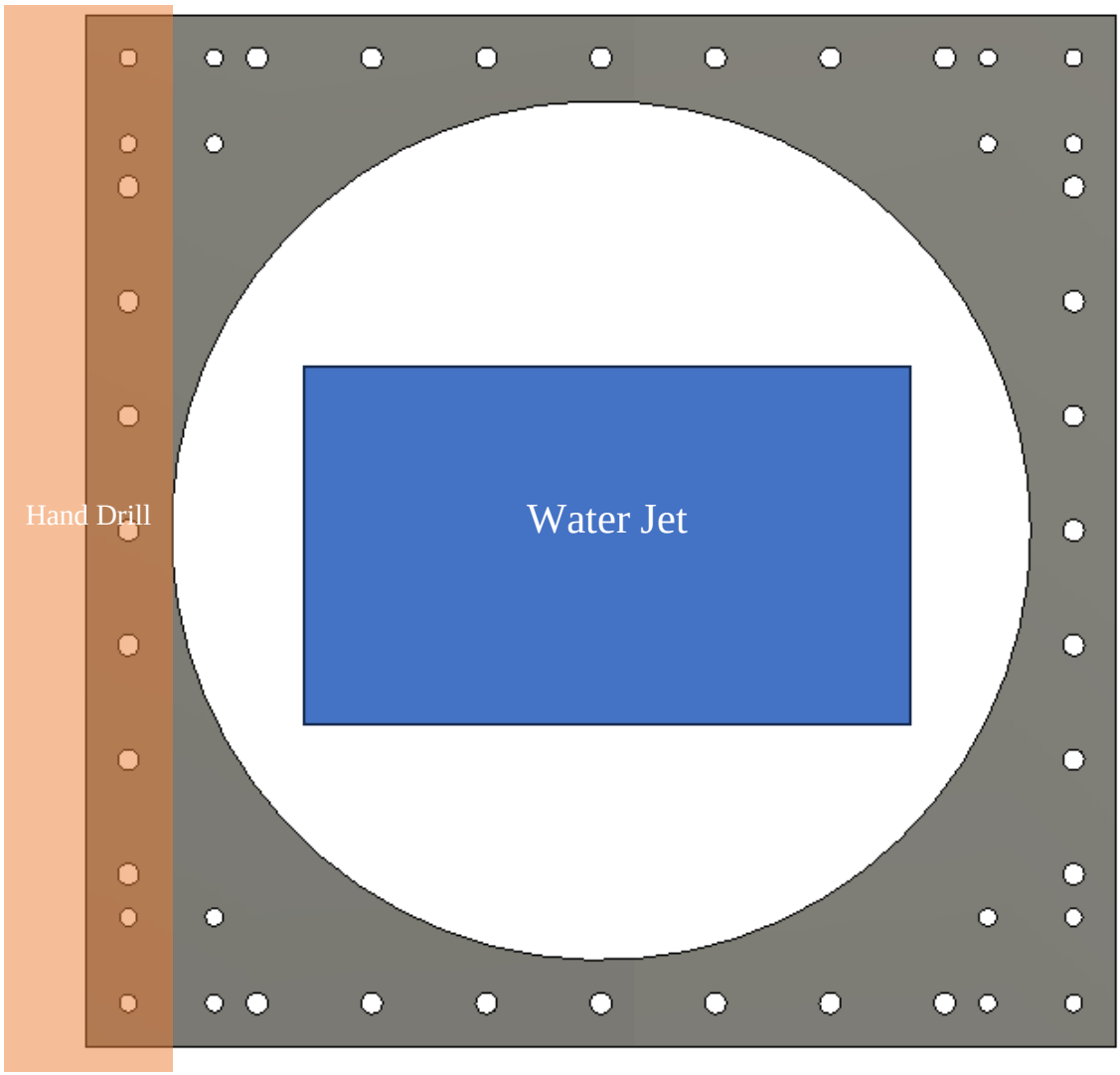

Figure 51: Bulkhead Plate Drill Areas

With all the frame sections and connection plates cut, the test frame could be bolted together and assembled. Assembly was aided by using drop-in slider brackets in the aluminum extrusion. These slide-in mounts allowed for additional support and hardware to be located anywhere along the extrusion. This construction method facilitated the quick initial assembly of the test frame, as shown in the figure below.

Figure 52: Initial Frame Assembly

After the initial assembly of the test frame, the next step was to fabricate the lifting point section. This section had to be manufactured with extra care as it would support the entire weight of the unit while lifting and testing. The lifting point was tapped into steel bar stock and secured to the test frame with aluminum plates.

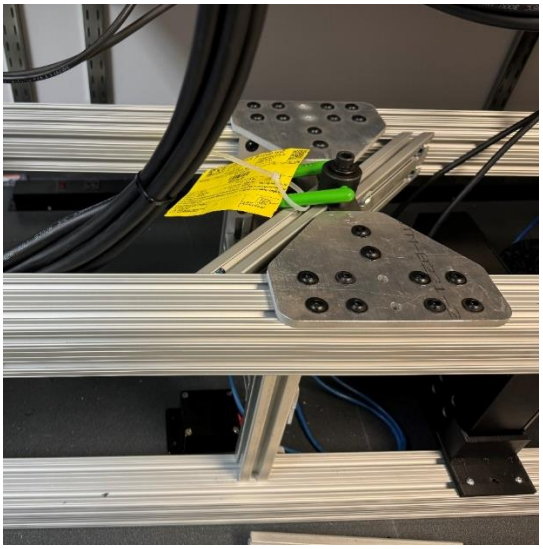

Figure 53: Lift Point

After the lift point was installed, the payload tube was installed in the front section. The payload tube was constructed from a 6” PVC pipe and secured onto the unit with hose clamps. The figure below shows the installed payload tube.

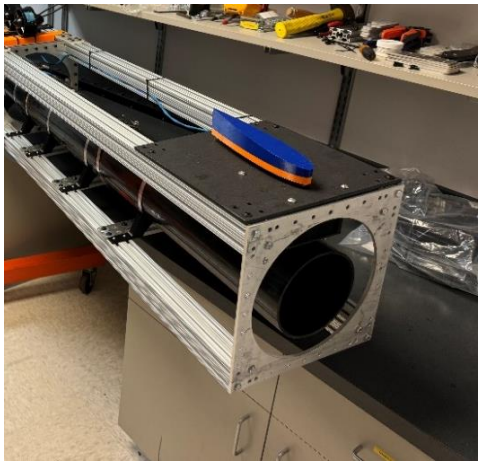

Figure 54: Payload Tube

The final step in the mechanical assembly for the unit was to hang it with an engine hoist to ensure it was secure and stable, along with gathering an initial dry weight of the frame.

Figure 55: Test Frame Hang Test

The hang test proved the lifting point was secure, and the test frame had an initial dry weight of 130 lbs. Additional ballast weight would need to be added during testing at NSWCCD. The fully assembled lift test represents the conclusion of the mechanical frame assembly.

Additive Manufactured Components

To support the fast construction of the test frame, many parts that would have been difficult to machine were manufactured with 3D printing. 3D printing was used in almost every area of the test frame. Thruster mounts, sensor components, and cable molds were manufactured using the Prusa Mk3, as described in the introduction section of this research. Below, the process for creating several vital components will be examined in detail.

Thruster mounts were a major component built with 3D printing. The figure below shows the slicing setup for a pitch thruster mount.

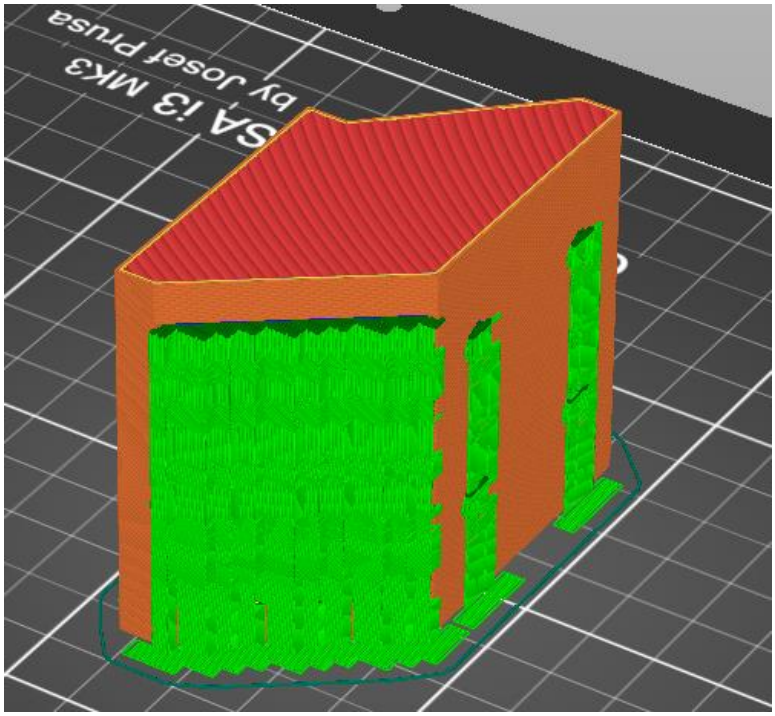

Figure 56: Pitch Mount 3D printing setup

All 3D-printed parts were printed in an orientation that would be best for their load case. For the pitch mount, the layer lines run perpendicular to the direction of the load. This makes the part less likely to split and fail when under load. This process of orientating the load lines was completed for each of the 3D-printed parts support loads.

Another group of printed parts were brackets and supports for the sensors located on the test frame. For the yaw sensor, a plate was printed to mount the IMU and bear it inside the waterproof case. The setup for this part is seen in the figure below.

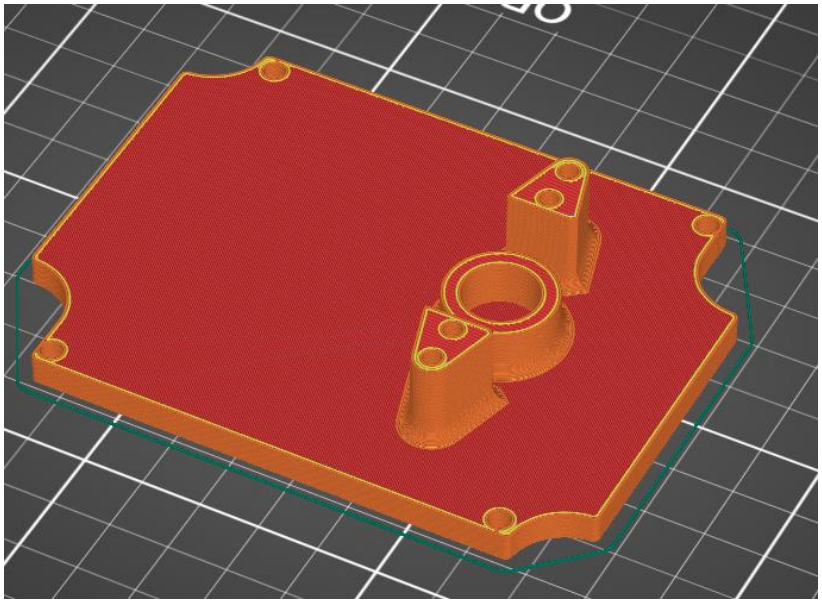

Figure 57: Encoder Mount

A critical parameter for the encoder mount and other sensor mounting parts was the hole and part size tolerances. If the holes were sized incorrectly, the encoder would not interface correctly or be misaligned. To correct for tolerance issues, the parts were printed, and then the printed dimensions were measured and compared to CAD. If the dimensions were incorrect, an offset would be applied in CAD to result in a part with the desired dimensions.

To support sealing the shaft on the yaw sensor, an Oring collar had to be produced. Since this part needed to stop water intrusion into the case, it needed to be printed using MSLA. MSLA printers can create solid parts that are not penetrable by water. The process followed for printing with MSLA is found in the introduction section of this research. The Oring collar was first created in CAD using the specifications in the Parker Oring Manual (29). The figure below shows a cross-section of the Oring collar.

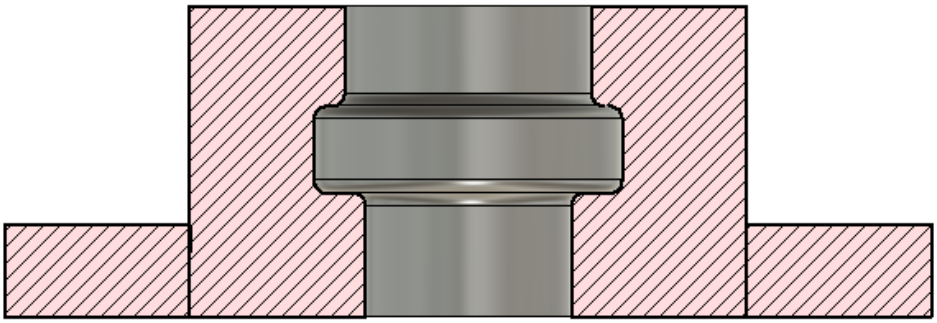

Figure 58: Oring Flange Cross Section

In printing this part, it was critical that the Oring cut-out was dimensionally correct within the tolerances given by the handbook. Like the FDM printed parts, an initial print was completed, and tolerances were adjusted through CAD. The result was an MSLA part, which an Oring was installed into. The part passed a vacuum check, which stressed the shaft Oring gland. Utilizing 3D printing for this part decreased manufacturing time and allowed for quick modification compared to making it on a lathe by hand.

Overall, 3D printing was critical to the assembly and function of the test frame. Many 3D printed parts were created, modified, and installed onto the frame. Since 3D printed parts can often be brittle and susceptible to drops or impacts, spare parts for every 3D printed part were made before transport to NSWCCD. This ensured that if any parts were to break, a spare would be ready to install to keep the testing going.

Electronic Assembly

The first step in creating the electrical system for the test frame was to prepare the thrusters. The thrusters used had short 18” power leads. These leads needed to be extended to larger, longer wires for connection to the surface. To do this, a cable mold was created. The cable mold was a 3D printed block that adapted the smaller thruster power wire to the larger tether wire. The block was then filled with adhesive to waterproof and strengthen the connection.

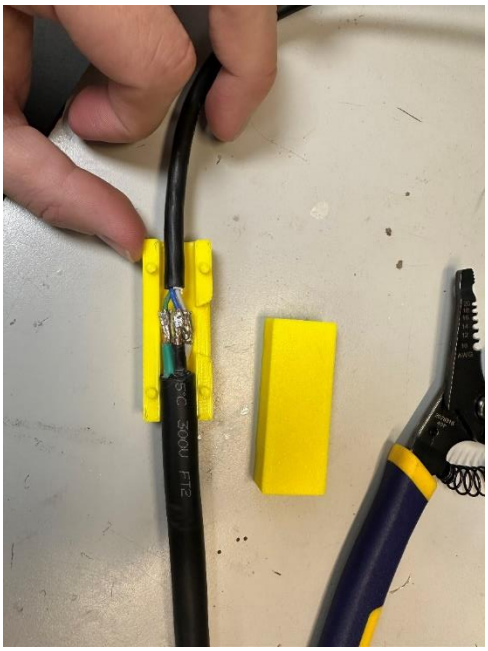

Figure 59: Thruster Cable Mold

The figure above shows the cables soldered together prior to potting. Before inserting the adhesive, it was important to ensure no solder connections were touching and test the operation of the thruster. After each of the eight thrusters were prepared, they were filled with adhesive during one mix-and-pour operation, as shown in the following figure.

Figure 60: Thruster Potting

After potting, the thrusters were retested before installation onto the test frame. All thrusters passed testing, and each cable mold was well sealed for underwater use.

The primary electrical component of the test frame is the surface control board. The surface control board needed to have space for the power supplies, motor controllers, and microcontrollers. A large sheet of finished wood was used as a backing plate for all the components. Initial assembly of the board included mounting the core components.

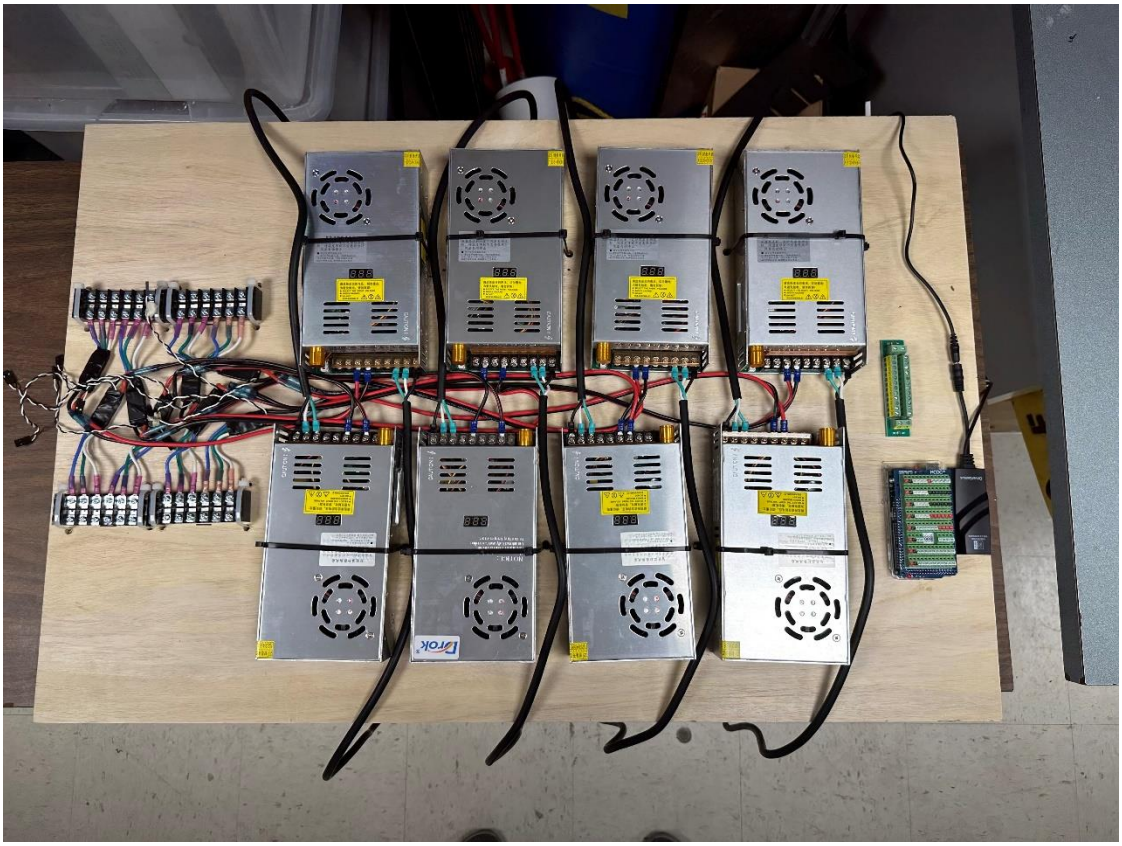

Figure 61: Core Components of Surface Control Board

In the figure above, the core components are installed on the backing board. The power supplies are each directly connected to a motor controller. The motor controllers are connected to screw terminals for easy connection to the thruster cables. The Arduino microcontroller and USB-to-ethernet converter are on the board's right side.

Additional equipment was installed to fully support the test frame's function, including sensor and motion capture light connections. The figure below shows the final configuration of the electronics board with callouts for the major components.

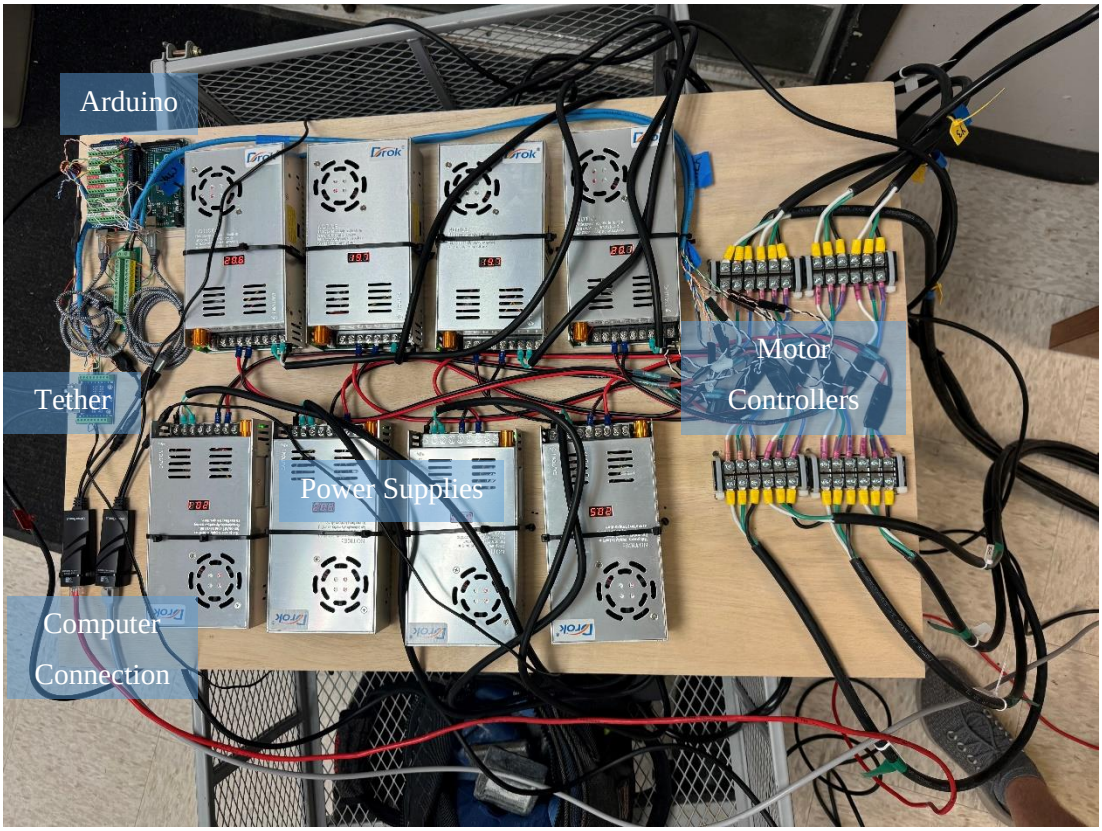

Figure 62: Final Control Board Setup Connected for Testing

Three different modules had to be constructed for use onboard the test frame. The central distribution box connected the sensors and motion capture lights to the model tethers. This box was made using a NEMA 6P-rated aluminum enclosure. These NEMA 6P enclosures are rated from the factory for continuous exposure at 6ft. Additional depth validation was completed at the Florida Tech Port Canaveral test site. A NEMA 6P enclosure was left in 15ft of water for five days. This test validated the performance of the enclosures and ensured they would not leak during testing at NSWCCD.

Figure 63: NEMA 6P Enclosure Sealed for Exposure Testing

Figure 64: NEMA 6P Enclosure Deployed at 15ft

After testing of the enclosure revealed no leaks over the 5-day exposure period, the hardware for connecting the sensors and motion capture lights was installed.

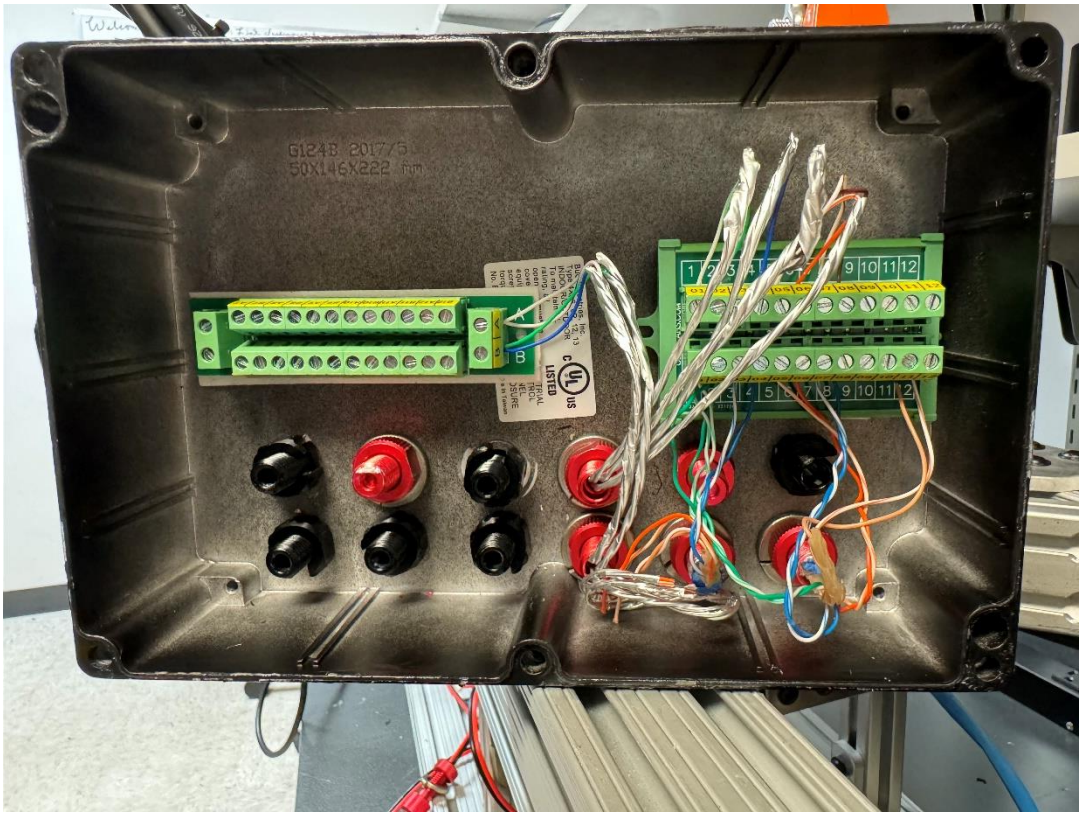

Figure 65: Test Frame Electrical Distribution Box

In the figure above, the components inside the distribution box can be seen. On the left side of the box, a screw terminal distribution strip is used to connect all the motion capture lights to the power leads in the model tethers. On the right-hand side is another screw terminal, but it is set up as a pass-through to connect the tether to the yaw and pitch sensor. Setting up the sensors through this screw terminal block allowed for easy wire reconfigurations and uninstalling of systems.

The pitch sensor was assembled into its NEMA 6P case using a 3D printed mount and connection wires. The sensor was connected with removal wire connections, so if a new IMU needed to be installed or tested, it could be simply swapped in. The figure below shows the IMU installed into the case.

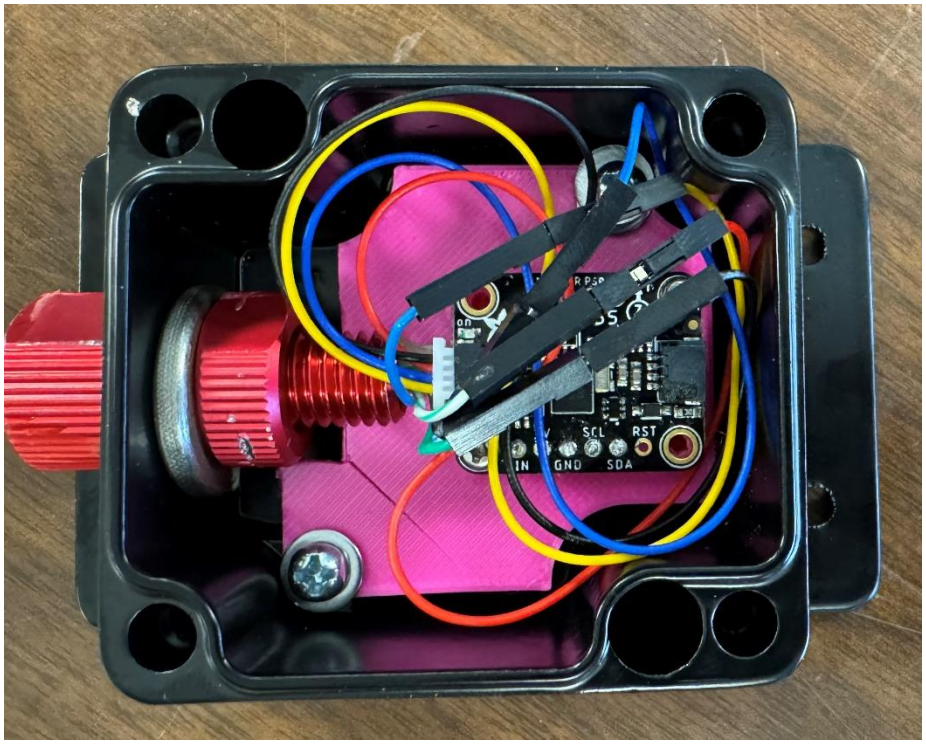

Figure 66: Assembled IMU Pitch Sensor

The final assembly of the yaw sensor included gluing the Oring collar into place. To find the correct alignment for the Oring collar, the encoder was first installed into the 3D printed bracket and case. Then, the shaft and Oring collar were set into place and glued. Installing the encoder allowed the alignment to be checked as the glue set. Aligning the shaft well with the encoder reduced friction and allowed the sensor to be more responsive to yaw motion. The figure below shows the Oring collar glued into place.

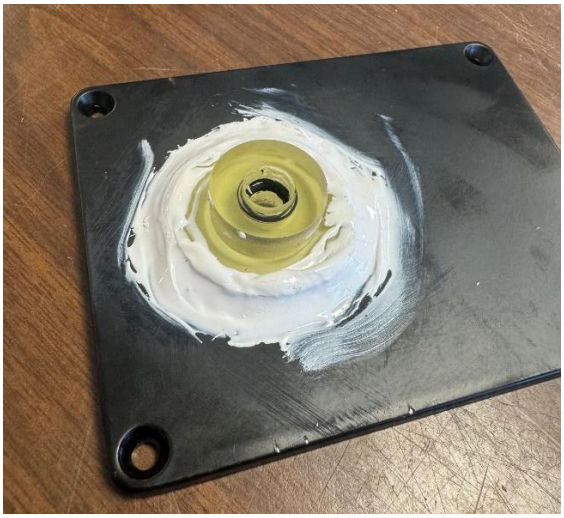

Figure 67: Glued Oring Collar

With the encoder mounted and collar glued into place the wiring of the enclosure could be completed. Similar to the pitch sensor, connectors were used for the sensor to make swapping out the encoder easy. The final yaw sensor enclosure is shown below.

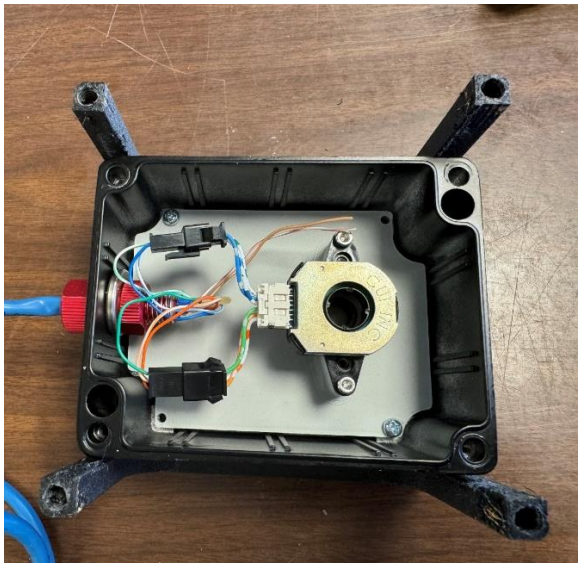

Figure 68: Yaw Sensor

Final Assembly

After all the system components were assembled and finalized, they were mounted onto the test frame. The yaw sensor was mounted to its plate and installed onto the front of the frame. The figure below shows the current vane fully ready for installation.

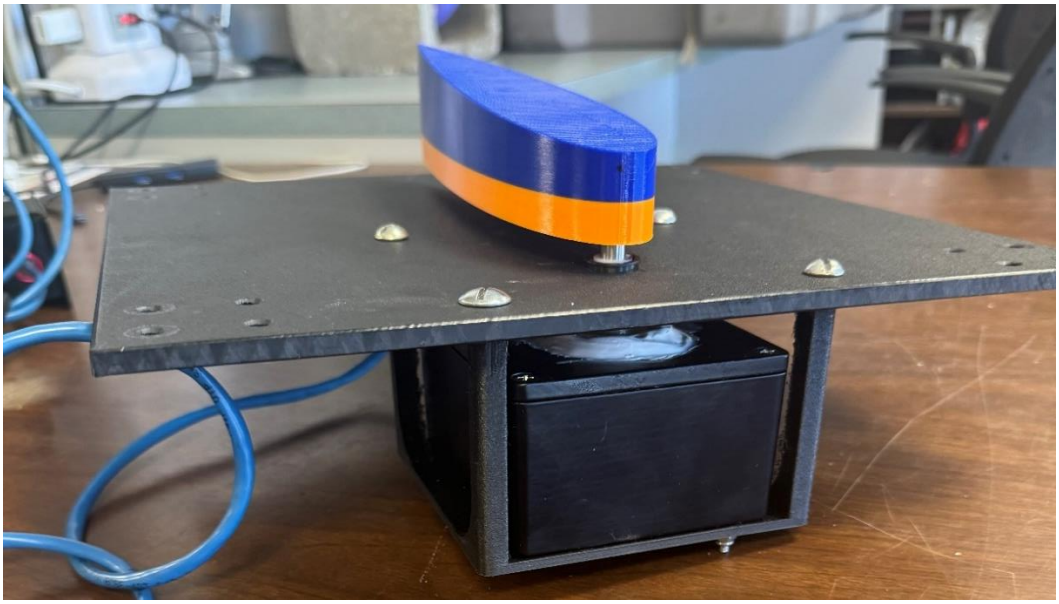

Figure 69: Yaw Sensor Installation Ready

In addition to installing the distribution box and yaw/pitch sensors, the motion capture lights were installed on the test frame and wired into the electrical box. The motion capture lights were wired into four different strings to facilitate wire management better. The markers were placed asymmetrically, as described previously in this research.

Figure 70: Test Frame Fully Setup with Electronics

With all the electronics assembled onto the frame, each system was tested and validated. The motion capture lights were powered up, and each light was checked for correct function. The yaw and pitch sensor outputs were checked for correct function. All thrusters were also tested to ensure correct performance and rotational direction. With all systems installed and tested, the frame was ready for transport to NSWCCD.

Chapter 4
Software Control of Model

MATLAB Simulink Setup

One of the critical elements for the testing unit is to be simplistic but capable of running different control configurations. The ability to modify the control system will allow other control types to be tested on the unit during future testing. Based on feedback from NSWCCD, many control systems have been developed and built through Simulink. Based on the use of Simulink, the Arduino microprocessor Mega R3 was selected. Arduino is connected to Simulink with the Arduino support package library. With this package, the board can be run in two different modes. The first mode takes the Simulink model and uploads it directly to the Arduino for code execution. Simulink can view the results and parameters of this model. The second mode allows the Arduino to act as input and output while the model computations are done onboard the computer hosting the model (30). Running the Arduino as IO will allow for quick execution of different Simulink blocks but does not result in a robust data connection. For longer simulation deployment, the Monitor and Tune function is recommended. Through this setup, different simulation parameters are controllable during the simulation. The ability to quickly change parameters will allow for successful system tunning during the in-water trials.

Simulink Arduino Sensor Connection

The Simulink library currently has several blocks that will aid in creating the control system. The following blocks will be used to easily interact with the Arduino and the connected sensors.

Figure 71: Arduino Simulink Blocks

The SPI block is used to interface with the current vane encoder. The BNO055 block will provide all the necessary data for vehicle pitch. This data can be pulled either from the sensor fusion algorithm as Euler angles or as raw values of the nine onboard sensors. Lastly, the PWM output block sends signals to each thruster's Electronic Speed Controllers (ESC). By utilizing logic controls in Simulink, the arming process of the ESCs can be executed before starting the full control loop and thrust outputs to the motors. These combinations of blocks will allow for effective sensing and control of the unit while connected to the topside laptop. The topside laptop will be able to monitor and record the sensor values and control loop performance.

A Simulink model was made to interface with each sensor and pull the required values from each data bus into the main simulation. For the IMU, the built-in BNO055 library block shown in Figure 37 was utilized.

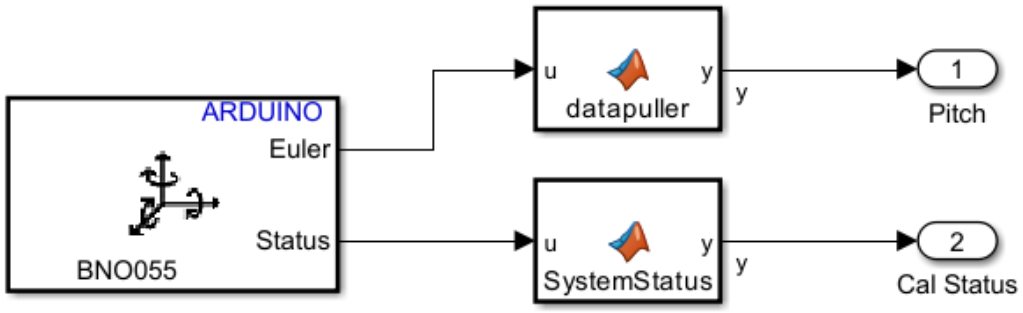

Figure 72: IMU Read Simulink

In the model shown above, the output of the IMU was set to sensor fusion and Euler angles. This method of pulling data from the IMU applies a sensor fusion Kalman filter. This filter improves the overall output from the block. The output of the block was set to Euler angles. The quaternion output would typically be preferred when interfacing with an IMU. Due to the reduced motion range of the testing frame, having a coordinate fixed Euler angle was more straightforward to work with. The Simulink block outputs a [1x3] matrix of Euler angles. The pitch value is the second Euler angle; the MATLAB function block shown in the model above pulls this portion of the matrix. The same method is used to gather the calibration status of the IMU. The portion of the matrix that outputs accelerometer calibration is pulled out separately with a MATLAB function. Both the calibration status and current pitch position are passed back upwards to the main Simulink model running the vehicle control.

There was no existing Simulink library for the encoder to retrieve data from the current vane sensor. The encoder works over the SPI data bus through a send/receive protocol. A read command must be sent to the encoder, and then the device responds with its current position. To do this, the SPI Write/Read block was utilized. Similar to the IMU read model, a separate model for encoder position reading was used.

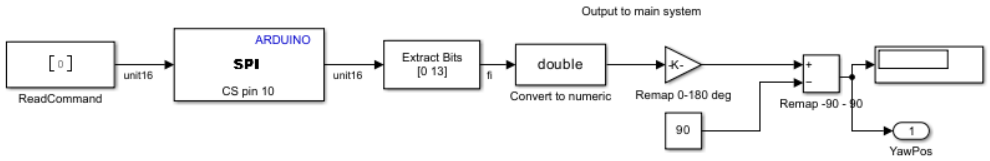

Figure 73: Simulink Model for Encoder Position Reading

From the diagram above, the model begins with creating a 16-unit vector of the read command. For this encoder, the read command is [0]. This read command is sent to the SPI block in Simulink. This block transmits the read command and records the encoder's response. When the encoder responds, the position is included in the data packet as a 14-bit precision number and a check sum (38). For use with this system, the check sum portion is ignored, and the positional data is retrieved by the extract bit block. The extracted bits are then converted to a numerical value. This numerical value can then be mapped to the encoder's 360-degree rotation range and transmitted to the main simulation model.

Model Control Setup

As described in the introduction for this project, a closed-loop control system was needed to maintain pitch and yaw angles. To improve system performance, these controllers were decoupled into separate Simulink simulations that ran onboard separate Arduinos. The implementation of this is shown in the following system diagram.

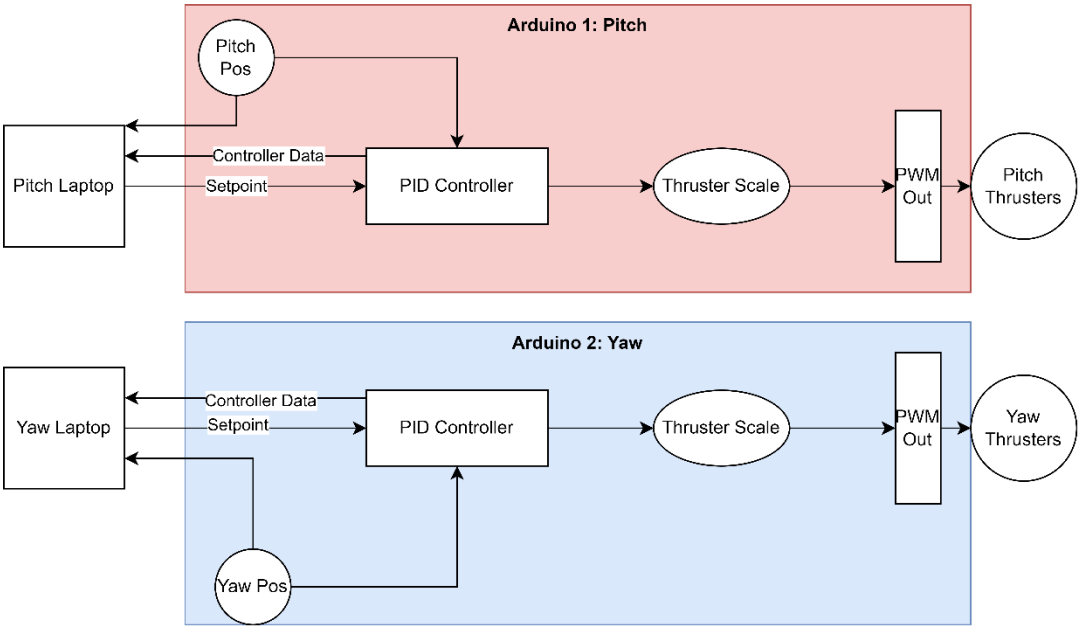

Figure 74: Laptop Arduino Connection Block Diagram

The primary goal of the PID control loops is to take the current pitch/yaw of the vehicle and use it to control how much power the unit needs to apply to hold the setpoint. The PID loop used to control the vehicle pitch is shown in the figure below.

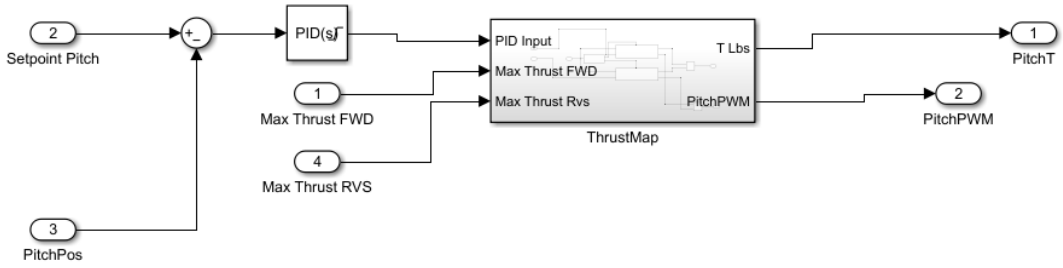

Figure 75: PID Control Loop for Pitch

In the figure shown above, the main function is to take the difference between the pitch setpoint and the current pitch position. This results in a measurement of error in pitch. This error is passed to the Simulink PID block, which uses Equation 1 to compute the output of

the PID block. The output of the PID block has a saturation limit of +-90; this output bound is used by the Thrust mapping block to scale the PID output to the force of the thrusters. If the PID block outputs +90, the thrusters will be actuated at their maximum set force. If the PID block values are between the max/min, then the value is scaled against the maximum thrust value set. The figure below shows the thruster mapping setup for the vehicle.

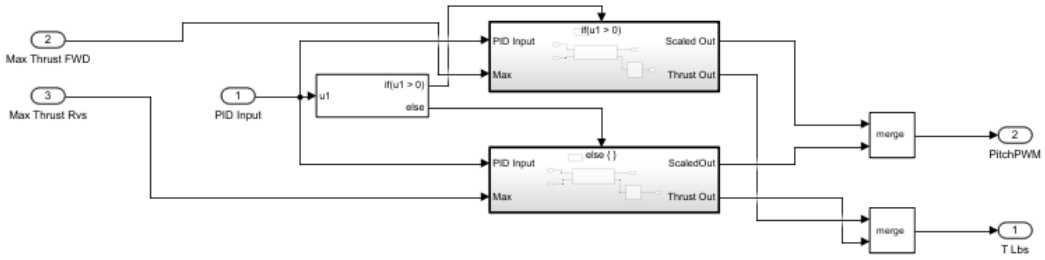

Figure 76: PID Thruster Mapping

In the figure above, the model for thruster mapping is shown. The Blue Robotics T200 thrusters used on the testing model do not output symmetric thrust. Due to the directionality of their accelerator nozzle, the thrusters output more force when running in the forward direction.

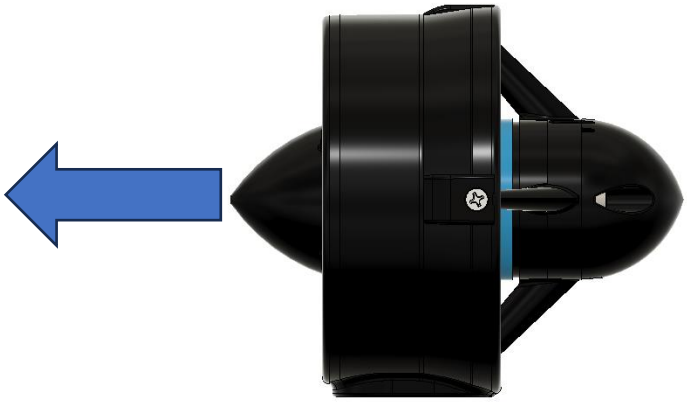

Figure 77: T200 Accelerator Nozzle (14)

Two different PID-to-thrust blocks were created to account for this difference in thrust. A different mapping function will be used based on whether the PID value is positive or negative. If the PID function calls for forward thrust, then the forward block is used. The same process happens when reverse thrust is commanded. This step ensures the vehicle responds with equal thrust, allowing the unit to operate consistently. Since the thrust mapping blocks all accept the thruster power limit, the system can be easily modified for different maximum thrust settings. The gains inside the PID block, along with maximum thrust values, can be tuned while the model is running. The PWM output from the thruster mapping functions is given to a set of blocks that will output the correct PWM frequency to the thrusters. The command set used for this is shown below.

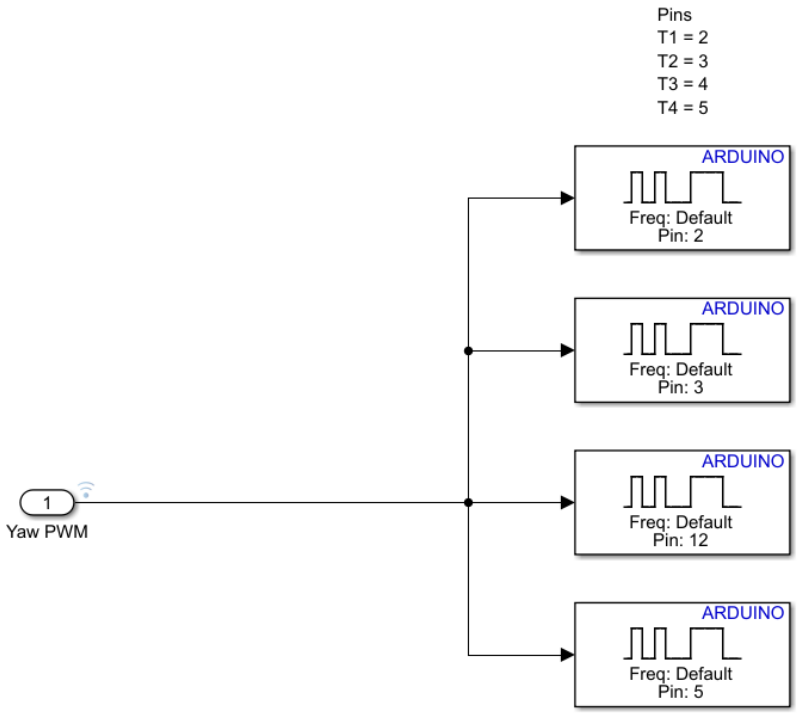

Figure 78: PWM Output to Thrusters

Returned from the PID section is the called thruster output. The PWM value called by the PID loop is referenced to the Blue Robotics T200 data table for PWM vs. Thruster Output. This output is displayed to the user and assists with tuning and diagnosing the system.

The PID control loops for the pitch and yaw control are very similar, as shown in the figure below. The main difference between the setups is that a separate derivative term was created for the Yaw controller to bypass the built-in MATLAB PID block. The PID model setup for the Yaw control loop is shown in the figure below.

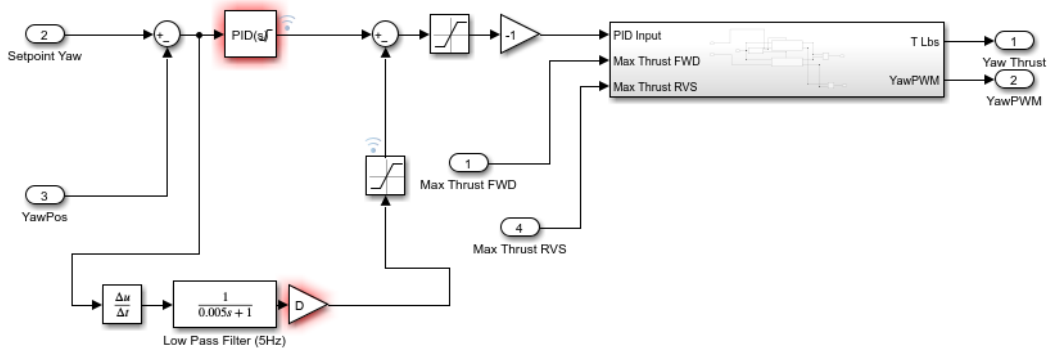

Figure 79: Yaw PID Controller

The setup for PID control over the yaw position of the test frame is shown in the figure above. Due to limitations with the Simulink derivative term inside the standard PID block, a separate D term had to be added. Testing revealed that the D term was not able to become negative, which would aid in slowing down the system's response. Further explanation of this behavior is discussed in Chapter 6. Since the D term was pulling directly from the calculated error between the pitch setpoint and the current pitch position, a filter needed to be applied so the D term would not act erratically. A low pass filter of 5HZ was applied to the signal; this smoothed the signal going into the derivative block, resulting in a more accurate D term response for the model. Since the derivative was separate from the Simulink PID block, saturation limits had to be applied so its effect on the overall PID output would be within the parameters set for the PI terms. The output of this PID controller setup was then passed into the same thruster mapping blocks as shown previously in this section.

Overall, the PID controller setup for the test frame was set up to effectively and simply control the test frame's yaw and pitch position. The control loops utilized real-time sensor feedback for control while passing important information back to the user to assist in the tuning process.

Hardware Software Integration

The individual models discussed in the sections above were combined into two models. Model 1 controlled the yaw position of the vehicle and logged corresponding signals. Model 2 controlled the pitch position of the vehicle and logged the corresponding signals for pitch. The figure below shows Model 1 setup in Simulink.

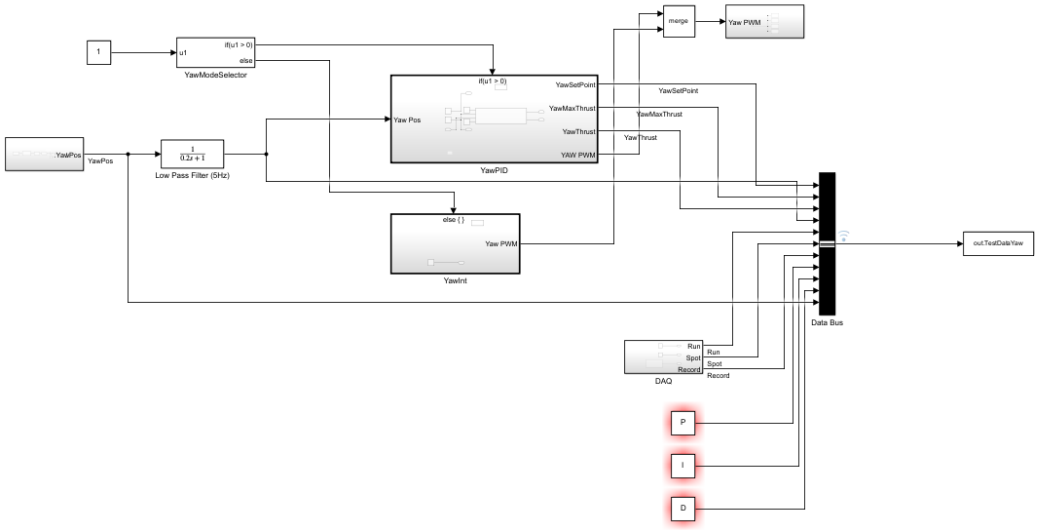

Figure 80: Simulation Model 1: Yaw Control

The figure above shows how the yaw sensor is used as input to the PID controller and thruster mapping block. From the model blocks, different outputs are mapped to a data bus, which is then recorded in the MATLAB workspace. This setup of inputs and outputs is the same between Model 1 and Model 2. The variables logged for Model 1 and Model 2 are shown in the following table.

Table 3: Simulink Logged Variables

Model 1	**Model 2**	**Description**
YawSetPoint	PitchSetPoint	Controller setpoint
YawMaxThrust	PitchMaxThrust	Max thrust allowed for individual motor
YawThrust	PitchThrust	Commanded thrust from controller
YawPos	PitchPos	Orientation data
PGain		gain setting
IGain		gain setting
DGain		gain setting

The data collected from the model can be used to tune the system in real-time and in data processing to better understand the motion observed by the motion capture system. A Simulink panel was created for each model to easily access critical parameters. The panels created for Model 1 is shown in the figure below.

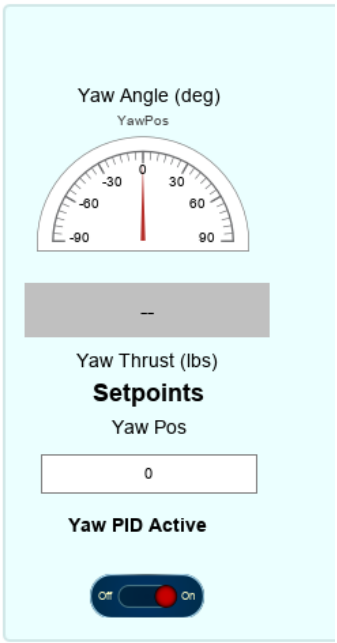

Figure 81: Simulink Panel

Simulink panels float in the workspace and can be easily accessed anywhere in the model, making them a great choice for displaying data to the user and receiving user input. For each model, a gauge was used to display the relative position of the test frame. A PID loop

activation switch was included to enable/disable the control loop. An input for setpoint was located on the panel; editing this parameter would change the desired orientation for the respective control loop. Lastly, there is an output box for the commanded thruster force. This box lets the user quickly see how much force the thrusters actuate. Working with these Simulink panels allowed for real-time testing and monitoring of the system.

To deploy the model to the Arduino controller, Simulink will compile the code into .hex files which are uploaded to the controller along with the Simulink server software. The code will execute on the Arduino based on parameters set in the simulation, the corresponding output is displayed back to the user.

In Simulink, different settings can be used to optimize the controller performance through the “Hardware Settings” work pane. The figure below shows the Arduino hardware settings that can be changed.

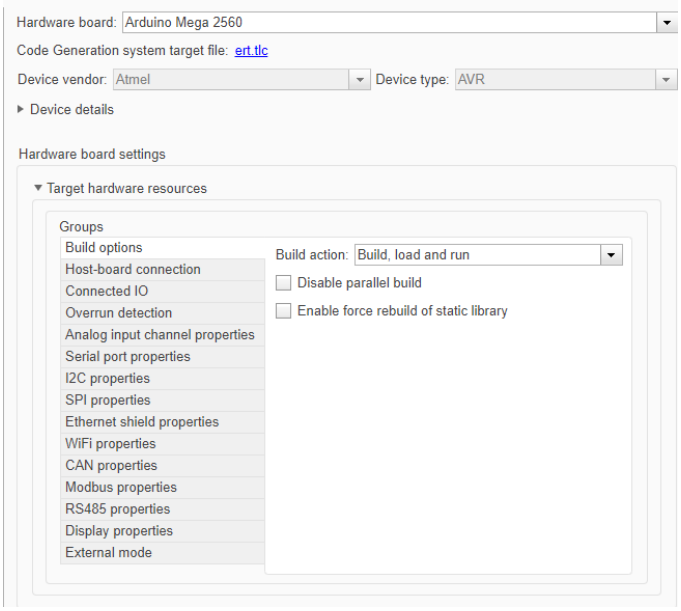

Figure 82: Arduino Hardware Options

During system optimization, it was found that the I2C bus and SPI bus clock speeds needed to be adjusted for the best data integrity. Due to overhead caused by the Simulink model loaded onto the Arduino, a lower clock speed and slower data collection rate was used to reduce the possibility of communication errors. Both the SPI bus and I2C bus were set to 1000Hz. The sample rate of the onboard sensors was set to 8.3Hz, as found using the equation below.

$$F = \frac{1}{sample\ time} \qquad \text{Equation 5}$$

Dry Test Trails

The system was validated with dry runs of the electronics/software system at Florida Tech before transfer to NSWCCD. The dry checkouts' goal was to check sensor input, control responses, and stamina.

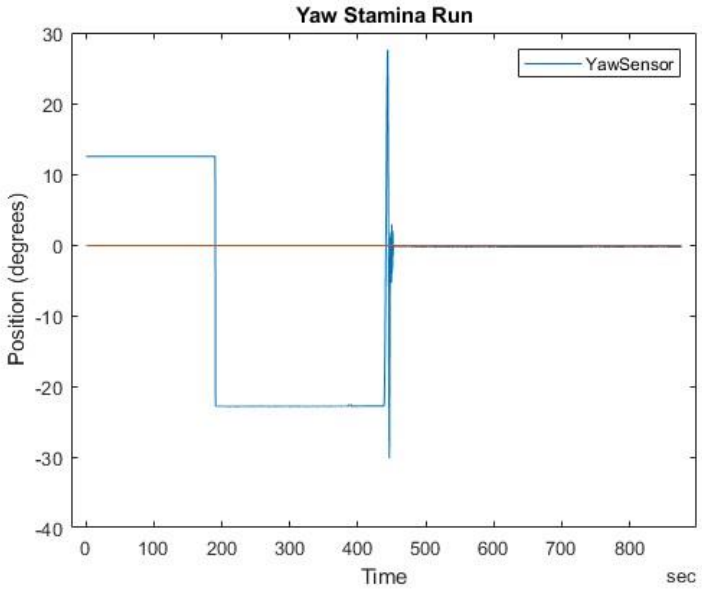

Figure 83: Yaw Stamina Run

The figure above shows a stamina run completed for the yaw sensor. The purpose of this test was to ensure the system was able to run a long data collection without sensor or control errors. In the graph above, the sensor values stay constant except near the 450-

second mark, where the sensor oscillates back and forth to check for proper response. The same process was completed for the pitch controller. The figure below shows a windowed view of the motion of the yaw and pitch controller.

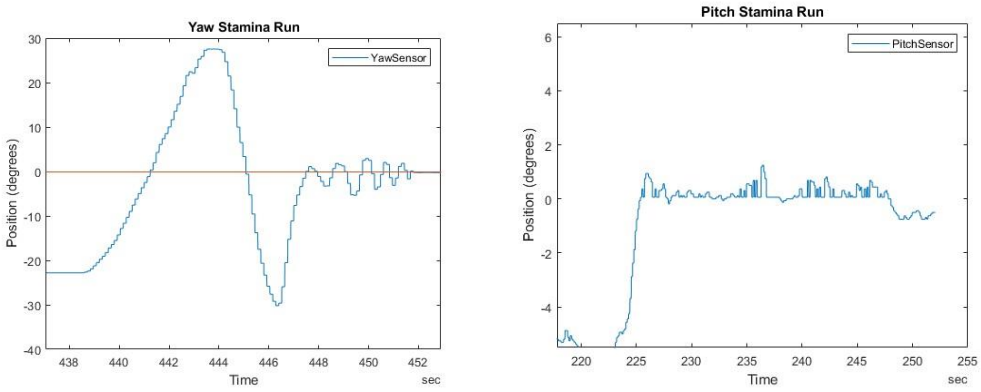

Figure 84: Yaw and Pitch Validation

The final assessment of the controller models was to validate that sensor motion would result in PID output to the thrusters. To do this, the yaw sensor and setpoint were adjusted to cause a thruster response. The same procedure was completed for the pitch controller. The figure below shows the output from the yaw output check.

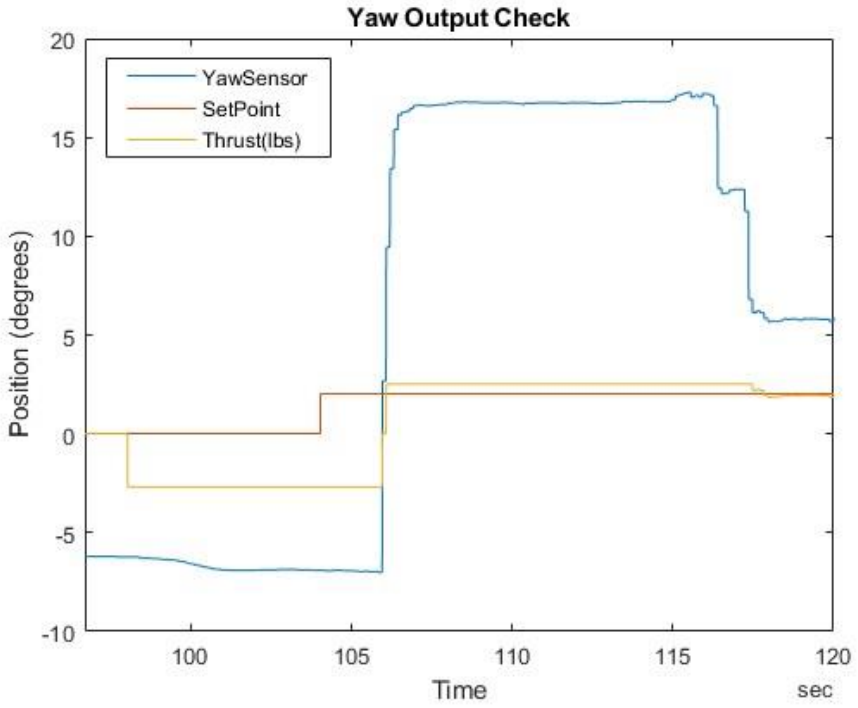

Figure 85: Yaw Controller Checkout

From the figure above, it can be seen that when the position and setpoint of the controller were adjusted, a response to the thrusters was generated. The maximum thruster output matched what was set as the limit in the Simulink control panel. Completing these tests for the yaw and pitch controller indicated that the software and hardware were working as expected and ready for testing at NSWCCD.

Chapter 5
Test Preparation

Proposed Test Setup

Testing was performed with NSWCCD in the CWC to analyze and evaluate the stability of the AUV capture system. This facility is a large water circulator that can produce uniform currents across a test section. The water flow is controlled by a constant-speed, motorized impeller with adjustable flow vanes.

Figure 86: Circulating Water Channel Scale Model and Testing Section

The water flows through the large open working section; this section has many features to facilitate model testing. Lighting and mounting points are placed along the working section. Adjustable bridge sections are located atop the working section on rolling tracks for quick model positioning. This is where the test frame will be mounted along with the needed sensors. The figure below shows a top-down view of the testing setup.

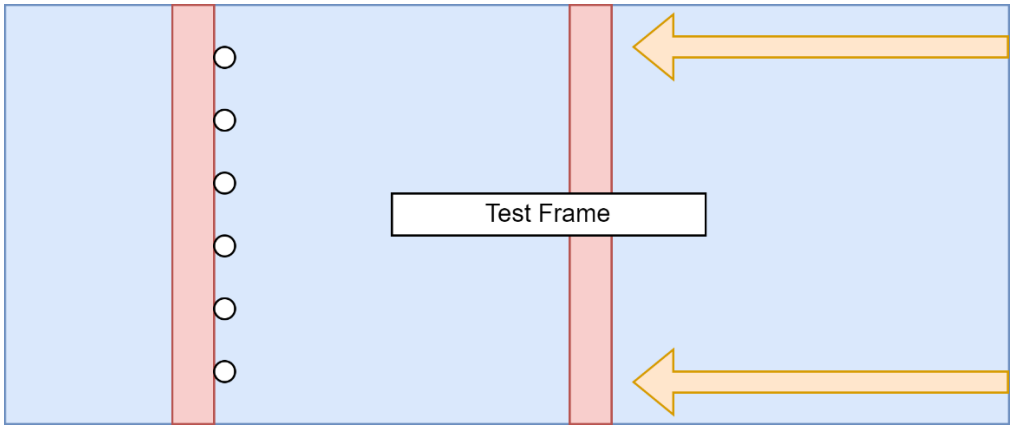

Figure 87: Overhead Test View

Underwater motion capture will be used to capture the exact motions of the device. This system is being analyzed and developed by the Unmanned System Hydrodynamics Division at Carderock, Code 881. This system utilizes OptiTrack Prime 13W cameras located inside underwater housings. To work with the underwater motion capture system, green LED lights were placed along the body, which will be tracked by the motion capture system. Based on previous testing by Code 881, the estimated resolution of the underwater camera system is <5.0 mm. The body's motions can be exported for further analysis with software such as MATLAB.

Data Collection Method

The goal of the instrumentation is to monitor the position and controller output of the test frame during each trial. For each test of the Frame, the primary data source will be an underwater motion capture system. This motion capture system will consist of six cameras placed along the rear carriage of the CWC. The six cameras will be focused inward, toward the center of the testing section. All cameras will also be angled 25 degrees downwards to prevent reflections from the water’s surface, which could impact the motion capture’s performance. The cameras’ field of view (FOV) was placed into a 3D model of the CWC testing channel to visualize the motion capture environment.

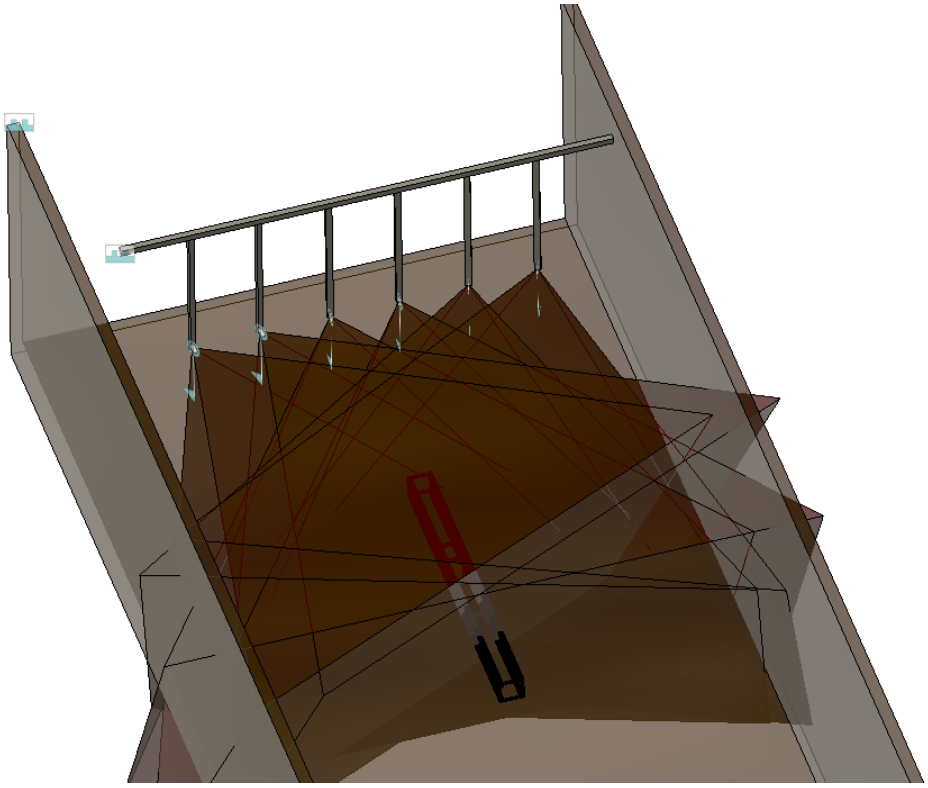

Figure 88: Motion Capture FOV Facility Overlay

Located onboard the test frame is a heading sensor and IMU. The data captured from the frame will include pitch, yaw, and controller output. Sensors will be time synchronized after testing using key events.

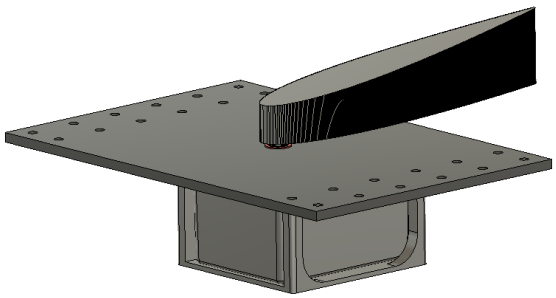

Figure 89: Yaw Sensor

The yaw sensor shown above uses the constant current of the CWC to monitor the angular deflection of the test frame against the current direction. This measurement will track the yaw position of the frame and feed into the closed loop PID yaw controller.

Control of the test frame is done through a Simulink controller and data acquisition (DAQ) setup, as described in the previous chapter. Dual Simulink simulation models connect to the dual Arduino MEGA 2560s in real-time. Using the data from the Arduino, Simulink PID controller blocks are used to command outputs to the frame's onboard thrusters. During testing, real-time tunning was completed by adjusting parameters within the floating control panels of each model.

Table 4: Measurement Devices

Equipment	**Measurement**	**Accuracy**	**Significance**
Natural Point MoCap	3-dimension body motions	~0.4 in	**Critical** to test data collection
IMU	Pitch	0.8 deg	**Critical** to Pitch control loop performance
Heading Sensor	Yaw	0.2 deg	**Critical** to Yaw control loop performance

The table above outlines the different sensors used during testing and their relative accuracies. Each sensor is critical to the success of the experiment's testing.

Test Readiness

To best prepare for testing at NSWCCD, a test plan outlines major test milestones, risks, procedures, and logistics. This test plan is reviewed during the Test Readiness Review (TRR). During the TRR, many personnel familiar with the project and facility discussed the test plan and suggested adjustments. The goal of the TRR was to ensure that the test was set up for success and to give feedback on any areas that needed improvement before testing. Action items that followed the TRR were sensor calibration, run matrix adjustments, and rigging procedure changes.

As part of the TRR and test plan, criteria must be established for when the test can begin and end. The purpose of creating the test entrance and exit criteria is to put in place the framework that outlines how the test will begin and what needs to be accomplished to conclude testing. Without these guidelines, the test could continue to other goals and stray from the original test plan. The following entrance and exit criteria were established with NSWCCD.

Test Entrance Criteria

- The test frame is functioning and shows proper controls response.
- The instrumentation on board frame is calibrated and functioning.
- Simulink control space is functioning and recording data.
- All required personnel are available.
- Test plan and matrix approved.
- TRR conducted and approved.

Test Exit Criteria

- Control loops turned for successful vehicle control.
- Yaw/pitch position tests completed for configuration 0.
- Estimates for power requirements obtained.

Another key area of the test plan is outlining the testing schedule and daily Go/No-Go criteria. The following schedule was the original estimate for the completion of the research testing.

Table 5: Initial Testing Schedule

Day	Title	Description	CWC Water Level
Monday 3/4	Rigging, Frame Setup	Assemble motion capture in CWC and calibrate. Assemble test frame and check system function.	Full
Tuesday 3/5	Frame tunning	Complete setup of frame and work on PID control loop tunning.	Full
Wednesday 3/6	Testing Runs	Complete testing for Yaw/Pitch Goals with initial test configuration.	Full
Thursday 3/7	Back-up testing runs, additional configuration runs	Complete any missed runs from Wednesday. Time permitting try additional weight and buoyancy layouts or thruster positions.	Full
Friday 3/8	Tear down	Disassemble system and pack back onto crate. Disassemble motion capture from CWC.	Full

The goal was to complete testing within one week and run the facility with flow for a total of 3 days. The requested water level in the CWC is shown on the right-hand side of the table. It was important to mark down this as filling and draining the basin can take up to 1 day, depending on water availability. Due to this, it was determined that rigging up the motion capture setup while the water was full would be the best option to minimize downtime. An additional consideration for keeping the water of the CWC full is the maximization of water clarity. Filters run at the bottom of the basin to clean particulates from the water; filling and draining the facility would remove any progress made by the filters to improve clarity.

Each day before flow can begin, the following set of Go/No-Go procedures are used to determine if testing can continue for the day.

Daily Go Criteria

- CWC and carriages are operational and safe, according to facilities personnel.
- Essential test personnel are present and ready.
- Test frame is in good condition, and all systems operate.
- Instrumentation is set up, calibrated, and communicates with DAQ properly.

Daily No-Go Criteria

- CWC nonoperational
- Required test personnel not present.
- Damaged or incorrect operation of test frame systems.
- Motion capture cameras moved or out of calibration.
- DAQ and Simulink control nonfunctioning.

If any no-go criteria is met, it must be correct before testing can continue in the facility.

Test Procedures

The following test procedures were used to conduct successful testing at NSWCCD.

Test Progression:

1. Weight and buoyancy
2. Sensor calibration
    a. Find the minimum speed current vane is effective.
    b. Check function of IMU
    c. Check function of Motion capture system
3. PID gain tuning
    a. Utilize Ziegler–Nichols tuning method
    b. Fine tune using Simulink control knobs
4. 0/0 runs
    a. Evaluate performance at 0 deg yaw and 0 deg pitch
5. Yaw positions 0, 1, 2, 3, 4, 5, 10, 15, 20, 25, 45, 90 both sides
6. Pitch Positions 0, 5, 10 Yaw setpoint 0

Weight and Buoyancy Procedures

1. Place estimated flotation and ballast onto vehicle.
2. Connect load gauge to hoist.
3. Lower unit into the water until fully below water surface.
4. Pitch frame up and down to ensure all trapped air is released.
5. Measure weight and pitch angle using motion capture and IMU.
6. Use trim weights/flotation foam to correct angle and system weight.
7. Stop adjustments when 200lbs negative and 0-degree pitch is achieved.

Gain Tunning Procedures

1. Place the frame into water.
2. With no current use Ziegler–Nichols method for tuning
3. Use table to estimate parameters for initial trail.
4. Hold unit into place with dock hook to allow flow to fully develop.
5. Enable PID controllers and monitor system behavior.
    a. Use dock hook to prevent extreme motion if observed.
6. Removed dock hook and fine tune PID gains to optimize system using real time monitoring.
7. Run 0/0 test to validate system baseline performance.

Daily Procedures

1. Overview of test plan for day
2. Check seals of all underwater chambers
3. Power on system and check function of all sensors and motors out of water
4. Check function of motion capture system
5. Check function of CWC facility

Run Procedure Yaw

1. Use dock hook to hold frame steady until current has stabilized at run speed.
2. Enable PID control at 0/0.
3. Enable system logging after system stabilizes.
4. Input new test setpoint.
5. Allow system to move to setpoint.
6. After system settles hold position for 60 seconds to record thruster power performance
7. Use dock hook to perturb system in yaw
8. Input 0/0 set point and allow vehicle to move back center.
9. Disable logging after vehicle settles at 0/0.
10. Repeat test procedure for all yaw positions.

Run Procedure Pitch

1. Use dock hook to hold frame steady until current has stabilized at run speed.
2. Enable PID control at 0 degree pitch only
3. Enable system logging after system stabilizes.
4. Use dock hook to perturb system in pitch
5. Disable system logging after system stabilizes.

Run Procedure Pitch

1. Hold test frame at 0 yaw position with PID loops disabled.
2. Enable system logging.
3. Input % yaw thrust until system reaches max tether length.
4. Allow the system to stop motion and disable logging.

Run Matrix

The initial run matrix for the experiment is shown in the following table.

Table 6: Initial Run Matrix

Run #	**Configuration**	**CWC Current Speed**	**Details**
1 – 5	0	0.0 kts / 1.0 kts	Yaw and Pitch Power Runs
6 – 10	0	1.0 kts	Tune PID Parameters
11 - 26	0	0.5 kts	Yaw movement validation. Check unit can move to multiple yaw positions
27 – 42	0	0.5 kts	Sweep through yaw targets
43 - 58	0	1.0 kts	Sweep through yaw targets
59-66	0	1.5 kts	Sweep through yaw targets
67	0	0.0 kts	Pitch perturbation

*All run numbers are approximate to the duration planned for each test goal

The run matrix above aims to set up how the experiment will progress. The experiment begins with yaw and pitch power runs. These experiments aim to assess how the unit will move in these directions. If the test frame acted uncontrolled during this testing, additional precautions would be needed for the following tests. The next portion of the run matrix focused on tuning the PID control loops and validating their performance. After each controller had been tested, the main experiment could begin with testing different yaw positions. The procedures found in the previous section were used during the yaw position tests. The last task on the run matrix was to introduce perturbation in pitch. Completing the run matrix is crucial to ensuring test goals are met and the experiment follows a logical order.

Chapter 6
Model Testing at NSWCCD

Testing Setup

At NSWCCD the test model had to be reassembled. The unit was broken down into three sections for transport, as shown in the figure below.

Figure 90: Model Broken Down for Transport

The model was unpacked and set up in the Code 881 mechanical lab. Set up of the test frame first began by reconnecting the wiring of the sensors and motion capture lights back into the electrical distribution box. After the electrical system was set up, the function of all the lights and sensors were validated. Validation testing was not initially successful. The connection to the IMU sensor was not stable. After 5-10 seconds, the encoder would enter an error mode that would stop data transfer on the I2C bus. To examine this problem, an oscilloscope was used to view the Serial Data (SDA) line.

The oscilloscope showed that at 30ft, there was excess noise on the data bus. This noise was causing the IMU to enter an error state where all outputs were set to zero. Shortening the length of the cable resulted in less noise as the capacitance of the cable decreased. The

I2C data bus can more easily transmit data and detect fewer errors with a lower noise level. This shortening of the cable resulted in a more stable system performance.

After the validation of all electrical systems, the unit was fully assembled and bolted together. All mechanical interfaces were tightened and checked. The lift point was torqued to spec using an adjustable torque wrench. After the mechanical setup was completed, ballast weight was added to the frame to increase its water weight.

The ballast weights used were steel blocks weighing 34 lbs. These blocks were placed into three different sections along the test frame. One block was placed in the forward and aft sections. Two blocks were placed near the center of the frame. Due to the frame construction, each group of ballast had to be mounted using a different type of ballast mount.

The rear ballast was clamped onto the short spans of frame running in between the main frame rails. The benefit of this mount was its easy mobility to move forward and aft.

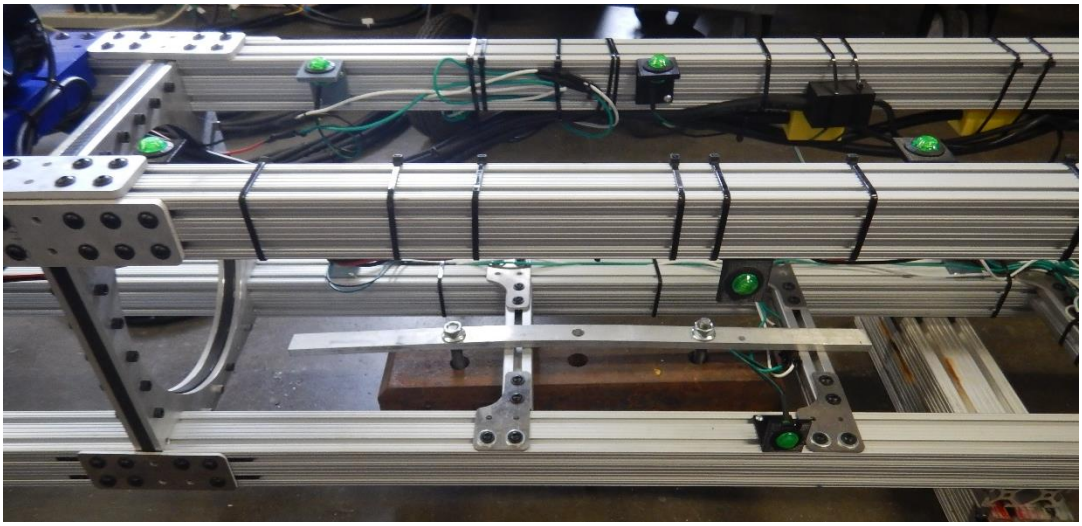

Figure 91: Rear Frame Ballast

Forward ballast was attached to the frame using drop-in T nuts. This method of fastening required no reconfiguration of the test frame. The forward weight is seen attached in the figure below.

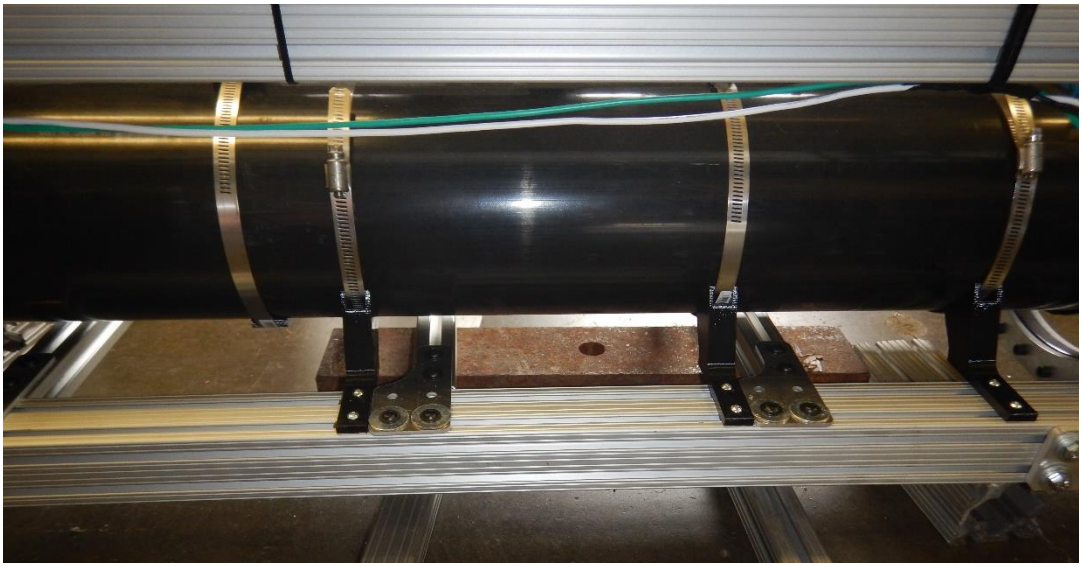

Figure 92: Forward Frame Ballast

Ballast in the center of the model was added along the frame rails with hose clamps. These weights could be easily shifted forward and aft to adjust the trim of the unit.

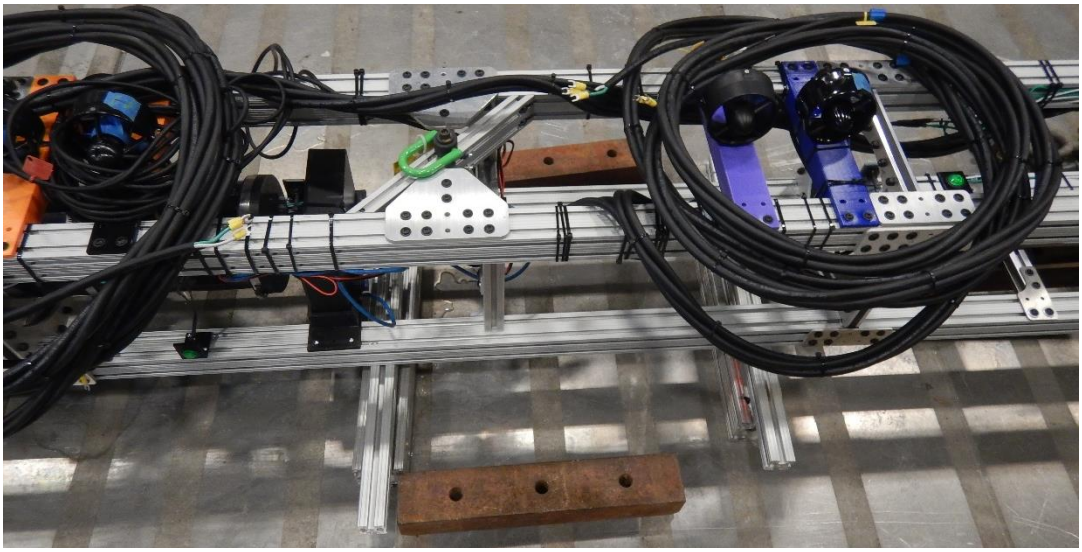

Figure 93: Center Ballast Area

After the installation of all the ballast weights, the test frame was lowered into the water for weighing. The total wet weight of the unit was 175 lbs; this weight was within the customer's requirements, so no additional ballast was added. The dry weight of the unit was 280 lbs. This operation also served as a hang test for the lift point on the model. The model observed no deflection or adverse effects with all ballast added.

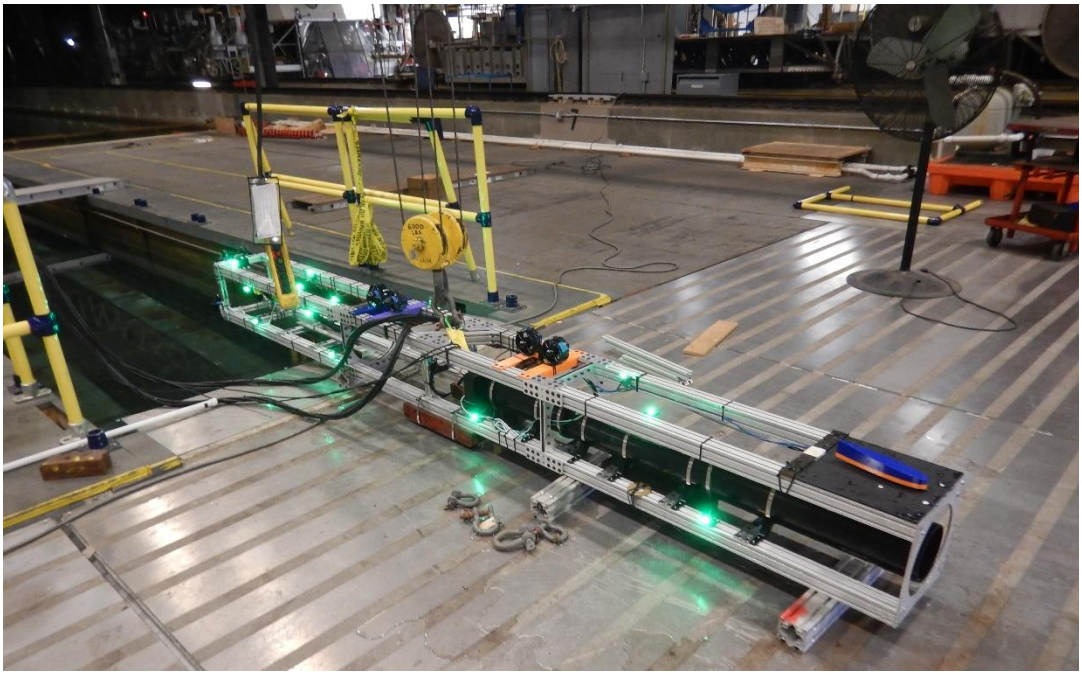

Figure 94: Test Frame Setup for Ballast

The photo above shows the setup used to weigh and balance the model. The dry dock located at the end of the tow tank was used due to its proximity to the mechanical lab. An overhead crane moved the test frame in and out of the water. While lifting, the unit was well-balanced and easy to control.

To transport the test frame to the CWC, the unit had to be placed onto a side loader. The side loader transported the fully assembled and ballasted frame to the loading bay at the CWC. In the loading bay, the unit had to be hoisted up four floors to the working deck of the test facility. The figure below shows this lifting operation.

Figure 95: Hoisting up to CWC Working Deck

For rigging the test frame in the CWC, the unit was connected to a wire cable and lifting sling. The lifting sling was connected to the overhead crane. Once near the water, the cable was attached to the tow point, and the load was transferred. With the unit suspended in the water, the tethers were run so that there was slack for the unit to move freely. The position of the unit and tethers can be seen in the figure below.

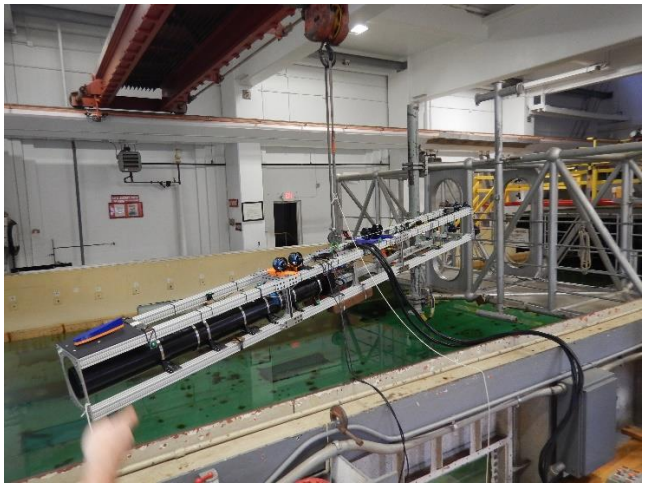

Figure 96: Lifting Into CWC Test Area

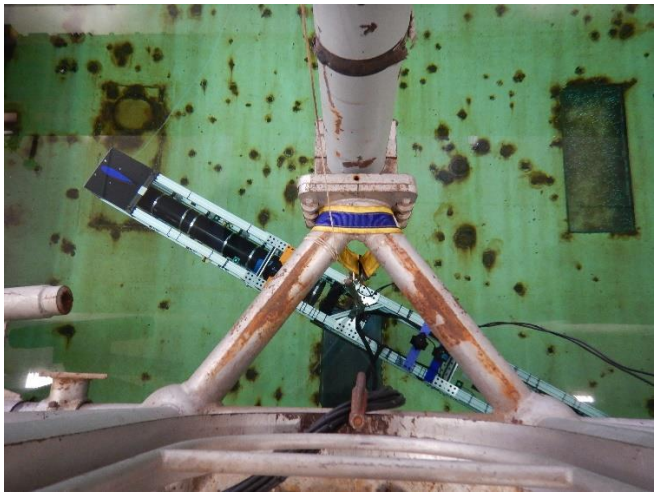

Figure 97: Test Frame on Lifting Sling

Tethers from the unit were connected to the topside control unit using screw terminals and RJ-45 connectors. The board was positioned near the side of the CWC so that it could easily connect to the required computers. The setup for the computers and control board are shown in the figures below.

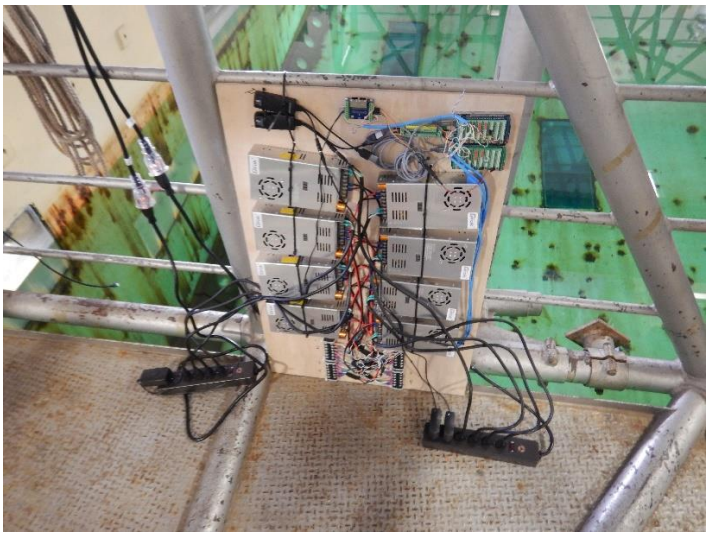

Figure 98: Control Board Setup on CWC bridge

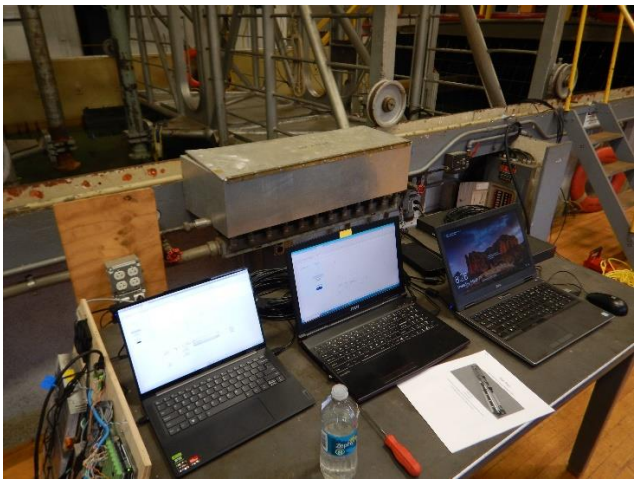

Figure 99: Frame control and motion capture laptops used for testing

Motion Capture Setup

The setup of the motion capture system was completed by NSWCCD Code 881 personnel. This process began by assembling a large, sturdy frame to which the motion capture camera struts were attached. Due to the water flow, fairings were added to the struts to reduce drag and limit turbulence. Turbulence around the struts could cause oscillations that reduce the system's accuracy. The motion capture frame and camera struts are shown in the figure below.

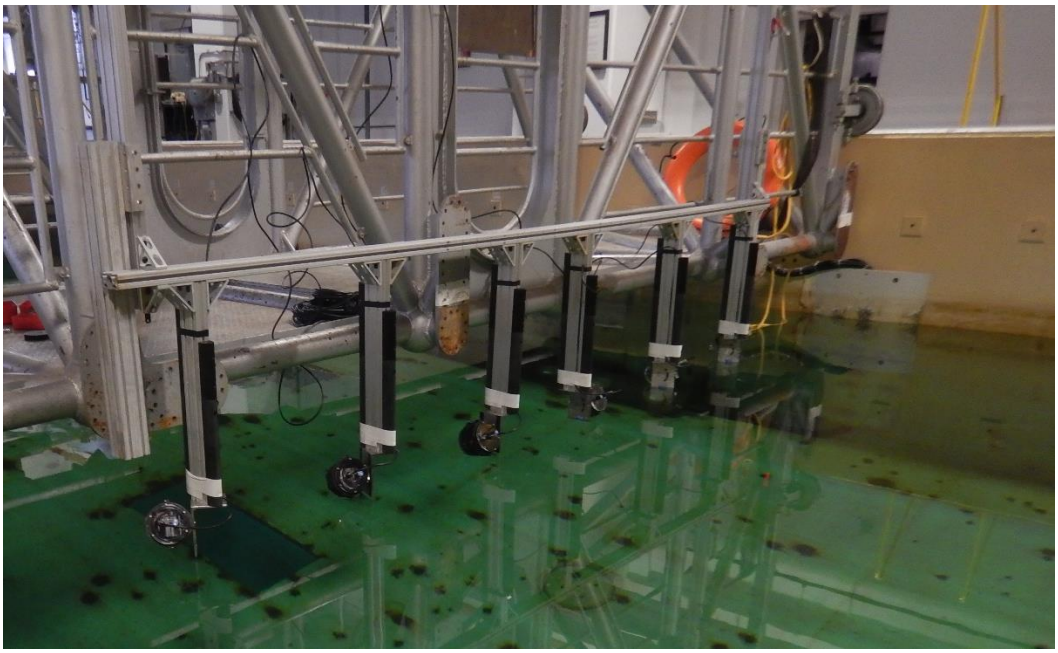

Figure 100: Motion Capture Frame Setup

After the cameras were mounted and lowered into the water, the next process was calibration and setting up the ground plane. A calibration light wand was used to calibrate the system. This calibration wand has LED markers at a set distance. The calibration procedure captures the marker position from each camera. Then, the software uses this data to solve where the cameras are in 3D space. After this step occurs, it is important not to move the cameras from their positions.

After the camera's calibration was completed, the next step was to align the ground plane. The ground plane is the reference plane for how all the measurements will be taken. To align the ground plane for this experiment, the windows inside the CWC were used. These windows allowed for alignment of the X and Y axis, as shown in the figure below.

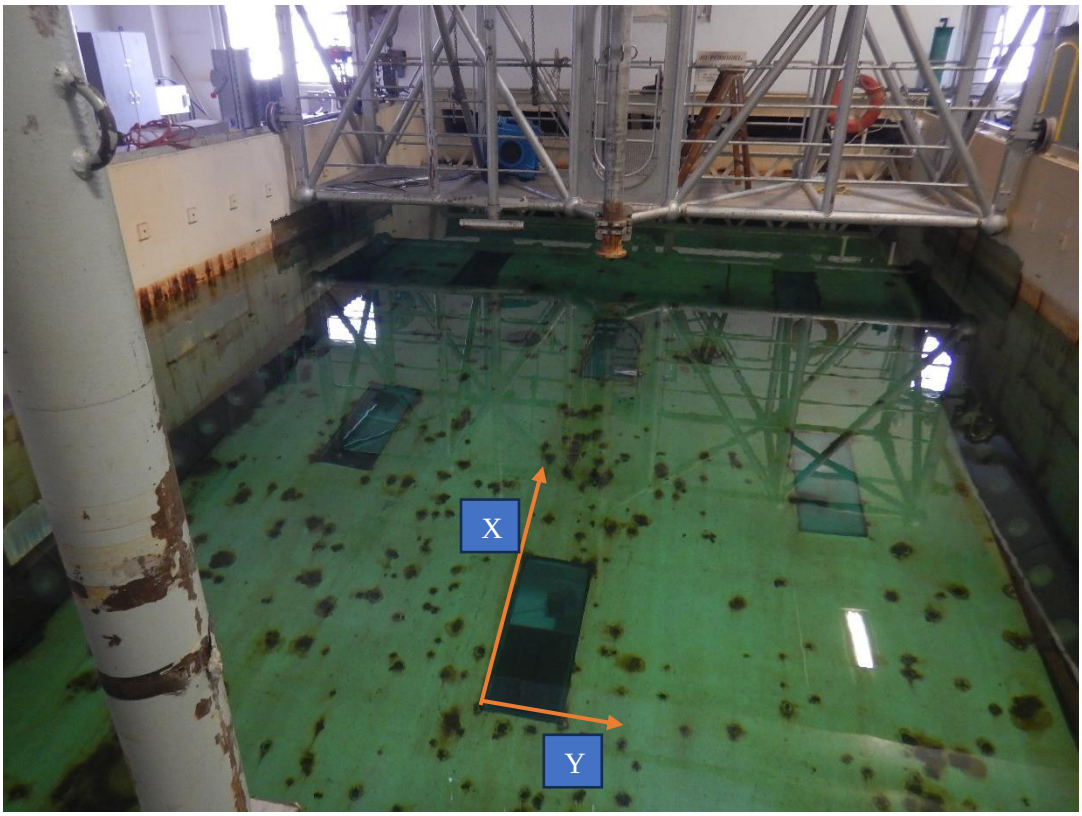

Figure 101: Motion Capture Axis Alignment

After calibration and alignment were completed, a process called "post calibration" was used to examine the capture volume and plan for where the model would be placed in the CWC.

The post calibration uses the LED marker wand from the calibration procedure. Using this known marker arrangement, details about marker accuracy and placement can be plotted for the capture volume. The following plots show the accuracy of the capture volume.

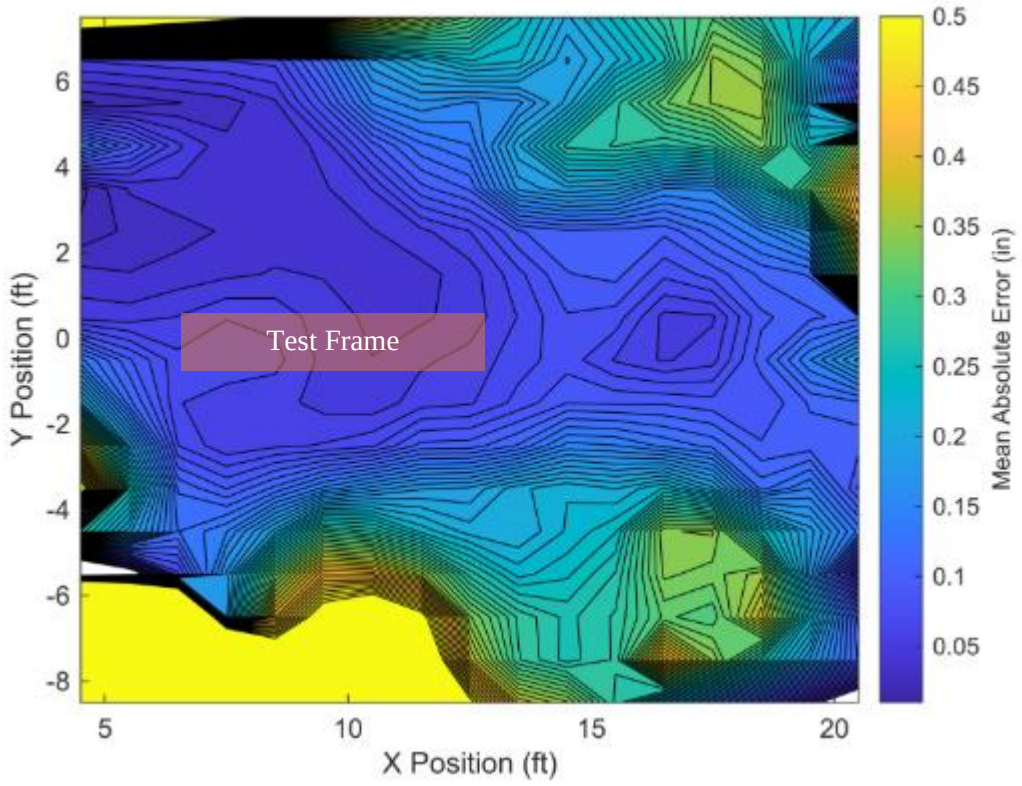

Figure 102: Mean Absolute Error at 4ft water depth

The figure above shows the accuracy at 4ft of water depth with the test frame overlayed 9ft from the cameras. The test frame is well within the areas with the highest accuracy. Based on the post calibration results, the test frame will be well-tracked with minimal errors.

Initial Testing Runs

In the dry dock basin, the unit was submerged about 6ft below the water's surface. With the unit submerged, the pitch thrusters were run up to 80% thrust to capture the pitch response motion. The result was quick but controlled motions. The unit would power up

and then reach a settling point when the pitching thrust equaled the resorting force of the test frame.

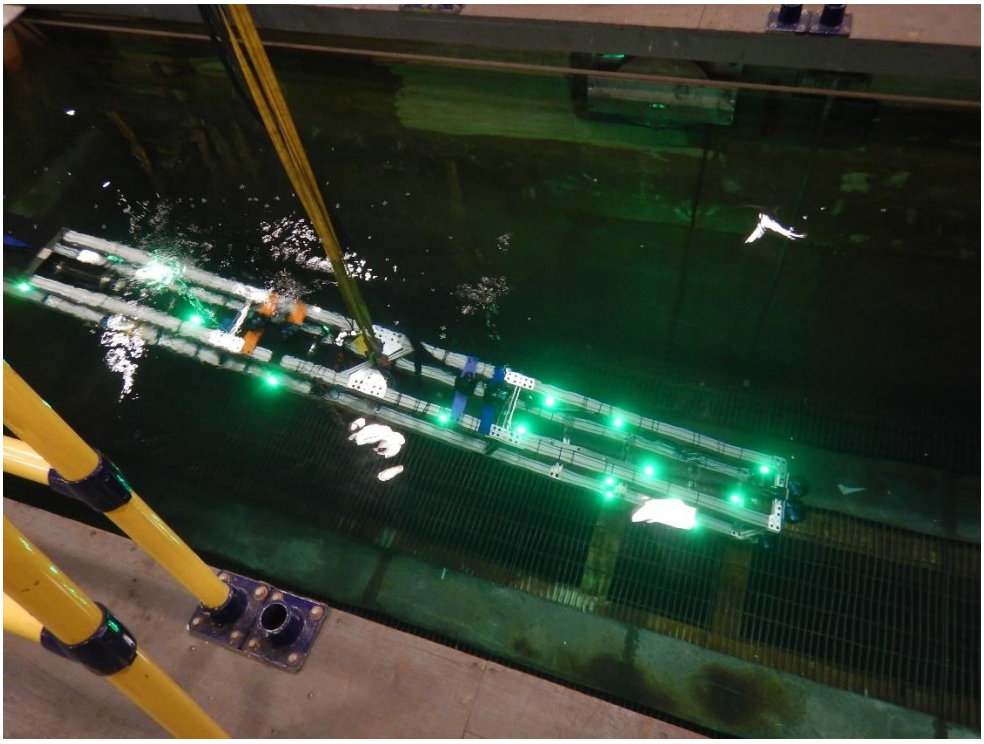

Figure 103: Pitch Power – Nose up Orientation.

Tuning of the pitch controller was completed using the Zeigler-Nicholas PID tuning method (16). This method forces the unit into a continual oscillation state; the period of this oscillation is used to derive an estimate for PID tuning parameters. The following graph shows the oscillation that developed using the Zeigler-Nicholas method.

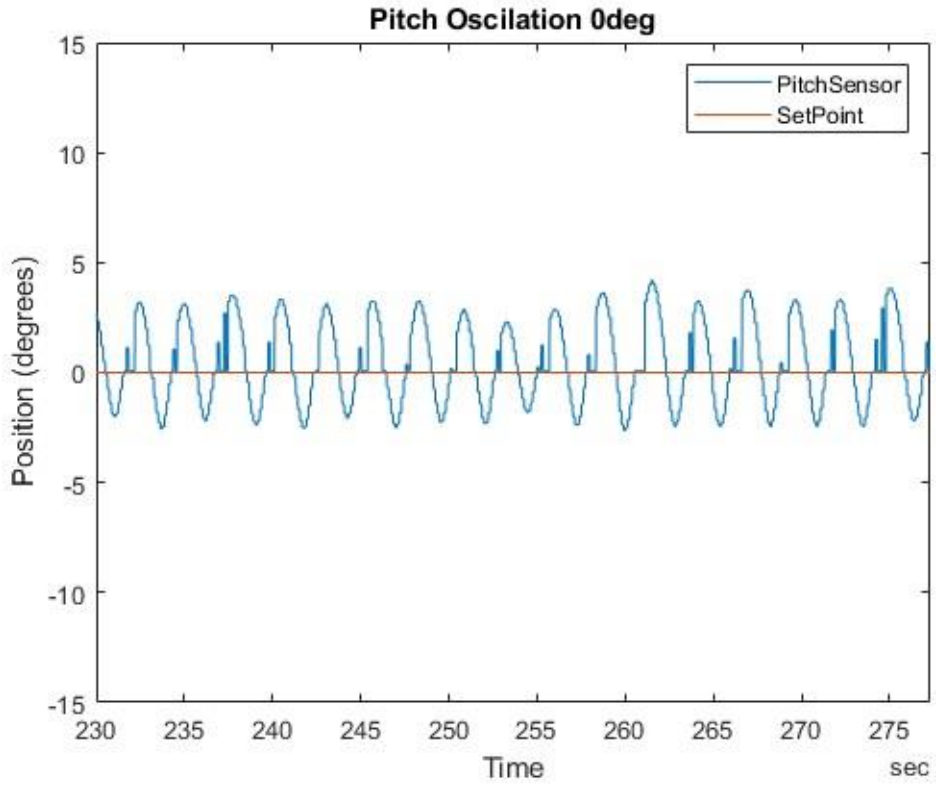

Figure 104: Forced Pitch Oscillation

As shown in the figure above, the unit was moved to a 10-degree setpoint and then back to a 0-degree setpoint to initiate the forced oscillation. From this disturbance, the P gain parameter was increased until the oscillation became consistent. 0-degree was chosen as it would be the most common setpoint at which the test frame would be set during testing in the CWC.

From the forced oscillation, the period was found to be 2.3 sec. From this period, the following set of equations was used to obtain the initial PID values.

$$P_U = 2.3sec\ K_c = 45$$

$$\boldsymbol{P = \frac{45}{1.7} = 17} \left| \boldsymbol{Ti\ = \frac{2.3}{2} = 1.15} \right| \boldsymbol{Td = \frac{2.3}{8} = 0.325}$$

The initial PID tune parameters located above performed well. The unit was able to maintain different pitch setpoints and respond to perturbations. It was observed that the first set of PID parameters resulted in the system being under-damped. This behavior is seen in the graph below.

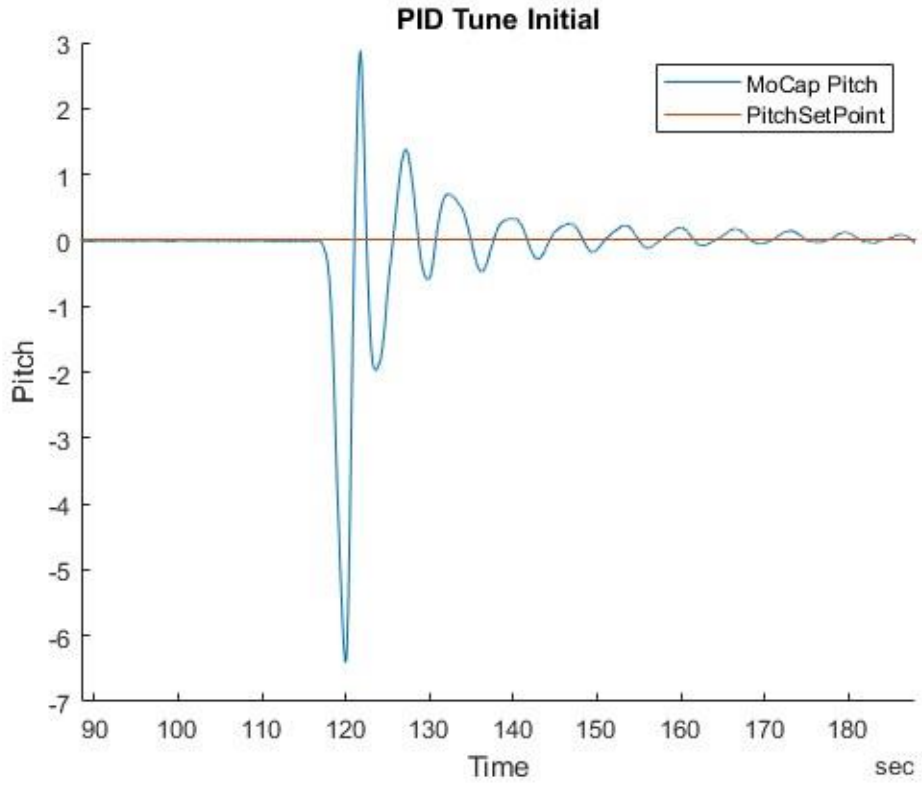

Figure 105: under-damped pitch response

The response from the unit is under-damped as it takes several oscillations to return to its setpoint. This indicates that the damping forces were not great enough, causing additional time for motion to reduce and the setpoint to be reached. To address this, the system was tuned with trial and error. The following set of PID values was chosen for the best pitch response.

$$\boldsymbol{P = 3 \mid I = 7 \mid D = 40}$$

The goal of these new parameters was to cause the system to be critically damped. With this characteristic, the unit will approach the setpoint with minimal overshoot and no oscillations. The effect of the final PID values is shown in the figure below.

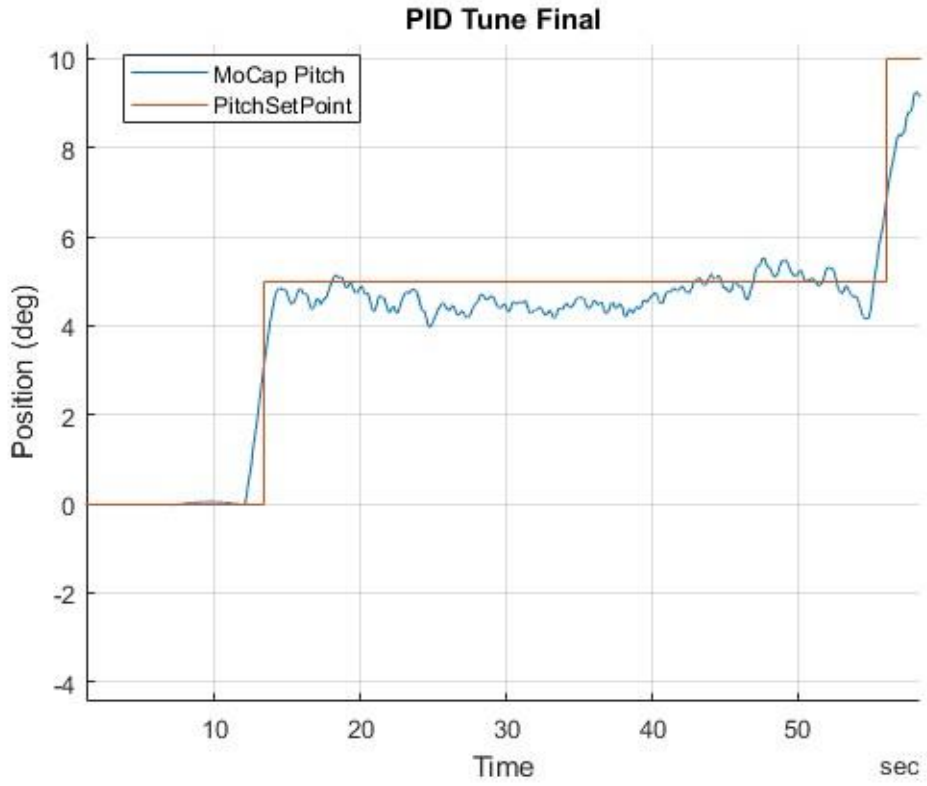

Figure 106: Final Pitch Tunning Step Response

The response above was caused by pushing down onto the test frame. Compared to the first response shown in Figure 91, this response damped out quicker and had less oscillation. This indicates that the additional dampening was effective at better controlling the pitch motions of the unit.

While in the dry dock basin, an attempt was made to tune the yaw controller. Due to limited width, the test frame contacted the side of the frame, breaking off the rear thrusters.

Figure 107: Broken Pitch Brackets

Completion of Run Matrix

The run matrix in Chapter 5 was completed while testing at the CWC. Several changes were made to the procedures and equipment configuration during testing to facilitate more effective testing. The first change was to perform multiple yaw setpoint locations in a single data collection because the system had to be restarted after each data collection time was saved, including multiple test frame positions in a single file. Due to the logistics of the test frame's location, it was more effective to combine pitch power runs and pitch PID tunning together at the dry dock basin. Yaw power and yaw PID tuning were still performed in the CWC as initially planned. The last significant change to occur during the

run matrix completion was two modifications to the current vane. The initial current vane geometry was not experiencing uniform flow from the CWC. The flat front of the test frame caused a dead zone to form along the top front of the system. To address this, a larger current vane was manufactured from a flat sheet and bar stock.

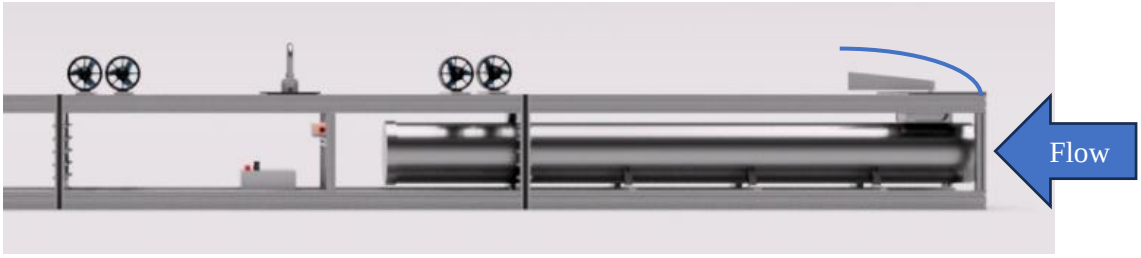

Figure 108: Flow Depiction over Frame Nose

After the taller current vane was installed, the sensor was able to record changes in angle. While it initially appeared that the sensor effectively identified the unit's angle to current, it was soon discovered that the yaw motion of the unit on the sensor caused it to deflect faster and act as an accelerator for the PID controller. This caused the unit to oscillate uncontrollably. To combat this, the current vane was moved behind the pivot point of the unit. With the vane behind the pivot point, the reaction force of the unit moving through the water will be opposite the direction of travel. This acted as a natural damping force, which was handled better by the PID controller.

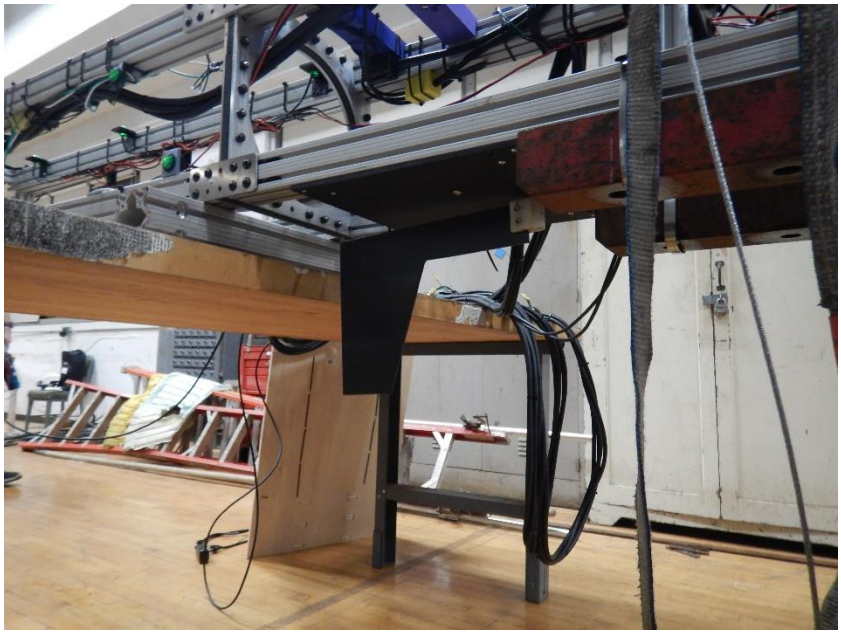

Figure 109: New Current Vane in Rear Position

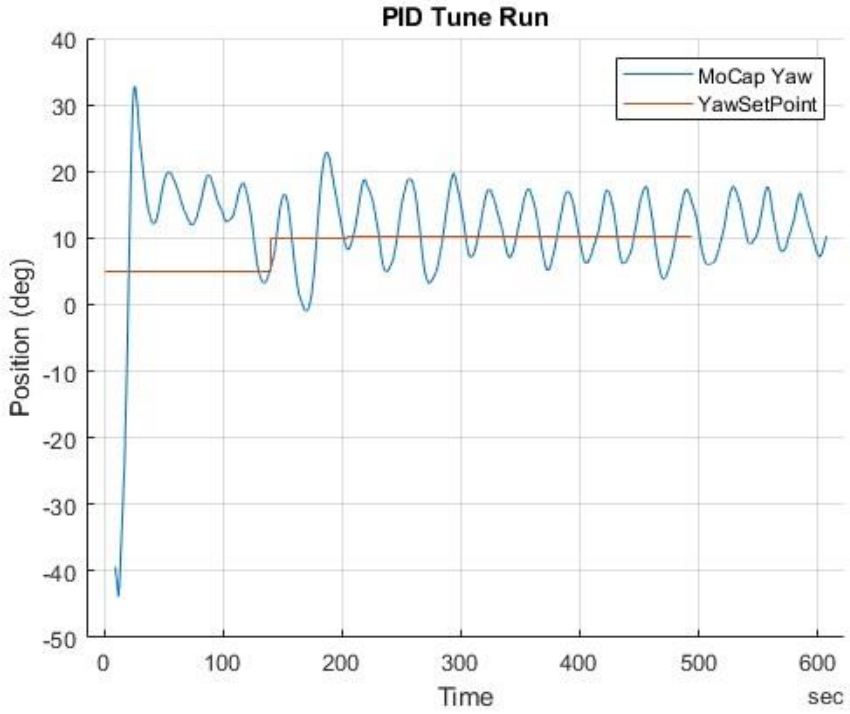

Figure 110: Yaw PID Controller Current Vane Initial Position

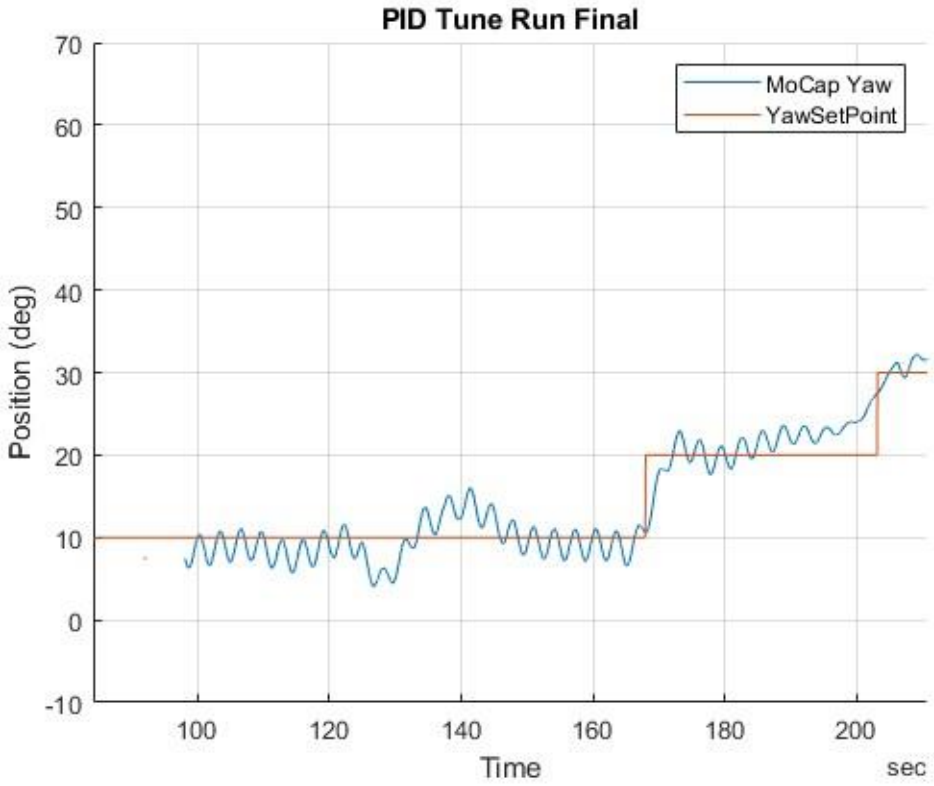

Figure 111: Yaw PID Controller Post Current Vane Position Switch

From the figures above, it can be seen how relocating the position of the current vane resulted in better unit performance. Even with the change of sensor location, the position hold performance for yaw was not perfect. The unit would still have oscillations. It was determined that improving performance was limited by the yaw sensor and PID controller. The following set of gains was used during the testing of the system.

Table 7: Yaw Controller PID Gain

Current Speed (kts)	P	I	D
0.5	10	-	2
1.0	20	0.25	2
1.5	30	0.5	2

Chapter 7
Model Testing Data Review

Collected Data

Data for this research was collected from two different sources: on board the test frame and the motion capture system. Data from onboard the test frame was collected at 8.3Hz, while the motion capture system was collected at 100Hz. When preparing the data for analysis, the motion capture data had to be time synced to the onboard sensor data. To do this, key events in each data set were matched together. During analysis, it was found that certain data sets experienced a timing error. This timing error began during the yaw PID tuning runs. The error caused the reported sample time to be less than real-time. When compared to motion capture, events captured by the yaw onboard sensors had different durations.

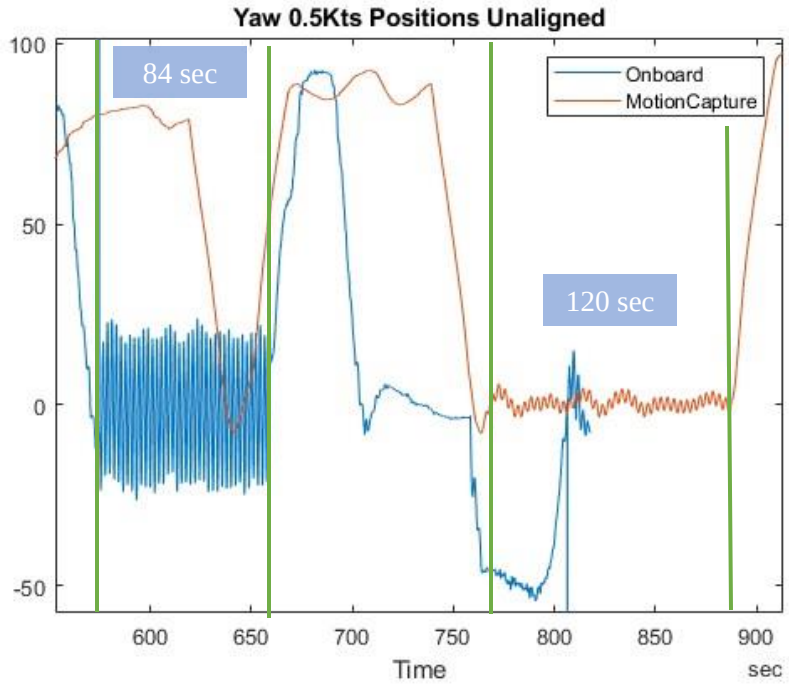

Figure 112: Event Duration Time Error

The event duration captured by the motion capture system was used as the ground truth, as there were multiple ways to validate the time reported by the system. Sample time from motion capture was validated by cross-referencing the frame time stamps, elapsed time, and frame rate. To correct the lower than real time sample time reported by the onboard unit, the data was remapped at a new frequency. Doing this added more time in between measurements. Fourier Analysis was used to convert certain events into the frequency space to validate that the corrected data was adjusted correctly. When examining the frequencies, the corrected data showed maximum power at the same frequencies as the motion capture data. This indicated that the adjusted data correctly displayed the test frame's response. While the data sets where the test frame’s sample time was incorrect were identified, an exact cause was not found. Additional examination will be required to find what change in the Simulink code caused this to happen. The graphs in this research will indicate what sensor the data came from. Those containing data from the onboard unit will have the correction applied. Data dependent on time, such as velocity, were taken directly from the motion capture system to eliminate possible errors in sample time.

With the data aligned, the primary analysis tool was graphing the data to observe overshoot, steady error, and thruster commands. In addition to graphing the data with controller data overlays, the average power used at each setpoint was calculated by taking the average power over the duration of the setpoint hold. The figure below shows an example of the data range utilized for average power.

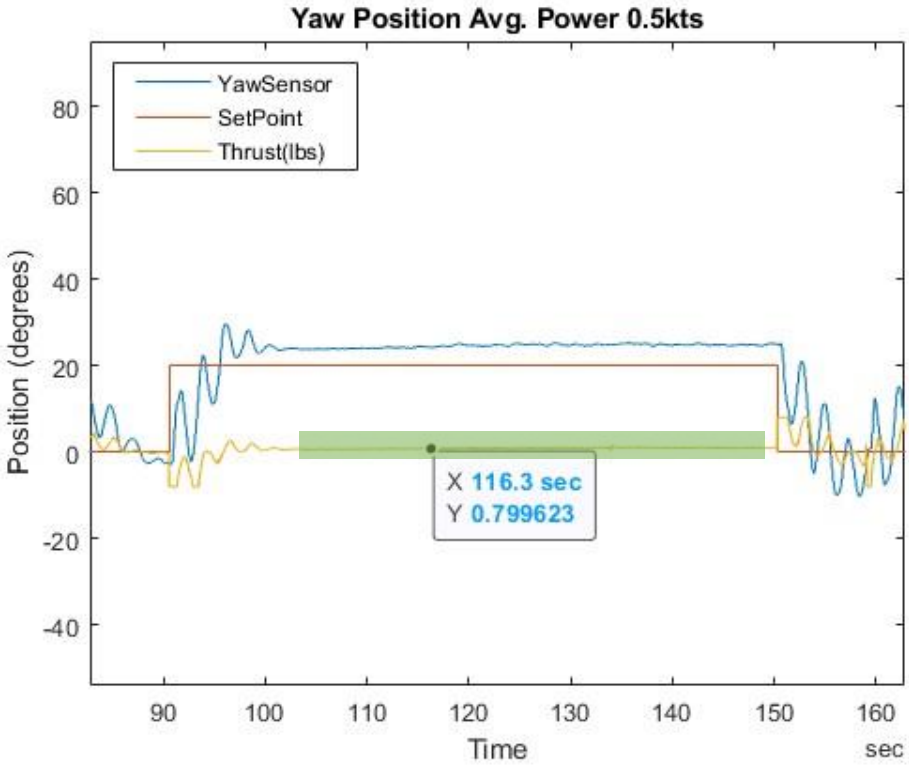

Figure 113: Yaw Position Average Power

The transparent green bounding box in the prior figure shows the area where the average power would be calculated for this setpoint.

The motion capture system gives a more accurate recording of position values. Reported error was low during this research. Error for a yaw position run is shown in the table below.

Table 8: Motion Capture Error Summary

	Error (in)		Error (deg)
X	0.0147	Roll	1.66
Y	0.0127	Pitch	0.19
Z	0.0054	Yaw	0.40

The motion capture data was of higher resolution and did not contain any of the sensor errors experienced by the onboard unit. The difference in these two data sets can be observed in the following figures.

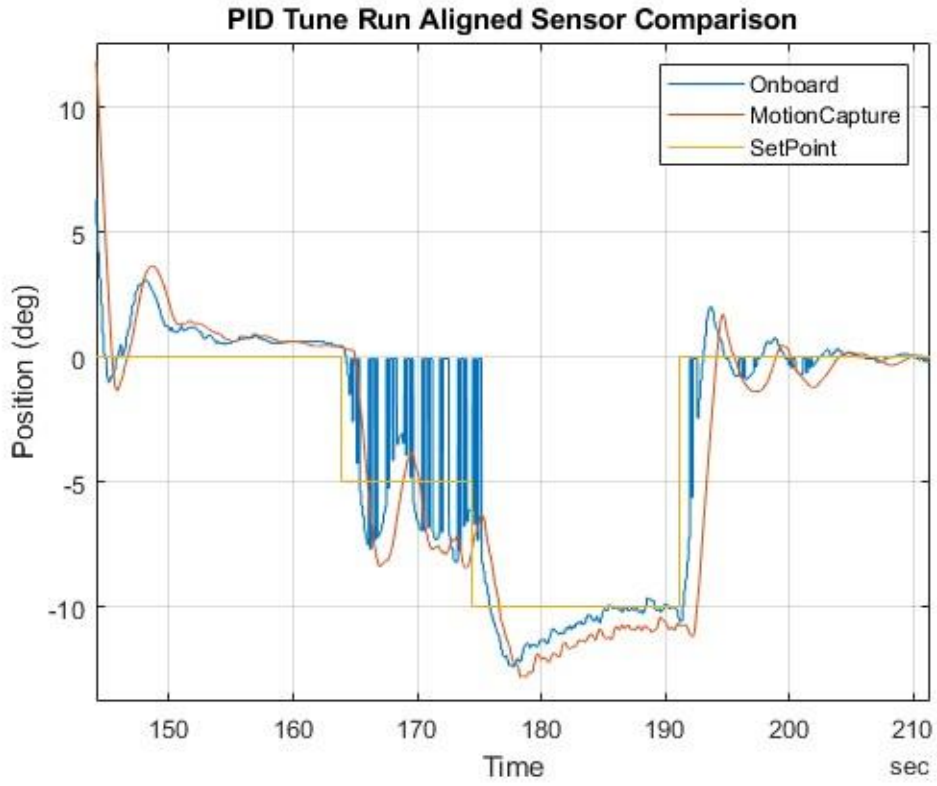

Figure 114: Onboard Position Data Vs. Motion Capture Event 1

In the figure above, the main advantage of motion capture is that it does not capture the errors in the sensor where the position was momentarily reported as -0.625 deg. This results in a more accurate data set tracking the frame position.

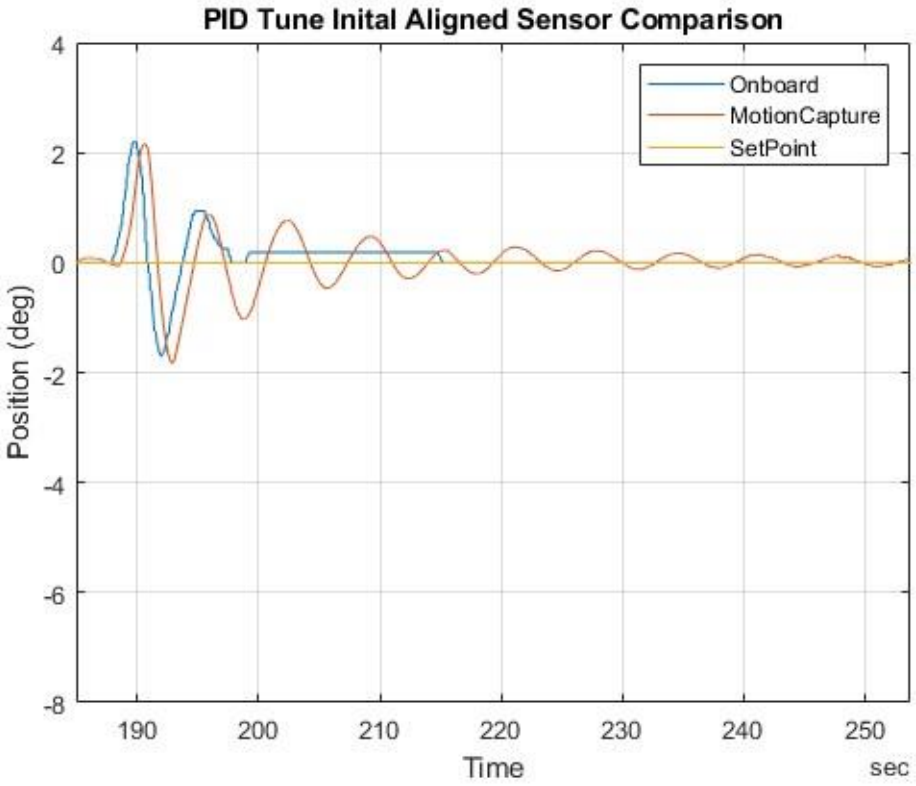

Figure 115: Onboard Position Data Vs. Motion Capture Event 2

The figure above shows how motion capture can track the unit's pitch position more accurately. The motion capture system has the resolution to track the small oscillations after they are no longer seen on the IMU.

The motion capture system is a valuable tool for tracking the motion of a body with high accuracy. The system is responsive and provided tracking with high accuracy for this research.

Yaw Control

Yaw control for the test frame was evaluated at three different current speeds: 0.5 kts, 1.0 kts, and 1.5 kts. Yaw control decreased as the current speed increased. The following set of graphs shows the range of motion and controller performance for the test frame in Yaw.

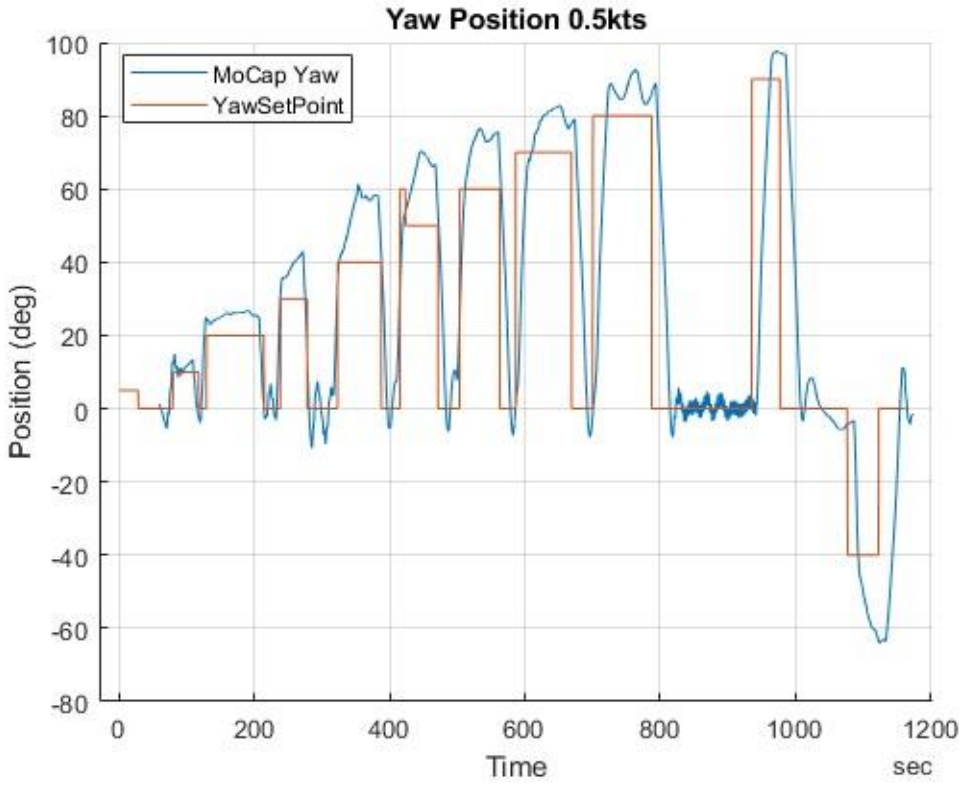

Figure 116: Yaw Position 0.5 kts full run

The figure above was collected during the unit test at 0.5 kts. From this plot, it can be seen that the unit struggled to maintain setpoints of 0 degrees. At this setpoint, the unit was prone to excess oscillation. This oscillation was likely caused by the limited response of the current vane at low speeds. A more accurate yaw sensor would reduce these oscillations and result in better control. At the 0.5 kts current speed, the unit was able to reach a maximum angle of 90 degrees in yaw.

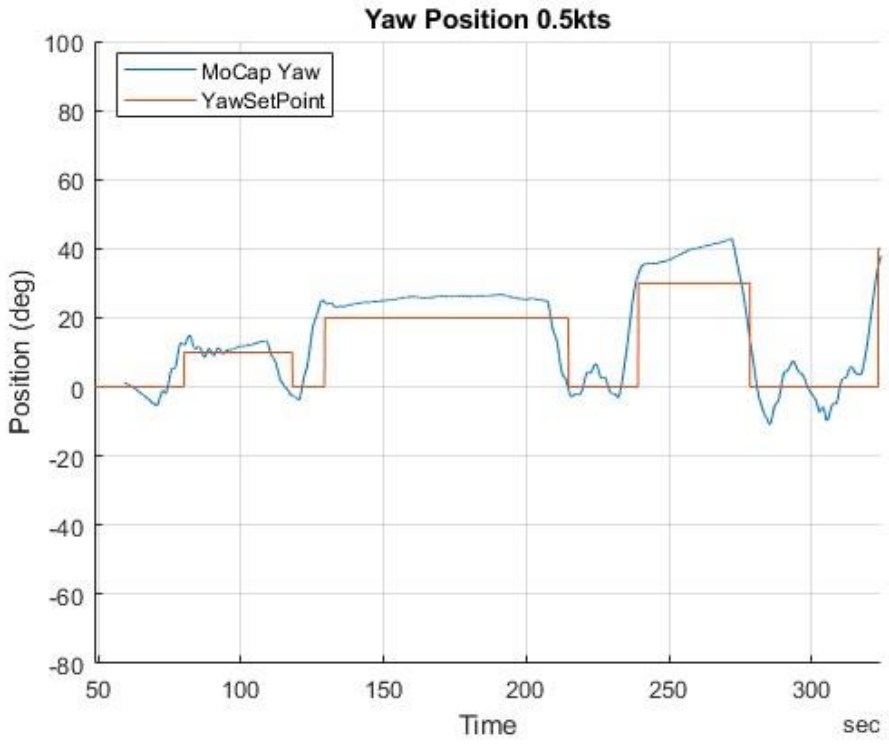

Figure 117: Yaw Detail Position 0.5 kts

The graph above shows a detailed view of the yaw response when adjusting setpoints. This detailed view shows how the unit transitions to a new setpoint with overshoot and eventual dampening. After dampening out, the unit settles out to constant thrust to maintain the current setpoint position.

When increasing the current speed to 1.0 kts, the maximum yaw position achieved decreased to 45 degrees. This was due to the increase in drag from the increased flow speed. More drag on the unit caused it to rotate, resulting in the thrusters working harder to maintain setpoint position. This trend continued when moving to 1.5 kts where the maximum yaw angle decreased to 20 degrees. At both 1.0 kts and 1.5 kts, it was observed that the unit was very sensitive to overshooting. Even though the thrusters were not reaching saturation holding the maximum yaw positions the unit was limited in the maximum angle achived by the pressence of overshoot. When overshooting occurred the thrusters would saturate and were unable to recover the vehicle back to the setpoint.

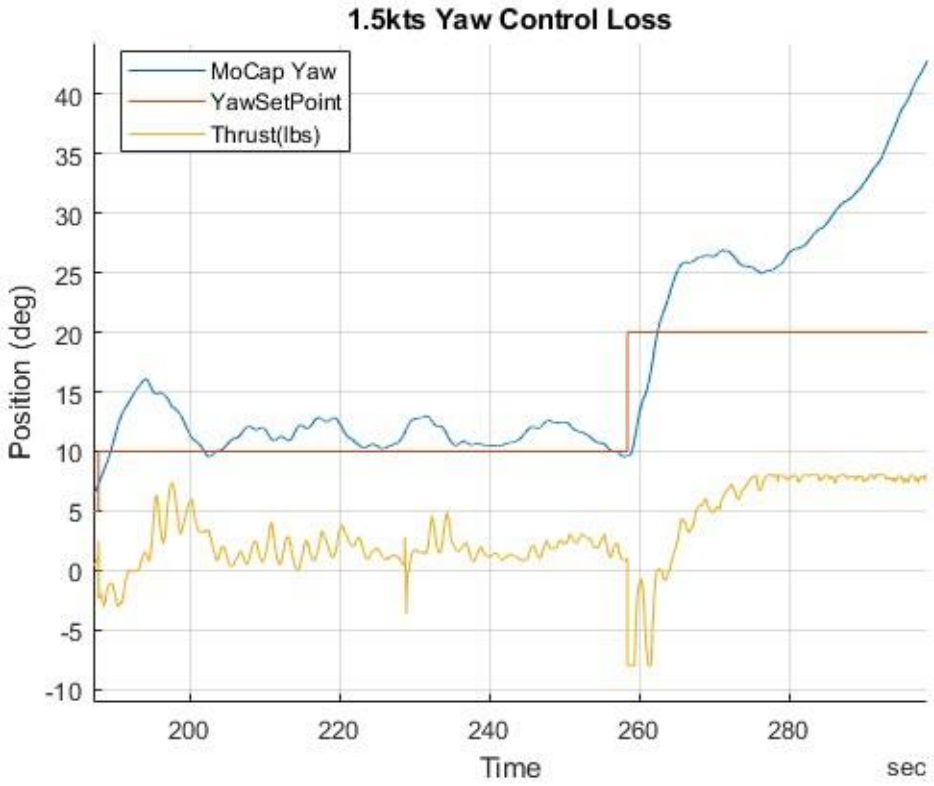

Figure 118: Yaw Control Loss

The figure above shows the position and thruster power for the test frame in 1.5 kts of current. The unit loses control when moving from the 10-degree setpoint to the 20-degree location. While the unit is moving to the setpoint, the thrusters begin to increase power to slow the unit and return to the setpoint. But due to the high inertia of the frame and moving into the flow, the thrusters are too slow to react, and the vehicle continues to move away from the setpoint despite the thrusters being fully saturated. This shows that while the unit has ample power to hold setpoints at higher angles, the process of moving and slowing the frame down requires higher thruster power. Finding this control loss location is highly important, as if the model was being used for a recovery mission and control loss occurred, the unit would have to be slowed down and reset. This process would be time-consuming, and the control loss could put the unit and AUV at risk of damage.

The following graphs and tables were produced to show the power needed at each setpoint based on the response and thruster power required to hold yaw setpoints.

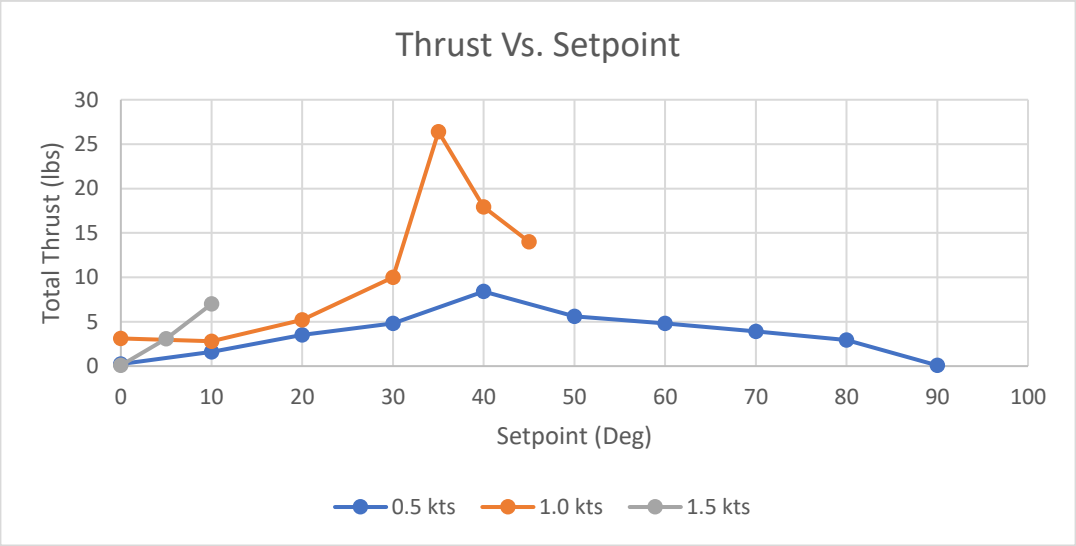

Figure 119: Thruster Power Vs. Setpoint

The graph above shows the total thrust required at each current speed to maintain different setpoints. Due to the control loss behavior detailed prior in this section not all yaw values could be tested for each current speed. The current speed of 0.5 kts allowed the unit to maintain yaw angles from 0-90 degrees. This allowed for an interesting trend to be seen in thruster power. The required thruster power maxes out at the 40-degree position and then decreases to near zero as the unit approaches 90 degrees. When in the 0/90 degree position, the unit has a limited amount of natural stability, allowing the thruster power to be near 0 lbs. However, when at the 40-degree position, the unit is furthest from either resting point, with a large surface area exposed to the current. This situation creates a large amount of drag, which tries to pivot the unit toward 90 degrees. While going past this yaw position, the total drag will increase with surface area, the required power to hold the yaw angle decreases as the setpoint becomes closer to 90 degrees.

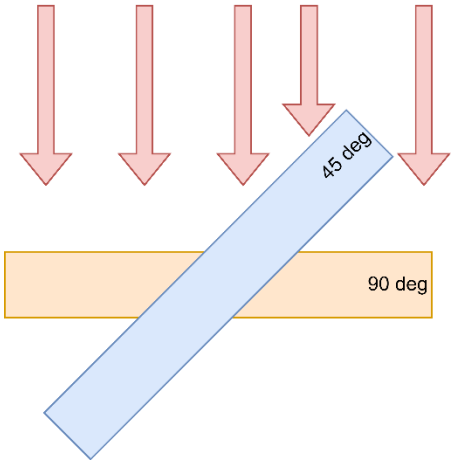

Figure 120: Exposed Surface Area to Flow 0.5 kts

This same behavior occurs for the 1.0 kts current speed. The maximum thrust required occurs at 35 degrees. Moving past this location, the required thrust decreases in a similar manner to that of the 0.5 kts trail. However, due to the control loss behavior associated with the higher current speeds, no data past 45 degrees was able to be collected. If more overhead in thruster power allowed the unit to maintain angles past 45 degrees, the required thrust should continue to reduce as the unit approaches 90 degrees. The following tables summarize the thrust required at each setpoint and current speed.

Table 9: Required Thrust and Setpoint

	Thrust (lbs)		
Yaw Position (deg)	**0.5**	**1.5**	**1**
0	0.24	3.12	0.08
5	-	-	3.08
10	1.6	2.8	7
20	3.52	5.2	-
30	4.8	10	-
35	-	26.4	-
40	8.4	17.92	-
45	-	14	-
50	5.6	-	-
60	4.8	-	-
70	3.92	-	-
80	2.92	-	-
90	0.08	-	-

The drag on the unit will increase greatly due to the velocity component of the drag equation.

$$F_d = \frac{1}{2}\rho v^2 C_d A$$

For the equation above, since all values except velocity are constant when at equivalent angles of yaw, the expected increase in drag and the resulting thrust will increase by a factor of v^2. The required total thrust can be plotted with the current speed with a trendline passing through a Y-int of zero to visualize this relationship.

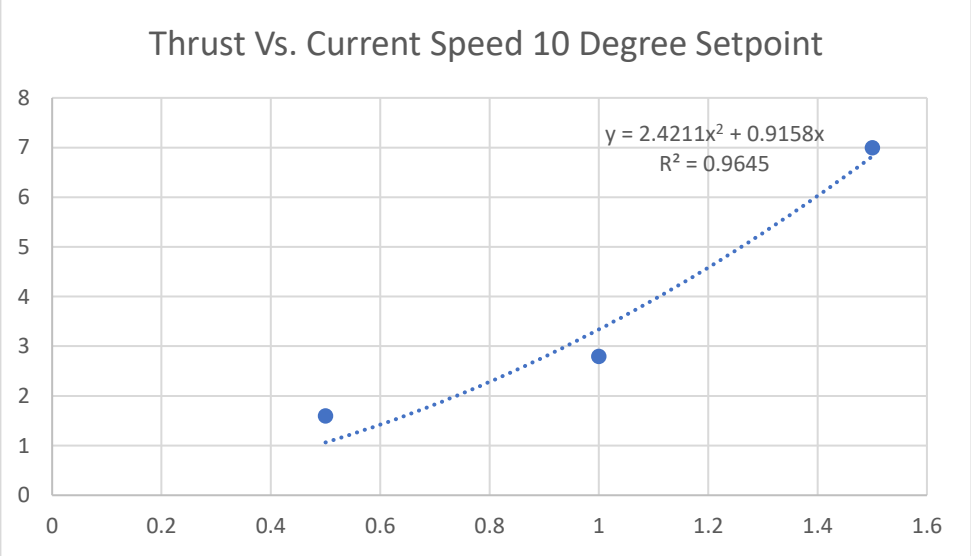

Figure 121: Required Thrust Relationship

The figure above plots the three data points on the graph with a base two polynomial line of best fit. This line of best fit follows the data points very well with an R^2 of 0.96, indicating that the trend line captures all the features of the original data points. This result shows that this experiment's drag relationship with velocity holds true, indicating that thrust measurements have been recorded correctly.

Different power settings were used to sweep the unit side to side to quantify the maximum yaw rates for the test frame. From these side-to-side motions, the angular rate could be calculated.

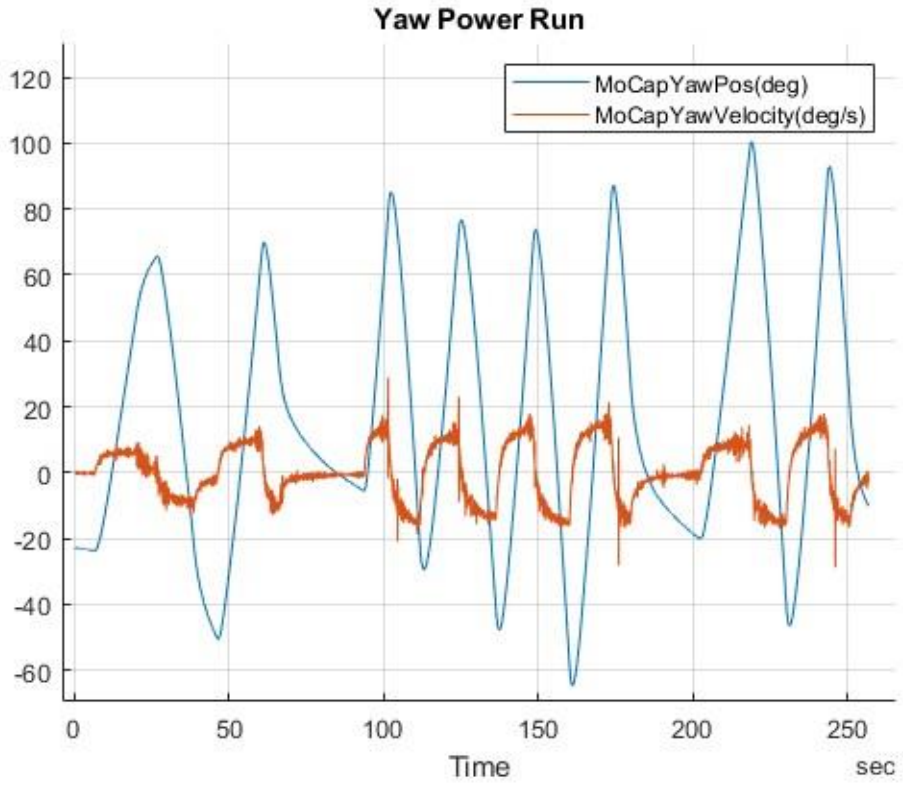

Figure 122: Yaw Power Sweep Runs

The maximum velocity reported by the motion capture system was used to calculate the yaw. The velocity represents the maximum speed the frame reached. The goal was to allow the frame to reach a constant velocity; however, due to tether limitations, the frame could not always reach a steady velocity.

Table 10: Yaw Rate

Yaw Power Sweep		
Thuster Power %	Rvs. Angular Velocity (deg/sec)	Fwd. Angular Velocity (deg/sec)
10	6.2	8.4
20	10.1	10.38
30	12.7	14.98
40	13.3	13.47
50	13.7	13.81
60	14.1	15
70	9.2	14.21
80	14.2	14.4

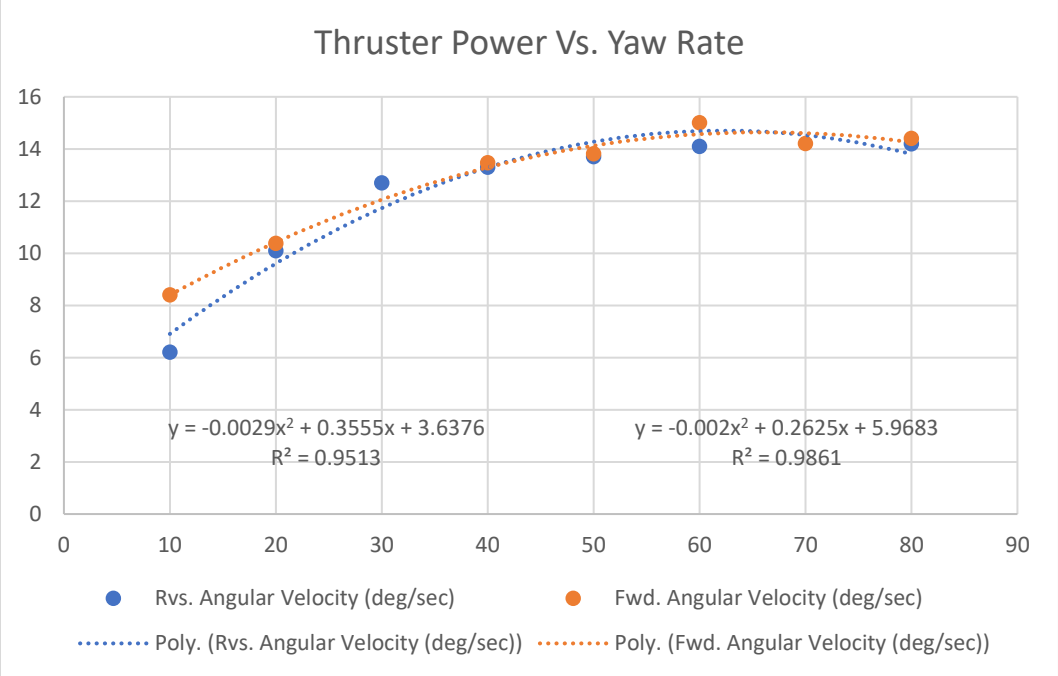

Figure 123: Thruster Power and Yaw Rate

The figure above shows the relationship between thruster power and yaw rate. To produce the figure above, two outliers from Table 8 were removed. When removed, a polynomial of order 2 trend line was fitted. These trend lines represent the estimated angular rate at a given thruster value. In the reverse thruster direction (clockwise), the R^2value was 0.95 and 0.98 for forward (counterclockwise), respectively.

Overall, the performance of the system in yaw was controllable but not ideal. The yaw sensor and PID gain tuning limited the performance of the system. However, despite not holding position with the utmost accuracy, the system could hold near the setpoints, allowing the required thruster power to be gathered. The required thruster power revealed an interesting behavior, where the maximum power is located between 40 and 45 degrees. Additionally, yaw rates for the frame at different thruster powers were documented. This information will assist in creating a digital hydrodynamic model for future research. Lastly, the drag equation current speed relationship was used to validate the trends observed in the required thruster power for the 10-degree yaw angle.

Pitch Control

The pitch control for the test frame was found to be highly effective at stabilizing the system and holding different angles. After PID tuning, the system was set to a 0-degree setpoint for most of the yaw position tests. In this configuration, the pitch controller worked to maintain a level system. The following graph shows the stability of pitch during a yaw position run.

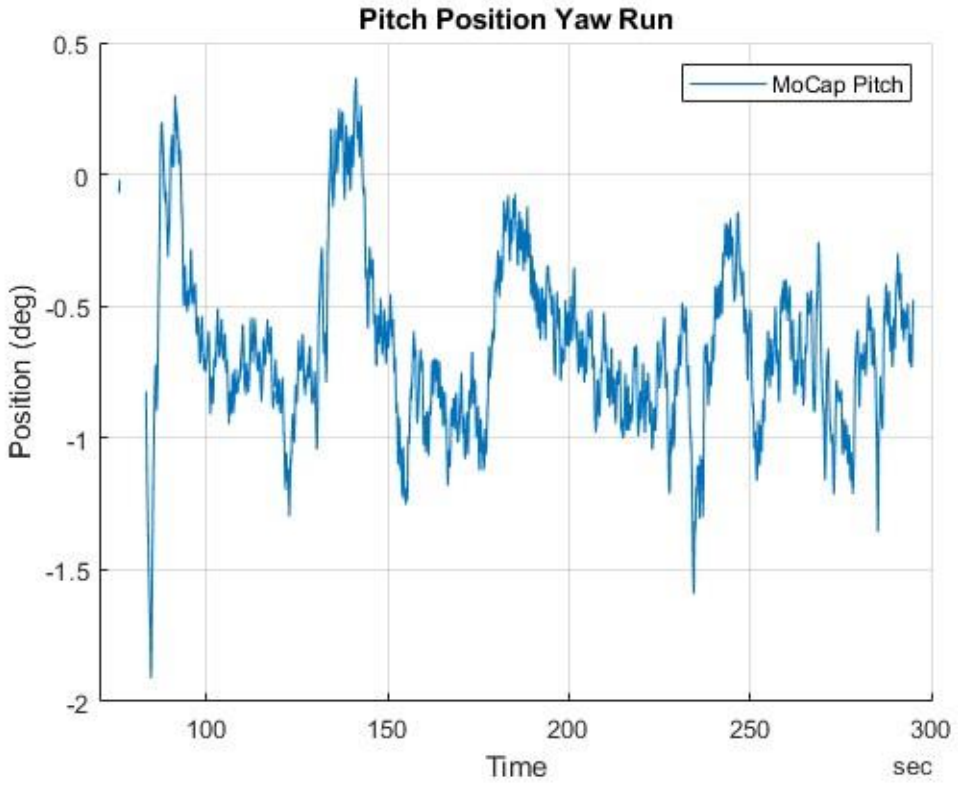

Figure 124: Pitch Stability

The graph above shows the pitch position of the test frame over the duration of a yaw data collection run. As seen in the graph, there are small oscillations in pitch centered around zero. The average pitch value for this run was -0.67 degrees, with a standard deviation of 0.29 degrees. This indicates that the controller and thrusters did an effective job of maintaining the 0-degree setpoint.

A pitch power angle test was completed to evaluate the performance of the pitch thrusters. This power test ran the thrusters at different power settings and recorded the angle at which the unit rotated to.

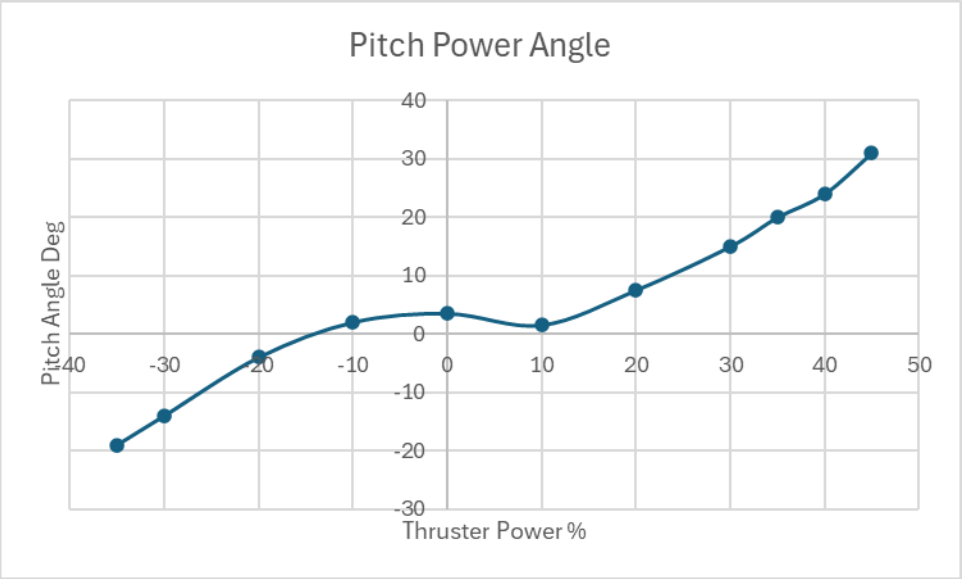

Figure 125: Pitch Power Maximum Angles

From the graph above, the unit had a resting state of just above 0 degrees of pitch. With no thrusters engaged, the unit rested at 3.5 degrees of pitch. Due to this offset, the graph does not have symmetry about 0 degrees. The pitch thrusters had ample power to move the unit in pitch. The data points in the figure above were limited due to the test frame's submersion depth. At the maximum pitch angles, a portion of the frame would be close to contacting the water's surface. If the unit had been suspended in deeper water, it would have likely been able to achieve high angles of pitch due to the combined power of the four pitch thrusters far from the pivot point of the frame.

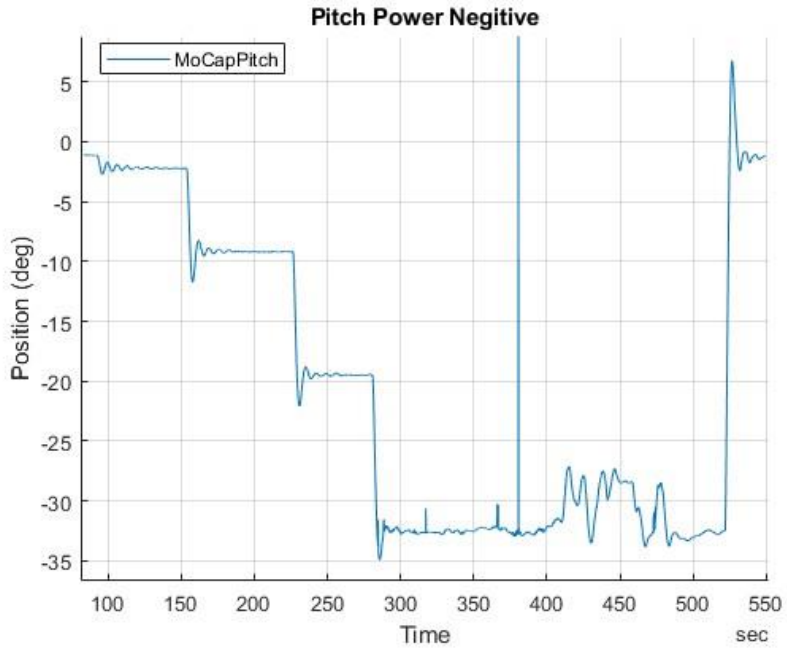

Figure 126: Pitch Angles Negative

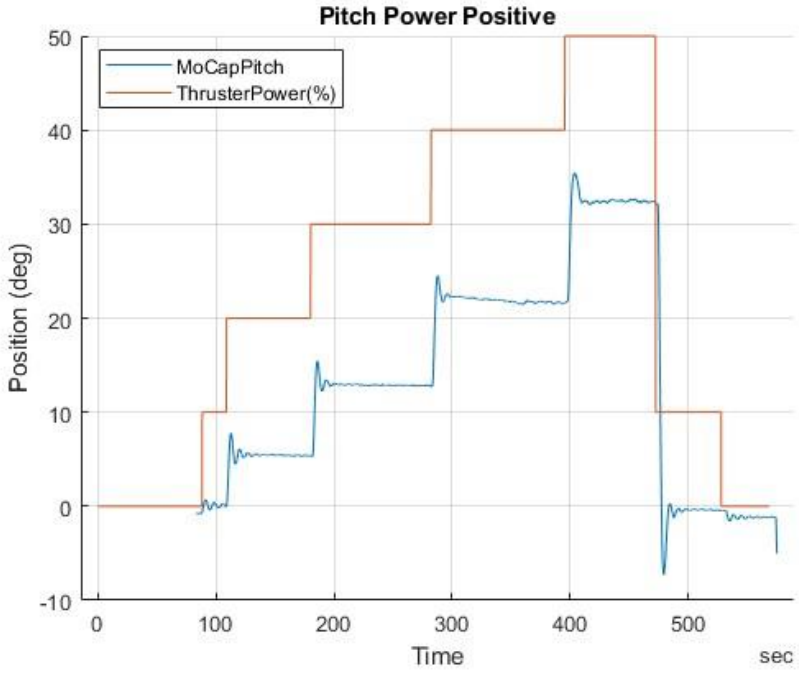

Figure 127: Pitch Angles Positive

Table 11: Pitch Power Maximum Angle

Pitch Power	
Thuster Power %	Max Angle
45	31
40	24
35	20
30	15
20	7.5
10	1.5
0	3.5
-10	2
-20	-4
-30	-14
-35	-19

Overall, the pitch control of the vehicle was very well controlled. The thrusters located on the back had ample control authority to position and maintain the desired setpoints. Due to the weight and natural pitch stability, the test frame was able to remain stable in still water without the need for PID control. When applying thrust, the unit would adjust pitch and then naturally dampen out. This dampening is shown in Figures 123 and 124. The behavior observed assisted the PID loop by providing a natural damping force.

Additional System Observations

In addition to the testing laid out in the run matrix, an experiment was conducted where the pitch setpoint was changed in combination with yaw. This aimed to show whether the unit could maintain yaw and pitch angles offset to the current. This setup would challenge both controllers.

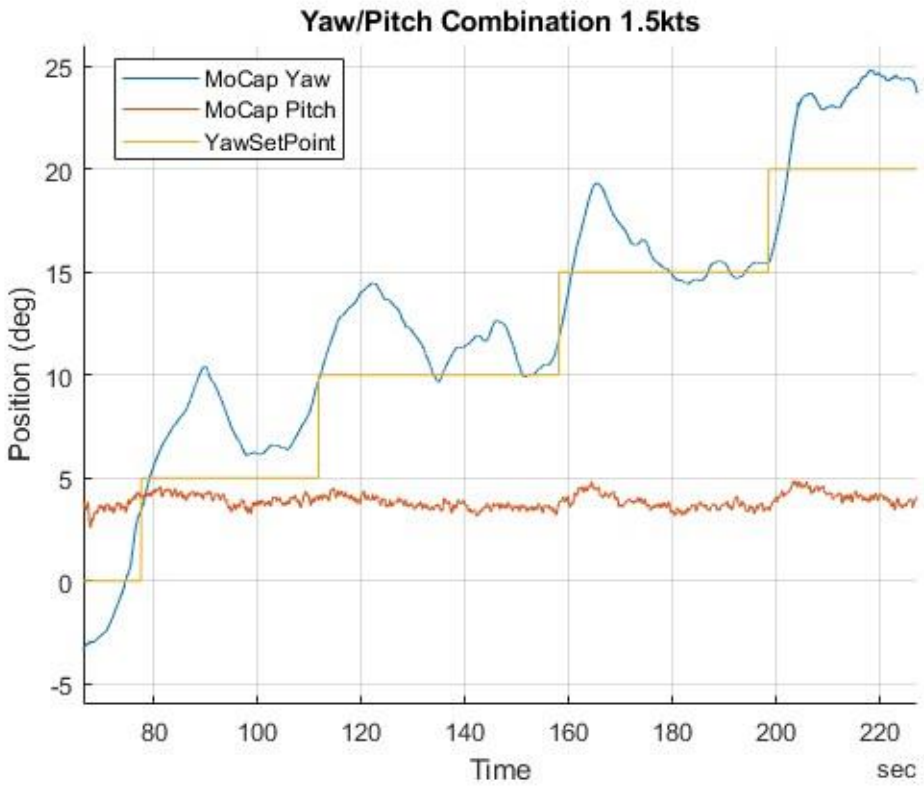

Figure 128: Yaw Pitch Combination Yaw Sensor

The figure above shows the output from the yaw sensor during the combination position hold. This run was completed with a current flow of 1.5 kts with the pitch position set to 5 degrees. The unit behaved very similarly to when the pitch setpoint was 0 degrees. This indicated that small pitch adjustments would not adversely affect yaw position hold performance even at the high current speed. When moved to the 5-degree setpoint, the average pitch over the duration of the setpoint was 3.8 degrees, with a standard deviation

of 0.33 degrees. The results of this trial show that at nonzero pitch values, the controller suffered from a minor increase in error. The pitch controller can control the pitch angle of the frame well and in higher current states.

The testing of the capturing frame in the CWC revealed several interesting behaviors. The first observation was the presence of sensor feedback errors. During some trials, the yaw or pitch sensor would return incorrect values for a single time step. This could sometimes cause a fast reaction from the PID controller, which perturbs the model. To limit the effect of these sensor errors, a low-pass filter with a cutoff frequency of 5 Hz was used.

Testing of the unit revealed the complex dynamics the system faced. The high inertial of the system, along with the current direction, could create more and less favorable conditions for approaching setpoints. The worst case condition is when the unit swings from one side to the other, for example, -45 to 45 degrees. During this action, the unit has to provide high thrust to push into the current and cross the 0-degree yaw position. After crossing zero, the unit then uses the thrusters to push in the current's direction, further accelerating the motion. This accelerated motion makes it difficult for the unit to stop due to the high inertia and continuing to move the frame. Due to this, the PID controller derivative gain needed to be set properly. With the gained tunned correctly, the unit could apply reverse thrust before approaching the setpoint when moving in the direction of the current. This was achieved by having a high D gain, which would work to cap the maximum rate at which the unit moved. This system was not perfect, and in some cases, the system still needed to react faster. To compensate for this problem, a more refined yaw controller could be developed, which would use a different set of gains when moving in or away from the current direction.

Chapter 8
Conclusion

Overall Model Performance

Testing in the CWC at NSWCCD revealed many promising and interesting operational characteristics of the test frame. The pitch control of the test frame was very strong, and the controller was easily tuned using the Zeigler-Nickolas method. Tests where the model was perturbed in pitch showed a strong and fast recovery response. During testing in flow, the unit was able to hold the pitch setpoint of 0 degrees with high accuracy and little fluctuation. In addition to success at the 0 degrees setpoint, the pitch controller was also able to hold setpoints of 0, 10, and -10 degrees without issue. This performance indicates that the positioning and power of the pitch thrusters were more than adequate to control the model's motion.

Yaw performance was limited by the accuracy and performance of the current vane. Due to the current vane being a flat plate, it had little corrective moment from hydrodynamic forces. This caused the vane to oscillate as it reacted to current contacting the sides of the plate rather than hydrodynamic stability. The limitation of this sensor can be seen in the yaw setpoint performance. At all setpoints, the unit suffered from small oscillations driven by the sensor. However, even with the oscillations, it was observed that the unit had the required power to hold yaw positions. The maximum yaw position the unit is able to maintain is driven by the current speed. At 0.5 kts of current, the unit was able to maintain a maximum angle of 90 degrees. At 1.0 kts, this value was limited to 45 degrees and at 1.5 kts this value lowered to 20 degrees. In addition to lowering the maximum yaw angle at higher current speeds, the unit became very sensitive to overshoot. When approaching the maximum yaw angle, if overshoot occurs, the unit may not be able to recover back to the setpoint due to a rapid nonlinear increase in the hydrodynamic drag forces. In this research, an attempt to stop overshoot was done, making the derivative term more significant. Due to limitations in the sensor and controller tunning time, overshoot was not able to be eliminated.

The motion capture setup used for this research performed very well. The camera rig was rigid and stable, requiring no maintenance during testing. The cameras provided a large capture volume with low error for data collection. The positioning of the lights along the unit performed excellent. The system was able to resolve the rigid body reliably with high accuracy. Data was easily gathered from the system, and the great operational capability of the motion capture system was demonstrated. The system was able to provide a reliable method of measuring 6 DoF motion without costly sensors installed on the test frame.

The mechanical structure and electronics setup for the test model performed excellent. There were no mechanical failures during CWC testing. The unit was able to successfully support all the ballast weight needed. All pressure enclosures remained dry, and no ill effects were seen on the onboard sensors. Connection to the surface through motor and data tethers was excellent. The chosen cables had ample strength and ruggedness to perform through multiple rig and de-rig procedures. Power supplies connected to the thrusters were able to provide all the needed power for the system without tripping any breakers in the CWC.

The Simulink control software setup was extremely valuable for tunning the model controllers and running the data collection runs. The ability to quickly reformat the control software allowed for the reconfiguration of the yaw PID controller, resulting in tuning success. The model setup allowed for real-time graphing of vehicle position, setpoint, and thruster values. These readouts, along with real-time tuning of the PID parameters, allowed for quick and efficient tuning of the control loops. The real-time tuning facilitated a great learning opportunity for the researcher, along with successful PID tuning.

Feasibility for Midwater Capture

Based on the observed controllability for Yaw and Pitch, capturing an AUV midwater with a garage-type structure would be feasible. While the test unit did not demonstrate a perfect yaw position hold, the yaw sensor performance limited this action. For creating an open water deployed AUV capturing device, accurate measurement of yaw position will be critical to the unit's success. Along with this, the control system will need to have a wide variety of inputs that can consider parameters such as current speed and direction of travel to adjust the PID settings accordingly. Increasing the amount of data going into the PID loop could also increase performance. In this research, only the yaw position was used for feedback. Adding yaw rate would improve the dampening performance of the controller. Addressing the issue of overshooting and required damping would be critical to a frame deployed in the ocean, as if overshooting occurs at higher current speeds, the unit would be unrecoverable. If this happens during an AUV recovery operation, the AUV would have to reset course, and the unit would need to be fully reset back to a stable position. Due to the system being naturally unstable with no fins or other corrective surfaces present, losing control of the system would introduce many undesirable behaviors that may damage the capturing device or AUV. With a more robust control system and additional sensor inputs, the precise control of an AUV garage has a strong likelihood of success based on the experiments in this research.

Summary and Future Work

Overall, this research proved the feasibility of midwater AUV capture and demonstrated the testing possibilities provided by a controlled flow facility. Performing these experiments in the facility allowed for a controlled current environment to be used. In the current controlled CWC environment, the pitch and yaw controllers' performance was well observed and optimized. Based on the performance of this research, two areas of future research can be proposed.

Model Testing

For the testing of this model, the performance was limited by the yaw sensor. To overcome this limitation inside the facility, the OptiTrack motion capture system could be used as a PID controller input. The OptiTrack motion capture system can export a real-time UDP data stream of rigid body position. Utilizing this output, the yaw controller would get a highly accurate and responsive yaw position for vehicle control. This type of system should be straightforward to implement as Simulink real-time can read a UDP stream and pull required values. These values could be mapped to the corresponding PID subsystem, where they would replace onboard sensor values. Future tests could also use a smaller tether section for the surface connection. While the tethers used in this experiment were rugged and performed well, they were bulky. This made working with them heavy, and their effects on the model had to be managed. If smaller tethers were used, there would be less impact on the model's motion. Like the tethers, a different lifting setup could also be implemented with a smaller connection point on the swivel hoist. The equipment used in this research limited the ability of the swivel hoist to move freely. While the hoist was still able to move, reducing the forces that can cause motion in the frame will improve the model's response. Lastly, a more robust communication method could be used to bring data from onboard sensors to the surface. While the SPI and I2C connections performed well during CWC testing, a more robust setup like CAN or RS-485 would have provided additional tether length and fewer sensor errors.

AUV Garage Feasibility

Based on the model's performance tested, future research should include the production of a fully dynamic simulation of the system. Developing a hydrodynamic model for the system and running it in a virtual environment would allow PID parameters and different control systems to be tested prior to in-water experiments. Due to the high nonlinearity of the forces experienced by the model while exposed to current, building this computer model would provide valuable insights into how best to control the system in difficult-to-control conditions. To make this hydrodynamic model, several areas must be refined and modeled in a computer environment. The distribution of all mass on the model would need to be known to calculate the Center of Buoyancy (CB), Center of Gravity (CG), and

Moment of Inertial. In addition to this, a hydrodynamic model of the vehicle geometry would need to be analyzed with Computational Fluid Dynamics (CFD) to develop various hydrodynamic coefficients, such as the drag coefficient for the unit at different orientations. Lastly, a model for the performance of the thrusters would need to be known. The combination of these studies could be used as input to a dynamic simulation based on the equations of motion present in Fossen's “Marine Craft Hydronamics and Motion Control” (13). Completing this work would allow for this complex system's controls development and PID tuning.

Overall, this research successfully examined the feasibility of AUV midwater capture. A physical model was developed and tested in a unique facility, revealing many interesting control and hydrodynamic attributes.

References

[1] Hobson, B. W., McEwen, R. S., Erickson, J., Hoover, T., McBride, L., Shane, F., & Bellingham, J. G. (2007, September). The development and ocean testing of an AUV docking station for a 21" AUV. *OCEANS 2007*. http://dx.doi.org/10.1109/oceans.2007.4449318

[2] Xie, T., Huang, L., Guo, Y., & Ou, Y. (2022). Modeling and simulation analysis of active heave compensation control system for electric-driven marine winch under excitation of irregular waves. *Measurement and Control*, *56*(5–6), 1004–1015. https://doi.org/10.1177/00202940221101666

[3] de Las Heras, Ana & Luque, A. & Cordoba, Antonio & Ramos Calderón, Teresa. (2022). Total Design in the Design and Development Process of a Remotely Operated Vehicle (ROV) with Particular Consideration of Sensorization. Sensors. 2022. 3284. 10.3390/s22093284.

[4] *Working offshore*. (n.d.). https://www.shipseducation.com/info/offshore/dynamic-position-5.html

[5] *Moonpool*. (2020, January 29). REV Ocean. https://www.revocean.org/vessel/moonpool/

[6] Stevenson, Peter & Furlong, Maaten & Dormer, David. (2009). AUV Design: Shape, Drag and Practical Issues. Sea Technology. 50.

[7] *What is an Underwater ROV?* (2019, September 23). Blue Robotics. https://bluerobotics.com/learn/what-is-an-rov/

[8] *Hydroid introduces the new generation REMUS 100 AUV*. (2016, March 14). Business Wire. https://www.businesswire.com/news/home/20160314005318/en/Hydroid-Introduces-the-New-Generation-REMUS-100-AUV

[9] von Oppeln-Bronikowski N,de Young B, Belzile M, Comeau A,Cyr F, Davis R, Emery P, Richards C,Hebert D and Van Der Meer J (2023) Best practices for operating underwater gliders in Atlantic Canada. Front. Mar. Sci. 10:1108326.doi:10.3389/fmars.2023.1108326

[10] *Description*. (n.d.). Retrieved April 9, 2024, from https://spray.ucsd.edu/pub/rel/info/spray_description.php

[11] Agarwal, T. (2020, July 24). *Open loop & closed loop control system and their differences*. ElProCus - Electronic Projects for Engineering Students. https://www.elprocus.com/difference-between-open-loop-closed-loop-control-system/

[12] Soper, M. (n.d.). *What is a PID loop?* Retrieved April 9, 2024, from https://www.setra.com/blog/what-is-a-pid-loop

[13] Fossen, T. I. (2021). *Handbook of marine craft hydrodynamics and motion control*. John Wiley & Sons.

[14] *Blue robotics - Underwater rovs, USVs, Thrusters and sonars!* (2020, January 7). Blue Robotics. https://bluerobotics.com/

[15] Wu, C.-J. (2018). *6-DoF Modelling and Control of a Remotely Operated Vehicle* [Master Thesis]. Flinders University.

[16] Libretexts. (2020, May 19). 9.3: PID tuning via classical methods. *Libretexts*. https://eng.libretexts.org/Bookshelves/Industrial_and_Systems_Engineering/Chemical_Process_Dynamics_and_Controls_(Woolf)/09%3A_Proportional-Integral-

Derivative_(PID)_Control/9.03%3A_PID_Tuning_via_
Classical_Methods

[17] plcynergyadmin. (2021, January 16). *What is A PID controller and how it works?* PLCynergy. https://plcynergy.com/pid-controller/

[18] *Motion capture systems*. (n.d.). OptiTrack. Retrieved April 9, 2024, from https://optitrack.com/

[19] : Schroeder S, Jaeger S, Schwer J, Seitz AM, Hamann I, Werner M, et al. (2022) Accuracy measurement of different marker based motion analysis systems for biomechanical applications: A round robin study. PLoS ONE 17(7): e0271349. https://doi.org/10.1371/journal.pone.0271349

[20] Sun, K.; Cui, W.; Chen, C. Review of Underwater Sensing Technologies and Applications. Sensors 2021, 21, 7849. https:// doi.org/10.3390/s21237849

[21] *Light penetration in water - Responsible Seafood Advocate*. (2014, November 1). Global Seafood Alliance. https://www.globalseafood.org/advocate/light-penetration-in-water/

[22] *Optitrack for Non-GPS Navigation — Copter documentation*. (n.d.). Retrieved April 9, 2024, from https://ardupilot.org/copter/docs/common-optitrack.html

[23] *Reconstruction and 2D mode*. (n.d.). EXTERNAL OptiTrack Documentation. Retrieved April 10, 2024, from https://docs.optitrack.com/motive/reconstruction-and-2d-mode#applying-changes-to-3d-data

[24] *CoordinateTransformations*. (n.d.). Retrieved 2024, from https://motion.cs.illinois.edu/RoboticSystems/CoordinateTransformations.html

[25] *Motive software setup and usage*. (n.d.). Stanford Flight Room. Retrieved April 9, 2024, from https://stanfordflightroom.github.io/motion_capture_motive

[26] *Original prusa enclosure*. (n.d.). Prusa3D by Josef Prusa. Retrieved April 9, 2024, from https://www.prusa3d.com/product/original-prusa-enclosure-3/?country=US&currency=usd&gad=1&gclid=Cj0KCQjwm66pBhDQARIsALIR2zAVHXO9ErV4gF-RWiKmnE8C85Z7q9ptTHIHrn-OFHVpkZop_PbSSWcaAk7YEALw_wcB\

[27] P. Baillon, S. Dixon, K. Faust, P. Herman, H. Seabring and S. Wood, "Stereolithography 3D Printed Resin Pressure Enclosures Applied in the Marine Environment," *OCEANS 2022, Hampton Roads*, Hampton Roads, VA, USA, 2022, pp. 1-7, doi: 10.1109/OCEANS47191.2022.9977042.

[28] *Anycubic Photon Mono X*. (n.d.). ANYCUBIC-US. Retrieved April 9, 2024, from https://www.anycubic.com/products/photon-mono-x-resin-printer

[29] Parker Hannifin. (2021). In *Parker O-Ring Manual*.

[30] *Arduino hardware - MATLAB & simulink*. (n.d.). Retrieved April 9, 2024, from https://www.mathworks.com/help/supportpkg/arduino/index.html

[31] *Fathom-X tether interface board*. (n.d.). Blue Robotics. Retrieved April 9, 2024, from https://bluerobotics.com/store/comm-control-power/tether-interface/fathom-x-tether-interface-board-set-copy/

[32] *Amazon.com: DriverGenius NT50 USB 2.0 Ethernet extender over cat5e/cat6/cat7*. (n.d.). USB Network RJ45 Extender Repeater up to 165ft (50M) Compatible for Win/Mac/Ubuntu (Driver Free Version) : Electronics. Retrieved April 9, 2024, from

https://www.amazon.com/dp/B01K9V7D18?psc=1&ref=ppx_yo2ov_dt_b_product_details

[33] *External Device Sync Guide: ESync 2*. (n.d.). EXTERNAL OptiTrack Documentation. Retrieved April 9, 2024, from https://docs.optitrack.com/synchronization/synchronization-hardware/external-device-sync-guide-esync-2

[34] Cario, G.; Casavola, A.; Gagliardi, G.; Lupia, M.; Severino, U. Accurate Localization in Acoustic Underwater Localization Systems. Sensors 2021, 21, 762. https://dx. doi.org/doi:10.3390/s21030762

[35] Siregar, S.; Trilaksono, B.R.; Hidayat, E.M.I.; Kartidjo, M.; Habibullah, N.; Zulkarnain, M.F.; Setiawan, H.N. Design and Construction of Hybrid Autonomous Underwater Glider for Underwater Research. *Robotics* 2023, *12*, 8. https://doi.org/10.3390/robotics12010008

[36] Ji D-H, Choi H-S, Kang J-I, Cho H-J, Joo M-G, Lee J-H. Design and control of hybrid underwater glider. Advances in Mechanical Engineering. 2019;11(5). doi:10.1177/1687814019848556

[37] *Electronic enclosures & accessories*. (2017, April 28). Bud Industries. https://www.budind.com/

[38] Devices, C. (n.d.). *AMT22 Series datasheet - modular | absolute | CUI devices*.

[39] *Serial peripheral interface (SPI)*. (n.d.). SparkFun Learn. Retrieved April 9, 2024, from https://learn.sparkfun.com/tutorials/serial-peripheral-interface-spi/all

[40] Weisstein, E. W. (n.d.). *Euler Angles -- from Wolfram MathWorld*. Retrieved April 9, 2024, from https://mathworld.wolfram.com/EulerAngles.html

[41] Campbell, S. (2016, February 13). *Basics of the I2C communication protocol*. Circuit Basics. https://www.circuitbasics.com/basics-of-the-i2c-communication-protocol/

[42] *T200 thruster*. (n.d.). Blue Robotics. Retrieved April 9, 2024, from https://bluerobotics.com/store/thrusters/t100-t200-thrusters/t200-thruster-r2-rp/

[43] *DROK*. (n.d.). DROK. Retrieved April 9, 2024, from https://www.droking.com/

[44] *Basic ESC*. (n.d.). Blue Robotics. Retrieved April 9, 2024, from https://bluerobotics.com/store/thrusters/speed-controllers/besc30-r3/

Appendix

MATLAB/Simulink Code

Pitch Plot Creator:

```
clear all
close all
clc

load("MoCap\YawHighPositions_002.mat")
load("PitchDataFiles2\YawPitchCombinationRun_002.mat")

%Create Time table of Frame Pitch
FramePitch = timeseries2timetable(TestDataPitch.PitchPos);
FramePitch.PitchPos = FramePitch.PitchPos*-1;

%Move Elasped Time into Time Collum of Timetable
FIT_Test_Frame_2.Body.Time = seconds(FIT_Test_Frame_2.Body.Time_Elapsed);

%Remove Data Error from IMU output
FramePitch(any(FramePitch.PitchPos == -0.0625,2), :) = [];
FramePitch(any(FramePitch.PitchPos == 0.0625,2), :) = [];

figure(1)
plot(FramePitch,"PitchPos")
hold on
plot(FIT_Test_Frame_2.Body,"Pitch")
legend("Onboard","MotionCapture")
title("PID Tune Initial Unaligned")

%%%%%%%%%%%%%%%%%%%%%%%%%%%
%Insert Offsets for time delay and IMU
tMFP = seconds(76);
offset = 0;
%%%%%%%%%%%%%%%%%%%%%%%%%%%

%Apply Adjustments to MoCap
FIT_Test_Frame_2.Body.Time = FIT_Test_Frame_2.Body.Time + tMFP;
FIT_Test_Frame_2.Body.Pitch = FIT_Test_Frame_2.Body.Pitch + offset;

%Plot to check results align
figure(2)
plot(FramePitch,"PitchPos")
hold on
plot(FIT_Test_Frame_2.Body,"Pitch")
```

```
plot(TestDataPitch.PitchSetPoint)
legend("Onboard","MotionCapture","SetPoint")
title("PID Tune Inital Aligned Sensor Comparison")
ylabel("Position (deg)")
grid on

%Plot Figure for Thesis Doc
figure(3)
hold on
plot(FIT_Test_Frame_2.Body,"Pitch")
plot(TestDataPitch.PitchSetPoint)
legend("MoCap Pitch","PitchSetPoint")
title("Pitch Position Yaw Run")
ylabel("Position (deg)")
grid on

figure(4)
hold on
plot(FIT_Test_Frame_2.Body,"Pitch")
legend("MoCap Pitch")
title("Pitch Position Yaw Run")
ylabel("Position (deg)")
grid on

%Average Position Hold Values
FIT_Test_Frame_2.Body = rmmissing(FIT_Test_Frame_2.Body);
TR = timerange(seconds(100),seconds(300));
Avg = mean(FIT_Test_Frame_2.Body.Pitch(TR));
Std = std(FIT_Test_Frame_2.Body.Pitch(TR));
```

Power Plot Creator

```
clear all
close all
clc


load("MoCap\YawPowerRun_002.mat")
load("YawDataFiles\YawPowerRun_002.mat")

%Create Time table of Frame Yaw
YawPower.Data = squeeze(YawPower.Data);
FrameYaw = timeseries2timetable(YawPower);

%Create Time from Elasped Time
FIT_Test_Frame.Body.Time = seconds(FIT_Test_Frame.Body.Time_Elapsed);

figure(2)
plot(FrameYaw,"YawPos")
hold on
plot(FIT_Test_Frame.Body,"Yaw")
legend("Onboard","MotionCapture")
title("PID Tune Run")

%%%%%%%%%%%%%%%%%%%%%%%%%%%
%Insert Offsets for time delay and IMU
tMFP = seconds(0);
offset = 0;
%%%%%%%%%%%%%%%%%%%%%%%%%%%

FIT_Test_Frame.Body.Time = FIT_Test_Frame.Body.Time + tMFP;
FIT_Test_Frame.Body.Pitch = FIT_Test_Frame.Body.Pitch + offset;

figure(4)
hold on
plot(FIT_Test_Frame.Body,"Yaw")
plot(FIT_Test_Frame.Body,"Yaw_Vel")
legend("MoCapYawPos(deg)","MoCapYawVelocity(deg/s)")
title("Yaw Power Run")
grid on
```

Yaw Plot Creator

```
clear all
close all
clc


load("MoCap\YawHighPositions_002.mat")
load("YawDataFiles\YawPitchCombinationRun_003Y.mat")

%Create Time table of Frame Yaw
FrameYaw = timeseries2timetable(TestDataYaw.YawPos);
FrameYaw.YawPos = FrameYaw.YawPos;

%Create Time from Elasped Time
FIT_Test_Frame_2.Body.Time = seconds(FIT_Test_Frame_2.Body.Time_Elapsed);

figure(1)
plot(FrameYaw,"YawPos")
hold on
plot(FIT_Test_Frame_2.Body,"Yaw")
legend("Onboard","MotionCapture")
title("Yaw 0.5Kts Positions Unaligned")

%%%%%%%%%%%%%%%%%%%%%%%%%%%
%Insert Offsets for time delay and IMU
tMFP = seconds(53);
offset = 0;
%%%%%%%%%%%%%%%%%%%%%%%%%%%

%Apply offsets to data
FIT_Test_Frame_2.Body.Time = FIT_Test_Frame_2.Body.Time + tMFP;
FIT_Test_Frame_2.Body.Yaw = FIT_Test_Frame_2.Body.Yaw + offset;

%Create Array to Be used for retime
FrameArray = FrameYaw.YawPos;
SetPointArray = TestDataYaw.YawSetPoint.Data;
ThrustArray = TestDataYaw.YawThrust.Data;

%Re time Frequency
Fq = 140;

%Retime data sets
ReTimedFrameYaw = array2timetable(FrameArray,"SampleRate",Fq);
ReTimedSetPoint = array2timetable(SetPointArray,"SampleRate",Fq);
ReTimedThrust = array2timetable(ThrustArray,"SampleRate",Fq);

figure(2)
plot(ReTimedFrameYaw,"FrameArray")
```

```
hold on
plot(FIT_Test_Frame_2.Body,"Yaw")
legend("Onboard","MotionCapture")
title("PID Tune Final Aligned")

figure(5)
hold on
plot(FIT_Test_Frame_2.Body,"Yaw")
plot(ReTimedSetPoint,"SetPointArray")
plot(ReTimedFrameYaw,"FrameArray")
legend("MoCap Pitch","YawSetPoint","CurrentSensor")
title("PID Tune Final Sensor Comparison")

figure(6)
hold on
plot(FIT_Test_Frame_2.Body,"Yaw")
plot(ReTimedSetPoint,"SetPointArray")
plot(ReTimedThrust,"ThrustArray")
legend("MoCap Yaw","YawSetPoint","Thrust(lbs)")
ylabel("Position (deg)")
title("1.5kts Yaw Control Loss")
grid on

figure(7)
hold on
plot(FIT_Test_Frame_2.Body,"Yaw")
plot(FIT_Test_Frame_2.Body,"Pitch")
plot(ReTimedSetPoint,"SetPointArray")
legend("MoCap Yaw","MoCap Pitch","YawSetPoint")
title("Yaw/Pitch Combination 1.5kts")
ylabel("Position (deg)")
grid on

FIT_Test_Frame_2.Body = rmmissing(FIT_Test_Frame_2.Body);
TR = timerange(seconds(70),seconds(221));
Avg = mean(FIT_Test_Frame_2.Body.Pitch(TR));
Std = std(FIT_Test_Frame_2.Body.Pitch(TR));

%% Use Power Spectrum To Match Frequency of Events
FIT_Test_Frame_2.Body = rmmissing(FIT_Test_Frame_2.Body);

%Select Time Range for Events to Compare
MTime = timerange(seconds(310),seconds(359));
FTime = timerange(seconds(246),seconds(284));

MoCapArray = FIT_Test_Frame_2.Body.Yaw(MTime,:);
YawArray = FrameYaw.YawPos(FTime,:);
[p1,f1] = pspectrum(MoCapArray,100);
[p2,f2] = pspectrum(YawArray,140);
```

```
%Plot Power
figure(10)
plot(f1,p1);
hold on
plot(f2,p2);
legend("MoCapYaw","OnboardYaw")
title("Frequency Analysis")
ylabel("Power")
xlabel("Frequency")
grid on
```

Camera Calibration Data

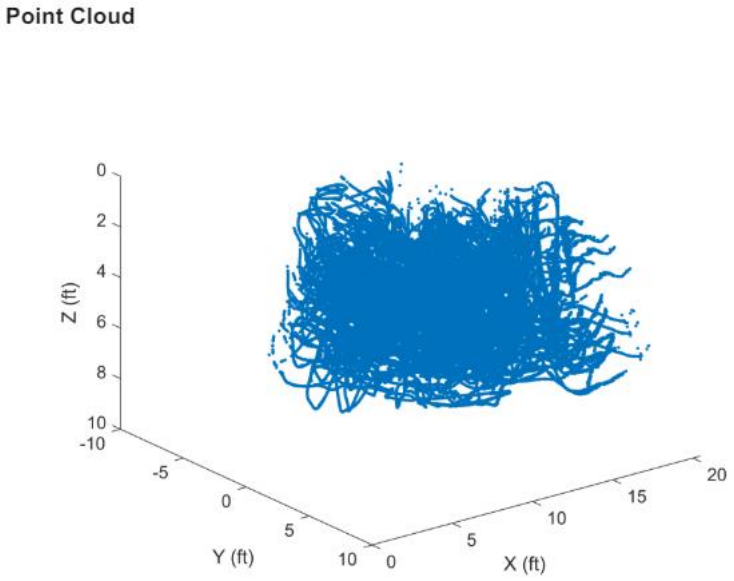

Figure 129: Calibration Points Collected

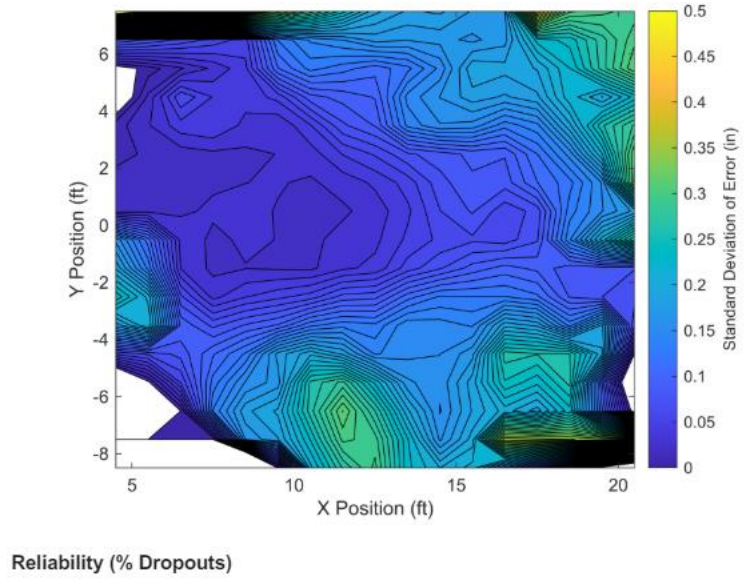

Figure 130: Motion Capture Reliability @ 4ft

Additional Media

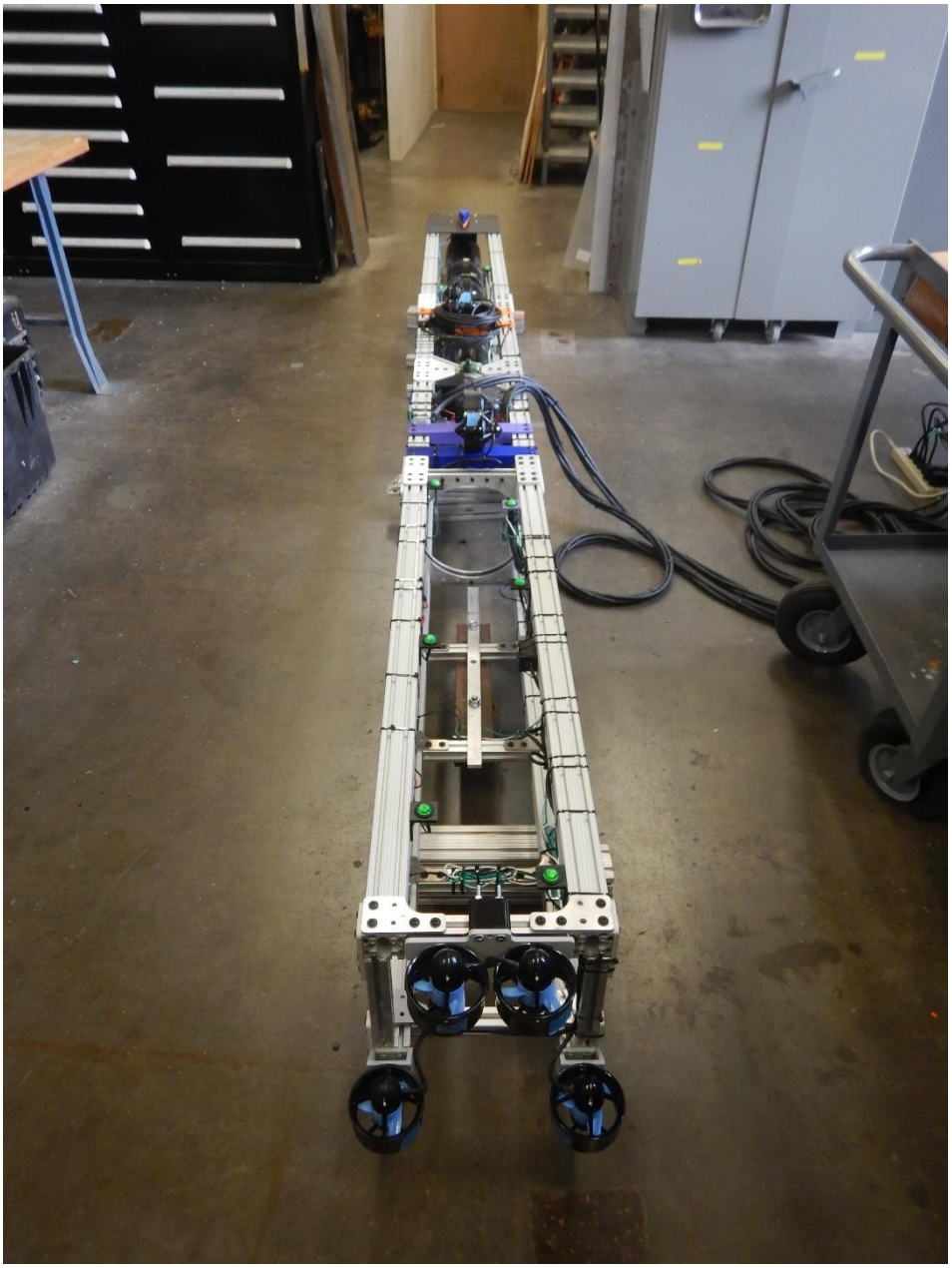

Figure 131: Fully Assembled Fame in Mechanical Shop

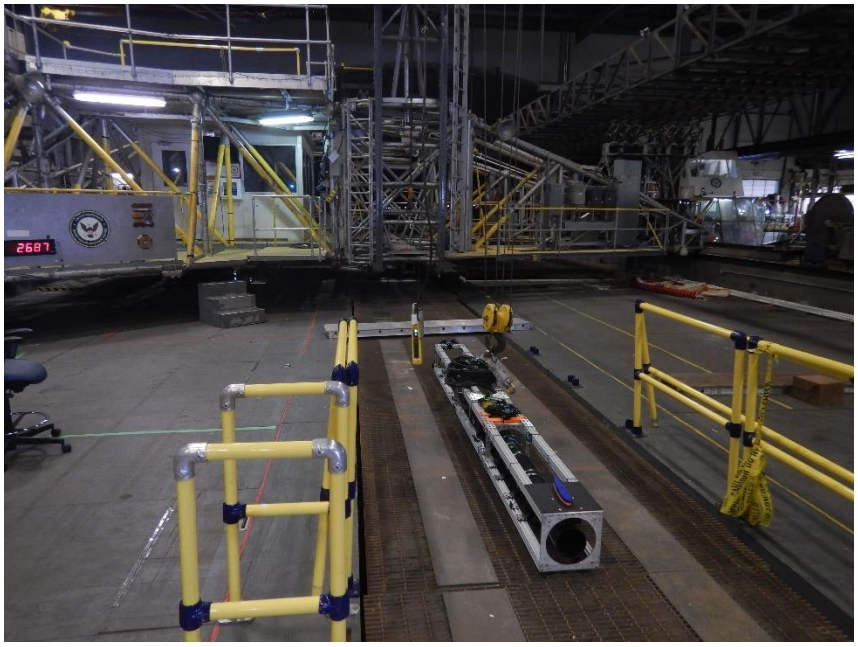

Figure 132: Model Loaded into Dry Dock at David Taylor Model Basin

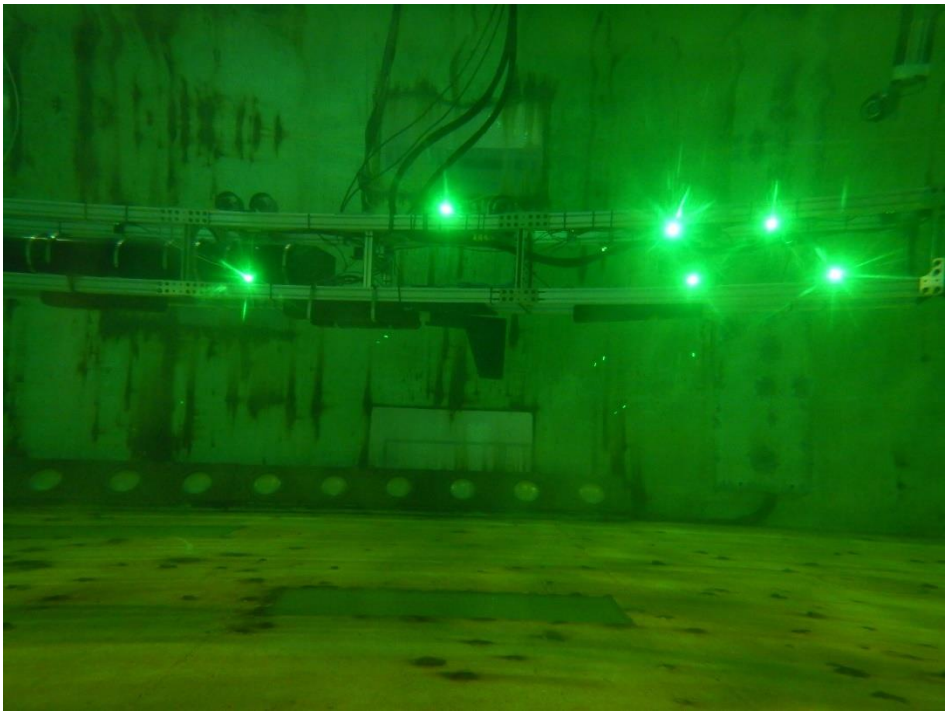

Figure 133: Underwater View from CWC

Figure 134: Underwater View 2 from CWC

Figure 135: CWC Observation Area

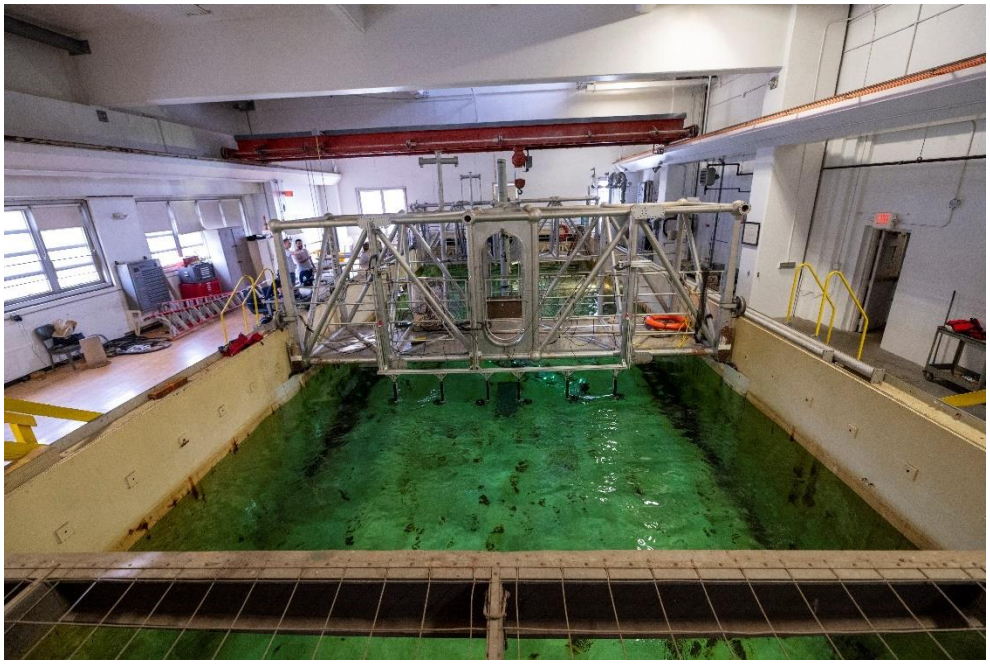

Figure 136: CWC Working Area

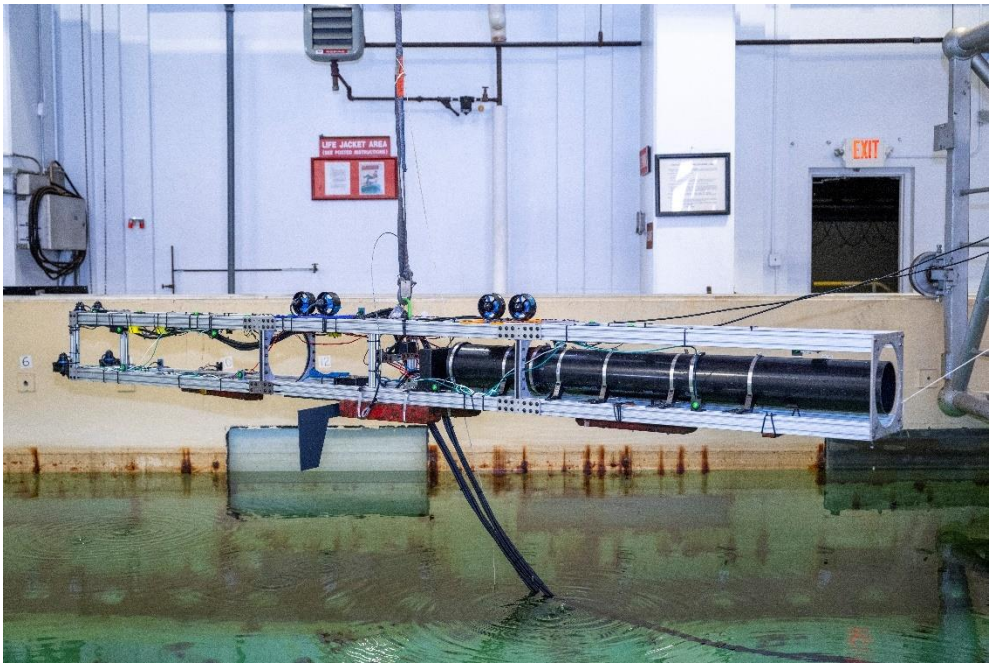

Figure 137: Test Frame on Crane